Computational Investigation of the Structural Response of Bistable Scissor Structures

Liesbeth I. W. Arnouts

Master thesis submitted under the supervision of
Prof. dr. ir. Thierry J. Massart

The co-supervision of
Prof. dr. ir. arch. Niels De Temmerman

Advisors
Prof. dr. ir. Péter Z. Berke
Dr. ir. arch. Kelvin Roovers

Academic year
2016-2017

In order to be awarded the Master's Degree in
Architectural Engineering

Computational Investigation of the Structural Response of Bistable Scissor Structures

Liesbeth Arnouts

in order to be awarded the Master's Degree in Architectural Engineering (2016-2017)

Abstract

In many civil engineering applications (emergency shelters, exhibition and recreational structures...), structures need to be easily moveable, or assembled at high speed on unprepared sites. For this purpose, preassembled deployable scissor structures, which consist of beam elements connected by hinges, are highly effective: besides being transportable, they have the advantage of speed and ease of erection and folding, while offering a huge volume expansion.

Intended geometric incompatibilities between the members can be introduced as a design strategy, to instantaneously achieve a structural stability at deployment that can be sufficient for small loads. In so-called bistable scissor structures, these incompatibilities result in compression and bending of some specific members that are under compression with a controlled snap-through behaviour. Despite the advantages bistable scissor structures have to offer, few have successfully been realized because of the complexity they add in the design process.

The main goal of this project is the development of a 3D nonlinear structural model for the simulation of the deployment of bistable scissor structures. Starting from an initial simplified polygonal module, the computational model is refined in several stages and the influence of the main design parameters on the structural response is investigated.

Since imperfections will unavoidably take place because of manufacturing defects, their influence on the deployment behaviour is studied. The main types of tolerances that are investigated are the finite hinge size, imperfections on the length of the beams, eccentricity of the pivot points, finite hinge stiffness, hinge misalignment and friction.

The computational tool is applied to structures consisting of multiple modules and the influence of imperfections on such structures is investigated.

Key words: numerical modelling, structural engineering and design, scissor structures, bistability, snap-through, nonlinear computational mechanics

Computational Investigation of the Structural Response of Bistable Scissor Structures

Liesbeth Arnouts

in order to be awarded the Master's Degree in Architectural Engineering (2016-2017)

Samenvatting

In vele bouwkundige toepassingen (noodopvang, expositie en recreatieve structuren ...), moeten structuren gemakkelijk verplaatsbaar zijn of snel gemonteerd worden op onvoorbereide locaties. Daartoe zijn voorgemonteerde schaarstructuren, die bestaan uit staafelementen verbonden door scharnieren, zeer effectief: naast transporteerbaarheid, hebben ze het voordeel dat ze snel en gemakkelijk kunnen gemonteerd en gedemonteerd worden, terwijl ze een gigantische volumevergroting teweeg brengen.

Geometrische incompatibiliteiten tussen de elementen kunnen worden gebruikt als een ontwerpstrategie, om ogenblikkelijk na het ontplooien een structurele stabiliteit te bekomen die voldoende is voor kleine belastingen. In zogenaamde bistabiele schaarstructuren resulteren deze incompatibiliteiten in druk en buiging in een aantal specifieke elementen met een gecontroleerd 'snap-through' gedrag als gevolg. Ondanks de voordelen die bistabiele schaarstructuren te bieden hebben, zijn er slechts weinig succesvol gerealiseerd vanwege de complexiteit die ze toevoegen in het ontwerpproces.

Het belangrijkste doel van dit project is de ontwikkeling van een niet-lineair 3D structureel model om het gedrag tijdens het ontplooien van bistabiele schaarstructuren te onderzoeken. Vertrekkend van een vereenvoudigde polygonale structuur, wordt het computermodel in verschillende fasen verfijnd en de invloed van de belangrijkste ontwerpparameters onderzocht.

Aangezien onvolkomenheden onvermijdelijk plaatsvinden door fabricagefouten, wordt hun invloed bestudeerd. De bestudeerde toleranties zijn de afmetingen van de scharnieren, onvolkomenheden op de lengtes van de elementen, excentriciteit van de gaten in de elementen, scharnierstijfheid, foutieve uitlijning van de scharnieren en wrijving.

Het computermodel wordt toegepast voor structuren die bestaan uit meerdere eenheden en de invloed van onvolkomenheden wordt onderzocht in dergelijke structuren.

Trefwoorden: numerieke modellering, bouwkunde en ontwerp, schaarstructuren, bistabiliteit, snap-through, niet-lineaire computermechanica

Computational Investigation of the Structural Response of Bistable Scissor Structures

Liesbeth Arnouts

in order to be awarded the Master's Degree in Architectural Engineering (2016-2017)

Résumé

Dans de nombreuses applications de génie civil, les structures doivent être facilement déplaçables ou assemblées rapidement sur des sites non préparés. A cet effet, des structures déployables pré-assemblées au départ d'unités en ciseaux sont très efficaces : en plus d'être facilement transportables, elles ont l'avantage de la rapidité et de la facilité de montage et de démontage, tout en offrant une grande expansion volumique.

Ces structures en ciseaux sont constituées de poutres reliées par des articulations. Pour obtenir une stabilité structurale instantanée après le déploiement de la structure, des incompatibilités géométriques entre les éléments peuvent être introduites intentionnellement dans la stratégie de conception. Dans ces structures, appelées structures en ciseaux bistables, ces incompatibilités géométriques intentionnelles ont pour effet la flexion-compression de certains éléments spécifiques générant un 'snap-through' contrôlé. En dépit des avantages de ces structures en ciseaux bistables, peu ont été réalisées avec succès en raison de la complexité du processus de conception et d'un manque de maîtrise des niveaux d'incompatibilité à utiliser.

L'objectif principal de ce projet est le développement d'un modèle 3D non linéaire pour la simulation du déploiement de structures en ciseaux bistables. À partir d'une unité polygonale simplifiée, le modèle de calcul est raffiné en plusieurs étapes et l'influence des paramètres de conception principaux sur la réponse structurale est étudiée.

Étant donné que les imperfections se produiront inévitablement en raison de défauts de fabrication, leur influence sur le comportement de déploiement est étudiée. Les principales tolérances étudiées sont les dimensions des charnières, les imperfections sur les longueurs des éléments, l'excentricité des points de pivotement, la rigidité des charnières et le frottement de celles-ci.

L'outil de calcul est appliqué pour des structures comprenant plusieurs unités et l'influence des imperfections sur ces structures est étudiée.

Mots-clés : modélisation numérique, ingénierie structurale et conception, structures en ciseaux, bistabilité, snap-through, mécanique non linéaire

Preface

I would like to express my sincere gratitude to my supervisor, Prof. dr. ir. Thierry J. Massart, and Prof. dr. ir. Péter Z. Berke for their interest in bistable scissor structures and their continued support during the whole year. Their great advice and our clarifying meetings helped me to understand the behaviour of bistable scissor structures and encouraged me to get the most out of it.

Special thanks go to my co-supervisor Prof. dr. ir. arch. Niels De Temmerman, who motivated me with his enthusiasm and suggestions like no one else could do. Without him being so obsessed with scissor structures, this thesis would have never seen the light.

At VUB, I would like to thank dr. ir. arch. Kelvin Roovers, whose PhD was a great starting point for my work. He was always available to explain concepts about the geometry and kinematics of scissor structures and his physical models helped me a lot in understanding this fascinating subject.

At ULB, I was lucky to meet ir. Murillo Bento Santana, who was interested in trying to model the deployment behaviour of bistable scissor structures with his own computational code. We had some fruitful discussions about bistable scissor structures and computational modelling.

Special thanks go to Prof. dr. ir. Charis J. Gantes, whose research in 1991 was essential for this work. I was fortunate to meet him and to discuss about my work. He was very eager to answer my questions when I needed some additional information.

I would also like to thank my friends and colleagues in the second year of architectural engineering. It has been a though year with a lot of pressure. Without the mutual support, it would have been a hopeless job.

My most heartfelt gratitude goes out to my parents, my brother and sisters for their unconditional love and never-ending support, and to my partner, Tijs Van Renterghem, for his interest in the subject and his love and encouragement when I was on the edge of breaking down.

Ixelles, May 2017
Liesbeth Arnouts

Contents

List of Figures

Nomenclature

α	Thermal expansion coefficient
$\bar{\theta}$	Temperature of the beam axis
$\Delta\theta$	Temperature change
Δl	Arc length
Δq	Displacement
Δt	Variation of the fictitious 'time' parameter
ϵ^{th}	Thermal strain
$\frac{\partial\theta}{\partial x_1}$	Gradient of temperature with respect to the local x_1 axis
$\frac{\partial\theta}{\partial x_2}$	Gradient of temperature with respect to the local x_2 axis
μ	Friction coefficient
ω	Load proportionality factor used in the Riks method
ϕ	Angle to describe the curvature of a curved module
ϕ	Misalignment of the hinge axis
Ψ	Parameter of dimensional consistency
θ	Temperature
A	Distance between the pivots at the hinges and the ends of the beam
a	Semi-length of rod
a_i	Coefficient to calculate the shape of the segments in the calculation of friction
B	Length between the pivots of a beam
b	Semi-length of rod in the geometric design
b	Width of a bar in the calculation of friction
b_h	Width of the slot of a joint
b_i	Coefficient to calculate the shape of the segments in the calculation of friction
C	Length between the pivots of a beam
c	Semi-length of rod
c_i	Coefficient to calculate the shape of the segments in the calculation of friction
D	Distance between the pivots at the hinges and the edges of the joint in the calculation of friction
d	Diameter of a member
d	Semi-length of rod
d_i	Coefficient to calculate the shape of the segments in the calculation of friction
E	Modulus of elasticity
f_{ext}	Unit force system
F_f	Friction force parallel to the surface
f_{int}	Current load magnitude
F_i	Concentrated transverse force

F_N	Friction force perpendicular to the surface
h_1	Heigth of the square module in the middle
h_2	Heigth of the outer elements in the square module
I	Moment of inertia
k	Factor slightly larger than 0.5 which depends on the extensibility of the pin at the pivotal connection
K_t	Tangent stiffness
L	Half the length of the diagonal in the square module
l	Length of a beam
L_i	Length of a segment in the calculation of friction
$M_{(i)}$	Bending moment
P_{11}	Deployment load for a single module
P_{mn}^{pred}	Predicted deployment load for multi-module structures
t	Parameter which allows defining the sequence of the different mechanical events (i.e. fictitious 'time' parameter)
t	Structural thickness of a member
$v_{(i)}$	Displacement at each segment in the calculation of friction
X, Y	Global Cartesian coordinate system
X_i, Y_i	Local coordinate system

Chapter 1

Introduction

1.1 Bistable deployable structures in civil engineering

In many civil engineering applications (emergency shelters, exhibitions and recreational structures, temporary buildings, maintenance facilities), structures need to be easily moveable in the course of normal use, which very often requires the building system to be assembled at high speed, on unprepared sites. For this purpose, preassembled deployable scissor structures are highly effective: besides being transportable, they have the advantage of speed and ease of erection and folding, while offering a huge volume expansion.

Figure 1.1: Deployable shelter (scissor structure + membrane) in the folded and unfolded configuration (Grupo Estran, n.d.).

Among the large scope of available technical solutions, scissor structures are transformable structures designed using the principle of the pantograph (Pellegrino, 2001). A pantograph, also called a scissor-like element (SLE), is the assembly of two beams connected through a revolute joint which introduces constraints of rotation normal to their common plane. By connecting such SLE's at their endpoints by hinges that allow for in-plane and out-of-plane rotations, a three-dimensional grid structure is formed (Kaveh & Daravan, 1996). This scissor grid can be transformed from a compact bundle of elements to a fully deployed configuration, offering a huge volume expansion (Figure 1.1). When folded, scissor structures occupy a reduced volume that can ease their transportation, which is a prime advantage for numerous applications, for example emergency shelters or bridges, temporary buildings or covers, lightweight camping, exhibition structures, greenhouses, travelling theatres (Gantes, Tsouknaki & Kyritsas, 1998).

Because of their simpler design process, 'stress-free' scissor structures have been used preferentially in the past (Hoberman,1990; Partyspace BVBA, n.d.; Nunes, 2016; Koumar, Tysmans, De Temmerman, Filomeno Coelho and Alegria Mira, 2014; Van Mele, De Temmerman, De Laet and Mollaert, 2010). Assuming a perfect 'wire' geometry, these structures are geometrically compatible before, during and after deployment; i.e. their beams remain straight during the deployment and the unfolding occurs without mechanical strain (De Temmerman, 2007). In the ideal case such structures can be considered as perfect mechanisms with an easy deployment, simplifying their design. By consequence, these mechanisms have the important disadvantage that they need external manipulation or stiffening to become structures and bear loads in the deployed configuration. The current design of such structures assumes idealized geometry and materials (perfect positioning of point-wise hinges, no friction). Subtle and inevitable changes in the geometry (manufacturing and assembly tolerances) and in the behaviour of the elements (e.g. friction in the links) can have dramatic effects on the deployed shape and can result in undesired mechanical behaviour (high deployment forces, spurious deformations) or no deployment at all, if incompatibilities become dominant. The structures then become self-locking and self-stiffening, which is not a desired effect in the design of compatible scissor structures, leading to uncontrolled residual stresses in their members (higher sensitivity to buckling).

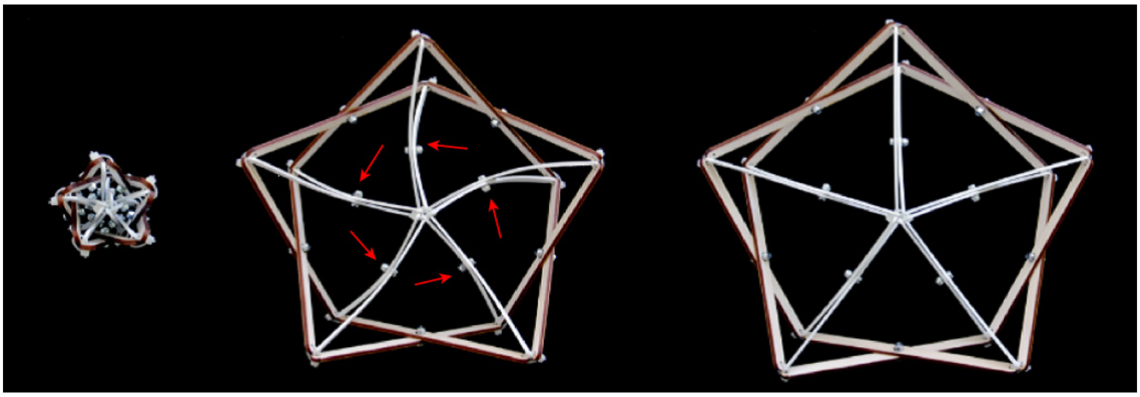

Figure 1.2: Three snapshots of the transformation from the compact (left) to the fully deployed state (right) of a bistable scissor module. The middle figure shows the controlled buckling of the middle beams, designed for this loading (Roovers, 2017).

Another approach consists of the introduction of intended geometric incompatibilities between the members as a design strategy. This is achieved by choosing a geometric or kinematic design that complies with the mathematical equations related to the straightness of the beams in the folded and unfolded configuration (Gantes, 1996a, 1997), while bending and relaxing of chosen elements during transformation is aimed at. The class of transformable structures with geometric incompatibilities meeting these terms is referred to as bistable. To summarize, bistable scissor structures are ideally geometrically compatible before and after deployment, but during deployment, the large displacements combined with the geometric incompatibilities result in intended bending of some of the members. By consequence, these structures exhibit a controlled snap-through behaviour during deployment to instantaneously achieve a structural stability that can be sufficient for small loads (self-sustaining under gravity for instance). The self-locking phenomenon can thus also be beneficial and desired because of the ease and speed of erection. Afterwards, the resulting stable structures are stiffened by attaching additional structural elements for regular use. The structural response is thus inherently nonlinear, requiring taking snap-through into account to investigate their transformation (Matijevic & Kovacevic, 2009). Because of the complexity of the deployment process (Figure 1.2, Figure 1.3), a computational approach is useful.

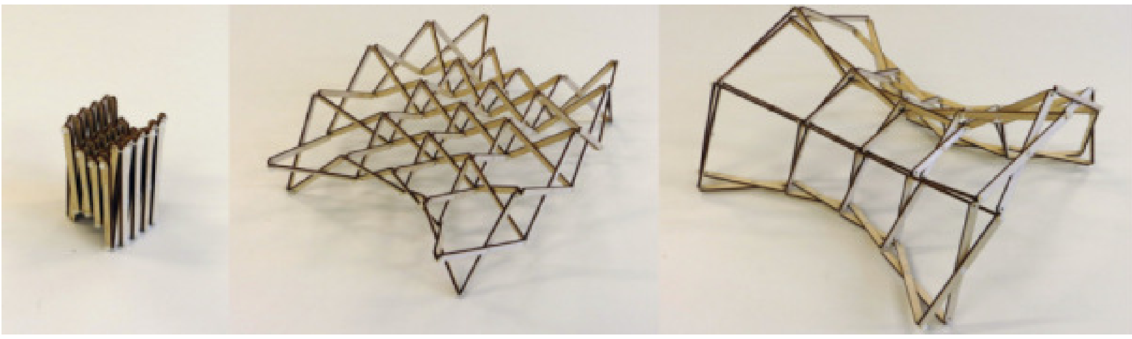

Figure 1.3: Reduced model of a complex bistable scissor structure going from the compact (left) to the fully deployed state (right). The middle figure shows the structure during deployment (Roovers, 2017).

Theodore Zeigler was the first to theoretically identify the 'snap-through' phenomenon in deployable structures (Zeigler, 1976). A disadvantage of earlier structures using the concept of the pantograph (Figure 1.4), introduced by Piñero (1961), was the requirement of an additional locking system, since these first structures were pure mechanisms. Zeigler patented a partial triangulated spherical dome (Figure 1.5), introducing a self-supporting feature that resulted from geometric incompatibilities between the member lengths associated with the way they are contained within the grid (De Temmerman, 2007). In subsequent patents (Zeigler, 1977, 1981, 1984, 1989, 1993), he tried to improve this structure and control the snap-through effect by experimenting with variations in the shape and the type of connections and by omitting some of the pivotal connections.

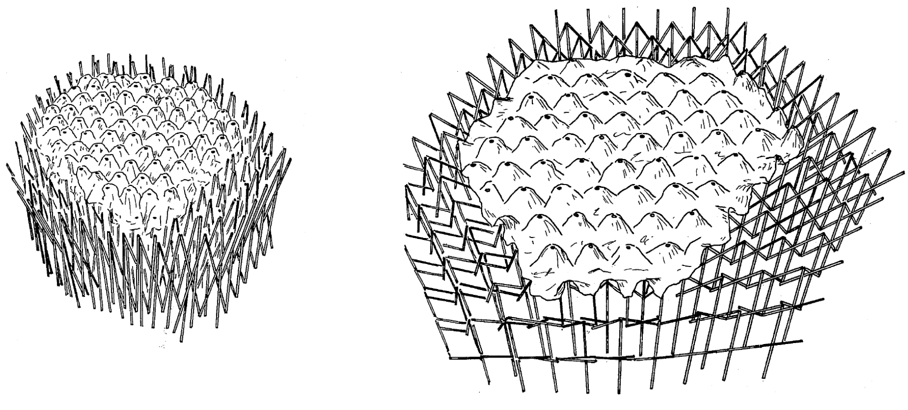

Figure 1.4: A three-dimensional reticular structure patented by Piñero (Piñero, 1965).

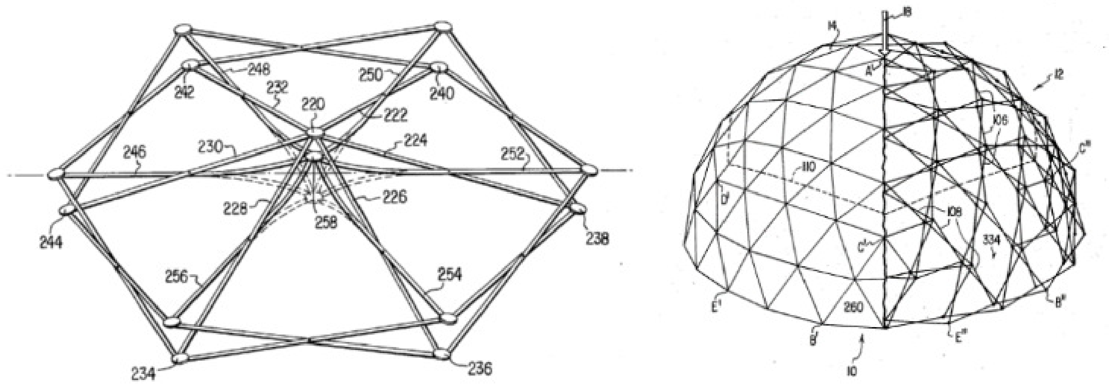

Figure 1.5: A single module and a spherical dome built from such modules (Zeigler, 1976).

Zeigler's work focused on limited geometric shapes and the design resulted in the existence of bent elements in the final deployed configuration. The structure was not fully geometrically compatible in the deployed configuration, meaning that in the idealised case, without taking into account gravity and external loads, there were still residual stresses in the members of the model (Gantes, 1991). This is not a desired effect in the design of bistable scissor structures, although it might prove helpful when folding the structure and to sustain loads. Nevertheless, several popular pop-up displays and pavilions were constructed in accordance with Zeigler's patents (Friedman, 2011).

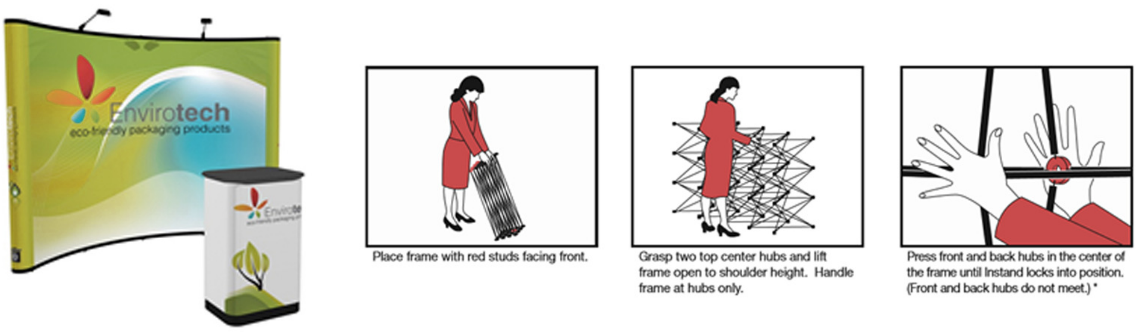

Figure 1.6: Pop-up display and schematic presentation of its installation (Nomadic Display Corp., n.d.).

W.P. Zalewski and S. Krishnapillai (Krishnapillai & Zalewski, 1985) improved the work of Zeigler and found a configuration for which the structure is stable and geometrically compatible before and after deployment. The strain energy that has built up in the members during deployment is released by a snap-through clicking into a self-sustained, load-bearing structure. The scissor-like elements of Krishnapillai's models are assembled in such a way that they form structural modules with a plan view of a regular polygon with three, four (Figure 1.7) or six sides. Each side and diagonal of the polygon is a scissor-like element. By combining several of these modules, structures of flat and curved geometric configurations can be created. For other types of regular polygons the assembly of flat structures consisting of many modules is not possible (Gantes, 1991).

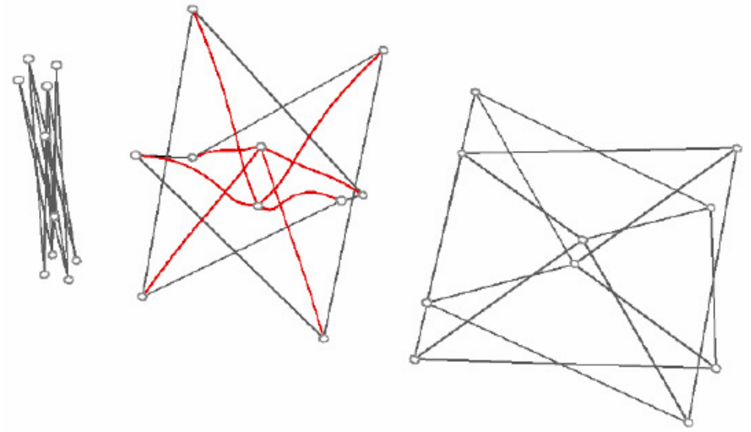

Figure 1.7: Bistable scissor structure with the plan view of a polygon (De Temmerman, 2007).

Based on this work, R.D. Logcher and Y. Rosenfeld did some structural analyses to identify the snap-through phenomenon and they carried out experimental work on these structures (Rosenfeld, Ben-Ami & Logcher, 1993). In parallel, C.J. Gantes developed a geometric design approach for flat slabs, curved grids (Figure 1.8) and non-circular arches which consist of assembled polygonal modules (Gantes, 1993). He studied the structural response of deployable structures as well as their structural behaviour in the deployed configuration, using the finite element package ADINA (ADINA R&D, 1987).

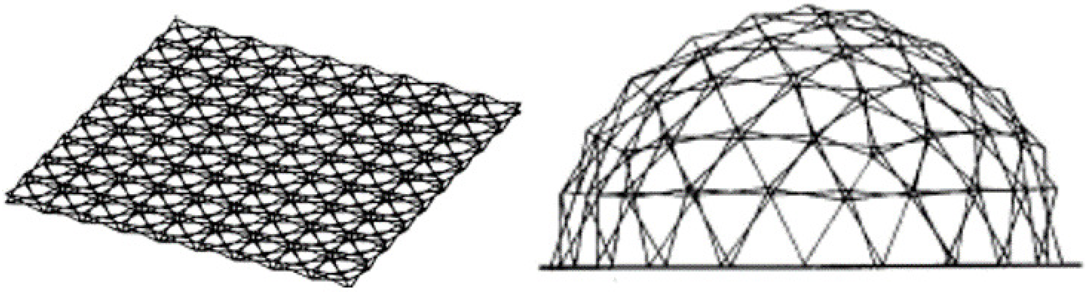

Figure 1.8: Flat slab and curved grid composed out of bistable polygonal scissor modules (Gantes & Konitopoulou, 2004).

The PhD thesis of Gantes titled 'A Design Methodology for Deployable Structures' (1991) is considered as a milestone in the study of the structural response of deployable scissor structures. Gantes made full size structures which he modelled during and after deployment with the finite element method.

1.2 Problem statement

Although bistable scissor structures have been known for a long time under the name of self-deploying, self-collapsing, self-supporting, self-stabilizing, self-locking or bistable structures, many researchers did not investigate the behaviour of this kind of structures in detail, since the underlying phenomena are complex. Although the structural behaviour in the deployed configuration can be approximated as linear, the response during transformation is characterised by geometric nonlinearities. Furthermore, even though large geometrical variations occur, the material behaviour in all phases must remain elastic to avoid permanent deformations. Simulation of the deployment process is therefore an important part of the analysis, requiring sophisticated computational modelling techniques (Gantes, 1991, 1996b, 1997, 2001).

Developing and analysing bistable scissor structures is a contemporary subject in civil engineering research, for example Kawaguchi and Sato (2015). K. Kawaguchi (Kawaguchi & Sato, 2015; Kawaguchi, Inoue & Ogi, 2012; Leaveanest Co.Ltd., 2012b, 2012a) and T. Sato improved the deployable geodesic sphere with scissor members designed theoretically by Zeigler and demonstrated successfully the viability of a deployable geodesic full sphere. Another group currently working on bistable scissor grids, is S.-D. Kim together with D.S.-H. Lee (Lee, Larsen & Kim, 2013, 2014, 2016). The most recent research about the geometry and kinematics of bistable scissor structures was performed by K. Roovers (Roovers, 2017), who investigated new configurations without taking their structural response into account. Although some of the researchers mentioned above are using the finite element method to do structural analyses, none of them is modelling the deployment behaviour of scissor structures.

Regarding bistable scissor structures, often an experimental approach is used (Rosenfeld et al., 1993; Kawaguchi & Sato, 2015; Hernandez, 1996) in which researchers try to combine an easy deployment process and adequate stiffness in the deployed state by making an initial guess and iteratively fine-tuning it to get a good balance between having a self-locking effect for stability with a limited force needed for deployment. Creating the structure and doing trial-error experiments to make it work correctly is however unaffordable as a rigorous design approach for the general problem. Other approaches (Gantes, 1991, 2001; Langbecker & Albermani, 2000) are based on idealised structures (i.e. no friction, point-like joints) which do not allow fully understanding their behaviour.

There is thus a need for a deeper understanding of the complex transformation behaviour of bistable scissor structures and their structural performance after deployment. Even though simple physical test models can give some insight to the behaviour of bistable structures, computational modelling can contribute significantly to defining a rigorous design methodology.

Designing the complete transformation behaviour (both in terms of kinematics and of applied forces) of bistable scissor structures is a pre-requisite for conceiving practical applications, which are currently rare in civil engineering (Rosenfeld et al., 1993; Kawaguchi & Sato, 2015). Additionally, the deployment process requires knowing how and which members to manipulate. A rigorous design includes the deployment response, linked to nonlinear mechanics, as well as the structural performance in the unfolded state. The main interest of the proposed work is the deployment response of these structures.

1.3 Objectives and methodology

The objective of this thesis is the development of a 3D nonlinear structural model for the simulation of the deployment of bistable scissor structures. There are three main goals:

- **Computational structural analysis using nonlinear finite element models:**

  The deployment behaviour of a simple structural model, which will be a bistable scissor structure with the plan view of a polygon with four sides (Figure 1.9), will be investigated. The load required for deployment and the stresses inside the beams will be assessed, the model will be extended to curved modules and it will be verified whether or not the deployment process is reversible. A parameter study will be carried out, to investigate the influence of the main design parameters on the structural response.

- **Implementing imperfections and tolerances in the nonlinear finite element models:**

  Since imperfections will unavoidably take place because of manufacturing defects, there will always be residual stresses inside the scissor structure. The main types of tolerances that will be investigated are imperfections on the beam lengths, eccentricity of the pivot points, finite hinge stiffness, hinge misalignment and friction.

- **Deployment analysis of realistic structures:**

  The resulting computational tool will be applied to larger structures; complex bistable structures or the interaction between combined basic structural models will be investigated during deployment.

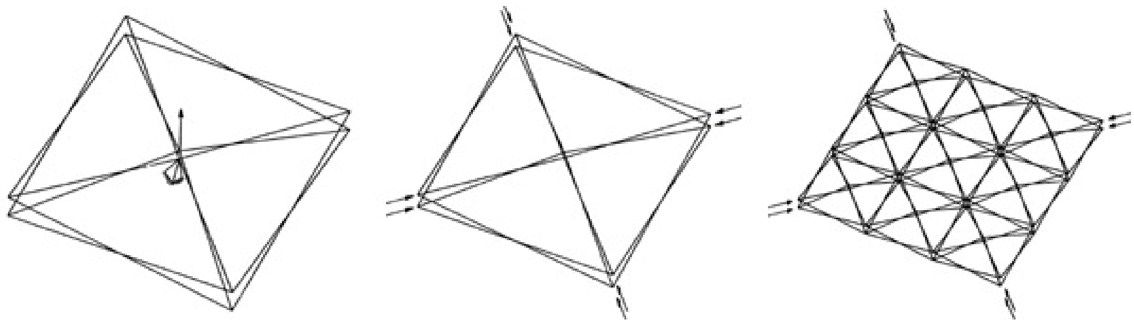

Figure 1.9: Dismantling mechanisms for a single module and for a multi-module slab (Gantes, 1991).

To reach these three main goals, existing research will be investigated first to get familiar with bistable scissor structures. To understand the structural behaviour, a structural model will be implemented using the nonlinear module of the Abaqus commercial finite element code (Dassault Systèmes Simulia Corp., 2012c), starting from an initial simplified model and going through several stages of model refinement. This model refinement includes considering discrete joint dimensions and gravity.

Next, imperfections and tolerances will be implemented in the computational model by considering the finite hinge size, by using 'fake' thermal strain to change the length of the beam elements in the assembled structure and by investigating the effect of hinge misalignment, finite hinge stiffness and friction.

At last, the resulting computational tool will be applied to larger structures. The interaction between combined bistable modules will be investigated as well as imperfections on such larger structures.

The used software package is Abaqus (Dassault Systèmes Simulia Corp., 2012c). The first reason for that choice are the capabilities of Abaqus to handle snap-through problems (e.g. path-following techniques). In addition, Abaqus is very user friendly, providing a complete library of tutorials and documentation. Furthermore, Abaqus uses the open-source scripting language Python for scripting and customization (Dassault Systèmes Simulia Corp., 2012b).

1.4 Originality and main contributions

This work will use Gantes' findings as an inspiration to investigate bistable scissor structures with finite element models starting from a simplified model going through several stages of model refinement, although other software packages and approaches will be used which were not available when he did his research.

For the first time, gravity is considered during deployment, which can have a huge influence on the required deployment load because it can be beneficial for the deployment process or it has to be overcome by the force required for deployment.

The influence of imperfections on the beam lengths, of eccentricity of the pivot points, of a finite hinge stiffness and hinge misalignments on the deployment behaviour of bistable scissor structures has never been considered before. When including such imperfections, a range can be determined for the tolerances to guarantee a proper deployability and a sufficient bistability.

Afterwards, the finite element tool is applied for larger structures. For the first time, discrete joint dimensions, gravity and imperfections are implemented on multi-module bistable scissor structures.

1.5 Outline of the thesis

To get familiar with bistable scissor structures, it is interesting to know the geometrical constraint equations supporting their purely kinematic design. In this work the ideal 'wireframe' geometry issued from design is considered without performing the design itself. The interested reader is referred to Appendix A.

To understand the structural behaviour of bistable scissor structures, a simplified structural model (e.g. frictionless point-like hinges) is investigated during deployment in chapter 2 using the Abaqus commercial finite element package. Subsequently, the model is refined in several stages, for example taking into account gravity. The load required for deployment and the stresses inside the beams are investigated. The tool is extended to curved modules and it is verified whether or not the deployment process is reversible. A parameter study is performed, to investigate the influence of the main design parameters (i.e. the height of the point in the middle, the height to width ratio of the module, the stiffness and the slenderness of the beams) on the structural response.

In chapter 3, he resulting computational tool is used to investigate the influence of discrete joint dimensions and of imperfections and tolerances on the deployment behaviour. Such imperfections will unavoidably take place because of manufacturing tolerances or defects. The main types of tolerances that are investigated are imperfections on the beam lengths, eccentricity of the pivot points, finite hinge stiffness, hinge misalignment and friction.

The computational tool will be applied to structures consisting of multiple modules in chapter 4. The interaction between combined basic structural models will be investigated and the effect on the load required for deployment will be examined. Finally, the effect of imperfections on multi-module structures will also be investigated.

Chapter 5 concludes the thesis by discussing the computational model and the influence of gravity and imperfections. Recommendations for further research are provided.

Chapter 2

Computational Modelling of a Single Idealised Bistable 3D Module

The structural analysis of deployable structures involves two phases, the analysis in the deployed configuration under service loads and the analysis during deployment. The analysis in the deployed configuration is quite straightforward, since the behaviour is expected to be linear (i.e. small displacements). The greater computational challenge is the assessment of the structural behaviour of bistable scissor structures during the erection and folding process. Large displacements occur, making the use of second order theory necessary. Plastic material behaviour during deployment should be avoided since it would result in reduced load-bearing capacity in the deployed configuration and permanent strains. Additionally, the load required for deployment and its variation should not be too high for practical reasons (Gantes, Connor & Logcher, 1990; Gantes, 2001).

The structural design process is thus very complicated and requires successive iterations to achieve a balance between the desired flexibility during deployment and the desired stiffness in the deployed configuration. In this chapter, the analysis during deployment is explained, starting from a simplified structural model and going through several stages of model refinement.

2.1 Idealised case based on the wireframe design geometry

2.1.1 Initial model

A square flat polygonal module has been used for the sake of simplicity. The module has been designed to be as similar as possible to the model Gantes studied and built (Gantes, 1991), which allows comparing the results. One side of the square flat polygonal module has a length of 76.2 cm, the height of the outer scissor-like elements is 23.1 cm and the height of the upper point in the middle of the module is 27 cm (Figure 2.1). Further conclusions (e.g. with regard to the weight) will depend on this choice. The trends obtained here were verified to hold for more complex curved modules as well.

The inner scissor-like elements, which lie on the diagonals of the square module, are made in HDPE (high-density polyethylene), while the outer scissor-like elements, which

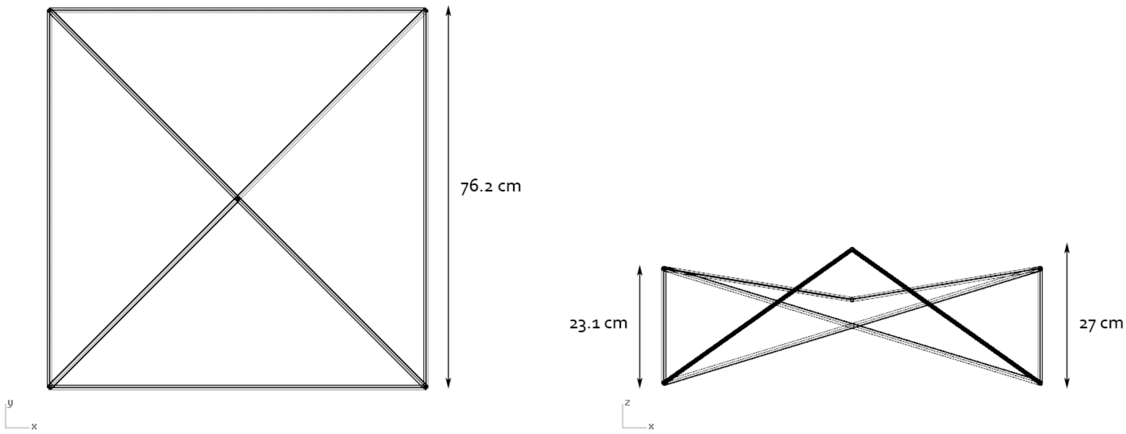

Figure 2.1: Top view (left) and side view (right) with dimensions of the square flat polygonal module.

lie on the sides of the square module, are made of aluminium (Figure 2.2 left). Two different materials were chosen to accommodate better the snap-through behaviour, because the inner SLE's bend during deployment, while the outer SLE's don't.

Scissor structures have two types of connections. The first one is the pivotal connection, that connects the two beams in a scissor-like element, while the second one is a joint which connects two or more scissor-like modules at their end points (Figure 2.2 right).

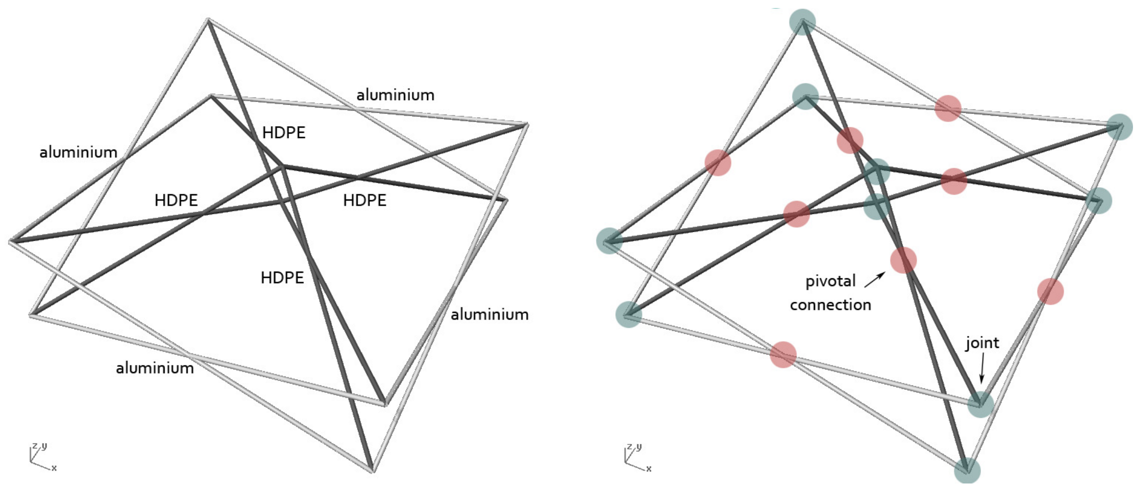

Figure 2.2: Materials of the different SLE's: HDPE and aluminium (left) and connections: pivotal connections and joints (right).

In this dissertation beam elements are used to model all the members, as opposed to Gantes, who used beam and truss elements (Gantes, 1991). Three-dimensional 2-node beam elements are used. In Abaqus, such a beam element is a one-dimensional line element in three-dimensional space that has stiffness associated with the deformations of the beam's axis. These deformations consist of axial stretch, curvature change (bending) and torsion. They offer additional flexibility associated with transverse shear deformation between the beam's axis and its cross-section directions. These elements in Abaqus are formulated according to the Timoshenko beam theory. Shear locking is addressed, which means that the elements degenerate correctly into beam elements according to the Euler-Bernoulli beam theory (which should be used for thin beams).

First, every semi-length of each beam was modelled as a beam element. Refinement of the beam elements (i.e. increasing the number of finite elements along the structural members) in the outer scissor-like elements was not necessary, since they were stressed in almost pure tension throughout deployment (Gantes even used truss elements). However, refinement of the beam elements of the inner scissor-like elements was necessary because they are subjected to both bending and compression (Gantes, 1991). If not enough elements are used to model the inner SLE's, the structural response will be too stiff. A converged mesh with four elements on each semi-length of the beams (Figure 2.3 left) gives sufficient accuracy for design and engineering purposes (Figure 2.3 right) and was used for subsequent analyses.

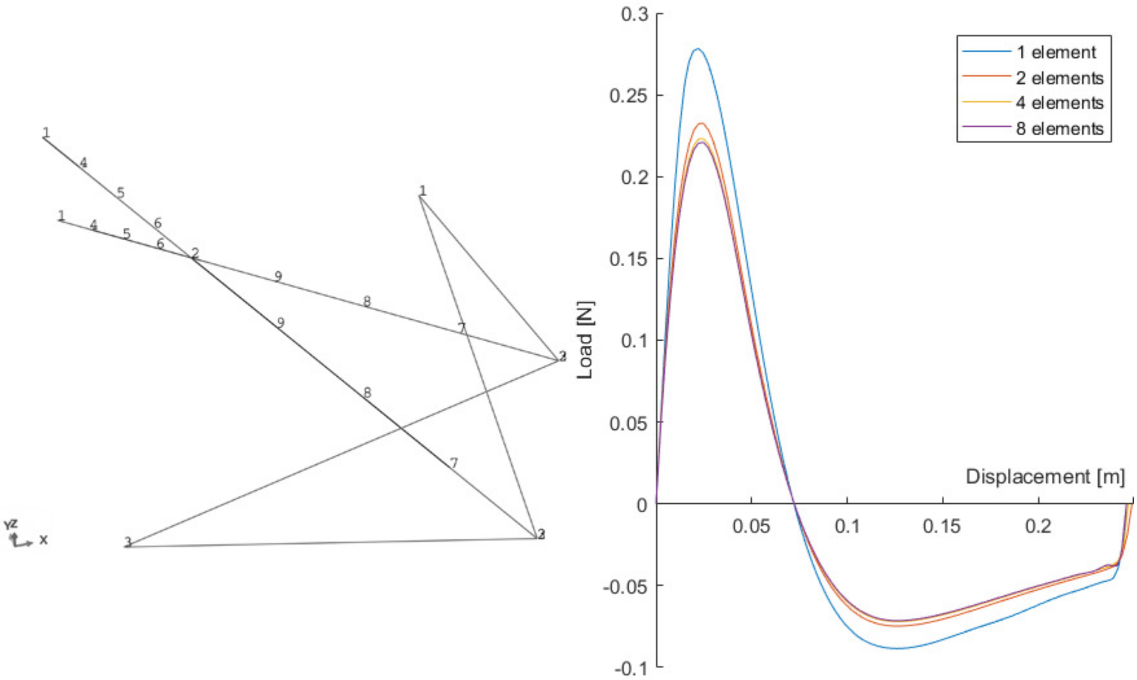

Figure 2.3: The finite element mesh for the idealised wireframe design geometry (left) and refinement of the mesh with 1, 2, 4 and 8 elements on each semi-length of the beams (right).

The effect of the pivotal connections was simulated by defining the two beams of an SLE as two parts (i.e. one leg is one part) with the Abaqus connector type 'hinge' in between, in order to model a realistic behaviour of the joints. Hinges join the position of two nodes and provide a revolute constraint between their rotational degrees of freedom. The hinges were defined perpendicular to the common plane of the two beams.

The model has been extended to include curved spherical structures as well. The main difficulty when modelling curved modules is the spatial reorientation of the joints during transformation (Figure 2.4). Connector elements in Abaqus have relative displacements and rotations that are local to the element. The connector element's orientation directions co-rotate with the rotational degrees of freedom at the corresponding node on the element. When the orientation directions of the hinges are correctly defined, the joints reorientate during deployment and remain perpendicular to the common plane of the two beams.

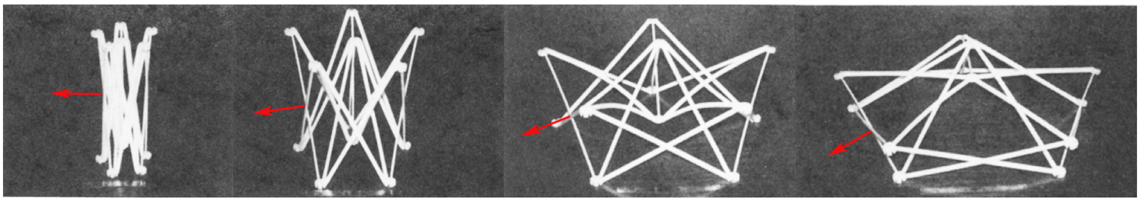

Figure 2.4: Reorientation of the joints during deployment: the joint in the middle is perpendicular to the common plane of the two beams (red arrow), which rotates in space during deployment (Gantes, Connor & Logcher, 1993).

Another technique that can be used to model the pivotal connections is the master node/slave node technique in which all the translational degrees of freedom of the slave node are constrained with respect to the corresponding degrees of freedom of the master node, while the rotational degrees of freedom are free. The disadvantage of this technique is that additional constraints are needed to prevent rotation of the beams around their beam axis. For the idealised wireframe geometry, the master node/slave node technique is used for the joints which connect the end points of the SLE's.

In general, foldable triangulated scissor structures always have a single kinematic degree of freedom. Additional kinematic degrees of freedom can only result from cells consisting of four units or more with parallel or concurrent unit lines, or from adding sliders or hinges to the structure (Roovers, 2017).

On the beam elements, material and section properties have to be applied. Rectangular cross-sections of 9 by 9 mm are used because they are easier to assemble than round cross-sections. The material considered is aluminium with a Young's Modulus of 70 GPa, a Poisson ratio of 0.35 and a density of 2700 kg/m^3. The elements which exhibit intended bending are considered to be HDPE (high-density polyethylene) with a Young's Modulus of 0.8 GPa, a Poisson ratio of 0.4 and a density of 940 kg/m^3. This material and cross-section has been chosen according to Gantes (1991).

The simplest possible method of deployment was used, which means that the lower centre node is considered fully supported, while the upper centre node is subjected to a vertical concentrated load (Figure 2.5 left). No gravity is applied for this initial analysis. Also a different set of forces is used later in this chapter, that is four horizontal loads at the upper corner points while the lower corner nodes are fixed in the vertical direction. These methods of deployment offer the advantage of having symmetry for a perfect structure, so only one fourth of the structure needs to be discretized using finite elements (Figure 2.5 right).

The deployed configuration is used as the initial state because in the folded ideal configuration, all nodes lie theoretically on a straight line and a small deformation has to take place before the structure can carry any loads.

Special attention has been paid to the boundary conditions at the intersection of the

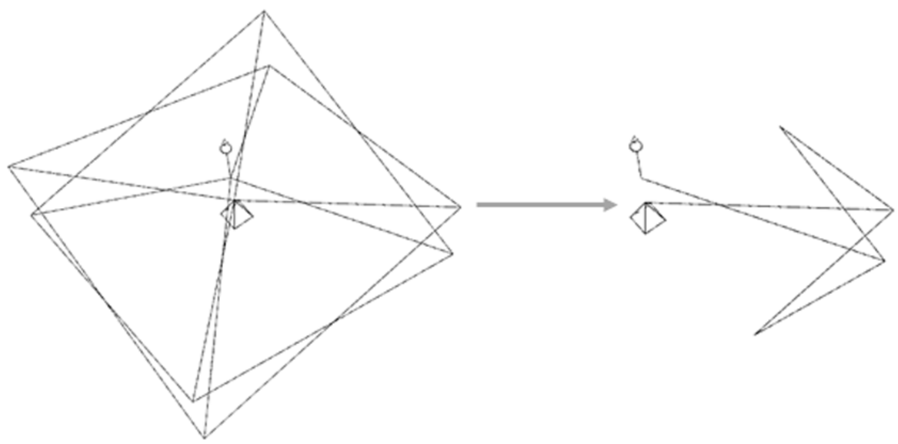

Figure 2.5: The method of folding of the flat square module (left) and one fourth of the module (right).

structure with the symmetry axes, so that the symmetry conditions would not be violated (Figure 2.6). At the same time, the assumption of equal radial displacements of upper and lower circumferential nodes was adopted and all nodes were only free to translate radially and vertically by using constraint equations, which reduces the number of degrees of freedom for the problem. This assumption has been made because of the hypothesis that the module is part of a bigger structure and by consequence connected to other modules (Gantes, 1991).

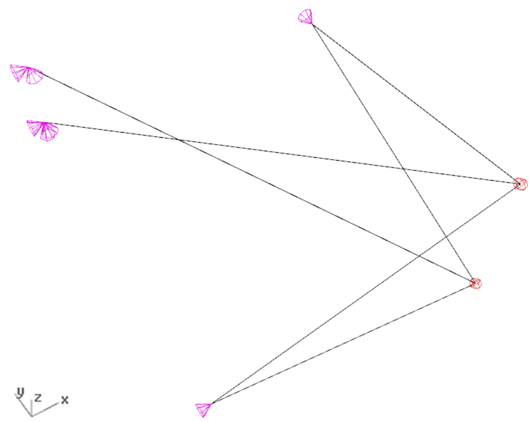

Figure 2.6: Boundary conditions for one fourth of the module. In purple, the fixed translations are shown. In red, the constraints are shown.

The modified Riks algorithm, which is called a path-following technique (Massart, 2016), has been used in the analyses (Crisfield, 1996a, 1996b), of which there is a version in Abaqus. The modified Riks method is an arc-length control algorithm that allows effective solution in cases where the load and/or the displacement may decrease during periods of the response as the solution evolves, which is the case in snap-through problems.

The snap-through behaviour of the beams of the inner scissor-like elements can be identified as a combination of in-plane bending and out-of-plane buckling (Gantes, 1991). Using the 'perfect' geometry, only the in-plane bending is represented. The out-of-plane buckling (Figure 2.7) cannot be represented with the 'perfect' geometry used for the initial analyses, because bifurcation points are not detected. Bifurcation points are points as from which several solutions exist to obtain equilibrium (e.g. buckling). At least two equilibrium paths exist in these points. Without perturbation, the fundamental path is obtained. Alternative paths can be obtained by perturbation (Massart, 2016). To analyse the problem, taking into account out-of-plane buckling, it must be turned into a problem with continuous response instead of bifurcation.

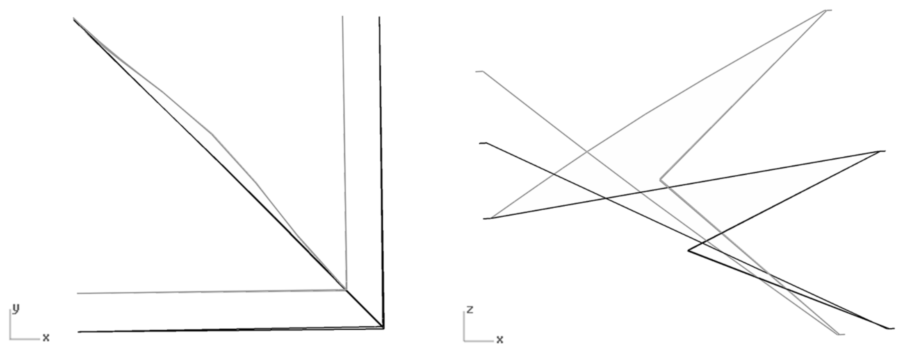

Figure 2.7: Initial configuration of one fourth on a module and in-plane bending (left) and out-of-plane buckling (right) of the inner SLE's during deployment.

This effect was accomplished by introducing an initial imperfection into the 'perfect' geometry (Dassault Systèmes Simulia Corp., 2012c). A linearised buckling analysis of the structure in its deployed state was carried out and its first buckling modes were obtained. Imperfections consisting of multiple superimposed buckling modes, multiplied by a very small scaling factor, were introduced as perturbations in the initial node positions.

2.1.2 Modelling deployment

The important information to consider during deployment is the following:

- The maximum required deployment load should be limited, to achieve the desired flexibility during deployment.
- The snap-through magnitude should be limited, to ensure safety throughout the deployment process.
- The maximum negative deployment load should be high enough, to make sure that the structure in the folded configuration does not move back to the unfolded configuration under its own weight.
- The stresses inside the beams should be limited, to ensure elastic material behaviour.

After performing the analysis, a load-displacement curve (Figure 2.8) is obtained, which describes the variation of the required external load as the structure folds. It has been verified that the snap-through process is reversible. By consequence, the polygonal module exhibits the same structural response during erection and folding under the simplifying assumptions used here (Figure 2.8).

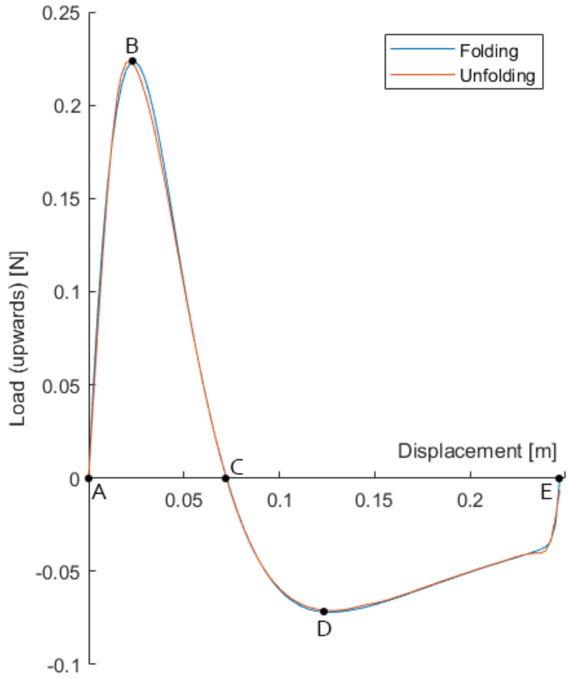

Figure 2.8: Comparison of load-displacement curves for unfolding and folding.

Point A in Figure 2.8 corresponds to the deployed configuration, which is given in Figure 2.9 and is assumed stress-free. When starting to fold the structure, first a vertical load has to be applied on the upper point in the middle of the module in the positive z-direction. In between point A and B, this force increases a lot, while the structure only folds slightly. This is due to the beams in the inner scissor-like elements, which first have to start bending before the structure can be folded.

Starting from point B, where the maximum folding load is required, the snap-through behaviour can be observed which corresponds to a negative slope of the graph. The load required for folding decreases drastically until the structure arrives at an equilibrium without any load applied at point C. This situation is unstable, which means that no force is needed to keep the structure exactly in this position (i.e. point C) of the folding, but the smallest perturbation is enough to cause the structure to move away from this point. The instability points are due to the fact that the second order variation of work is negative ($d^2W = dF.dq < 0$). Physically, the equilibrium positions from B to D are unstable because in these configurations, there is bending inside the beams of the inner scissor-like elements, which means that the stresses inside the beams are not zero.

The required folding load decreases below zero until the maximum negative force is required at point D. A negative force means that a load is required in the negative z-direction to keep the structure in the corresponding position. If there is no force applied in the negative z-direction, the structure will 'snap' until it reaches again a stable equilibrium state at point E. In between point D and E, the magnitude of the negative required folding load decreases because the beams in the inner scissor-like elements become straight again.

Point E corresponds to an equilibrium state of the structure under zero load, which can thus be considered as the folded configuration. In this case however, this state does not

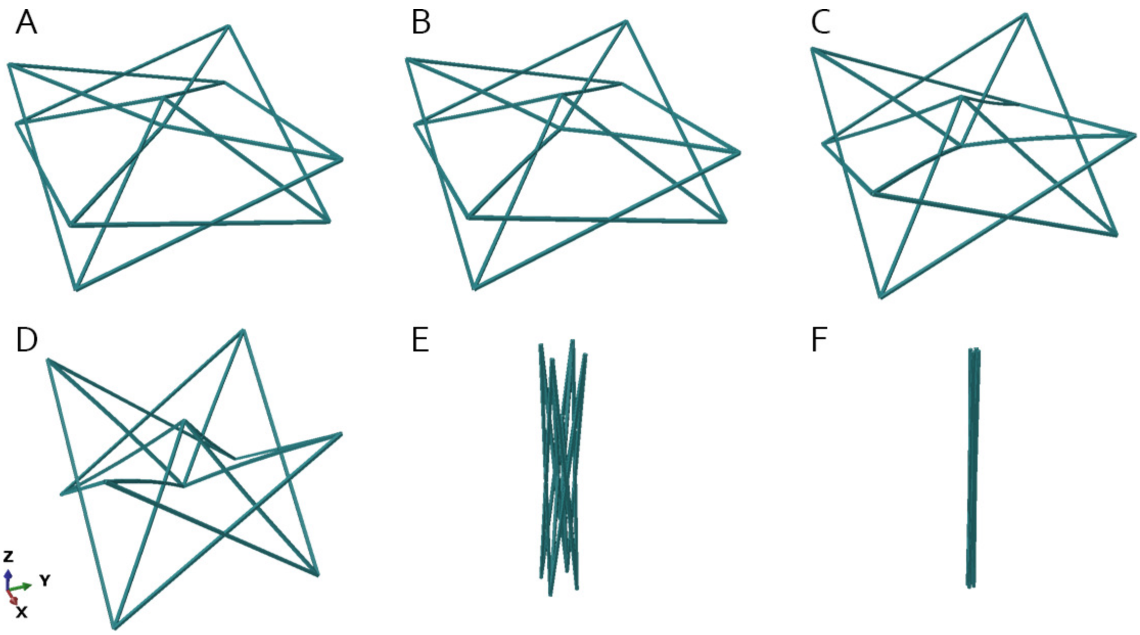

Figure 2.9: Deformed configurations corresponding to the points highlighted in Figure 2.8.

correspond to the theoretically folded configuration for a wireframe model (in which the beams are all geometrically located on one line). This phenomenon will be explained in section 2.1.3. If the structure is 'forced' to fold completely on a single line (configuration F in Figure 2.9), a huge force is required. After point E, the curve thus actually continues vertically.

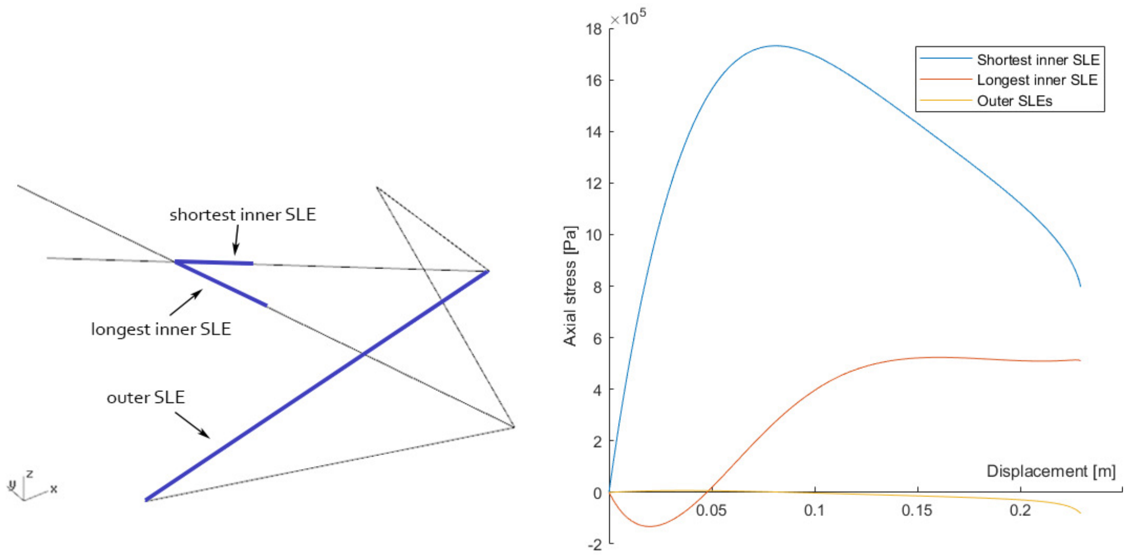

Figure 2.10: Elements for which the axial stress, normal force and bending moment are given (left) and stress variation during folding (right).

Load-displacement curves together with local stress distributions can contribute significantly to the understanding of the snap-through effect. They can then be used to achieve the desired flexibility during folding, for which the forces needed for folding should not be too high. They can also be used to ensure safety throughout the deployment process, for which the snap-through magnitude should not be too high for the operator.

Figure 2.10 (right) shows the variation of the axial longitudinal stress in the members of the structure during the folding process. For the outer members, this axial stress is mainly due to compression, while for the inner members, the axial stress is due to both compression and bending. The bending occurs inside the plane of the inner SLE's because there are no imperfections taken into account. The axial stress is displayed for a beam element in the shortest inner SLE, a beam element in the longest inner SLE and a beam element in the outer SLE's (Figure 2.10 left). The stress inside the other beam elements follows the same trend due to the assumption of perfect geometry and symmetry. The snap-through behaviour can be observed in the curve where the stresses inside the beams first increase throughout the transformation phase and then decrease again.

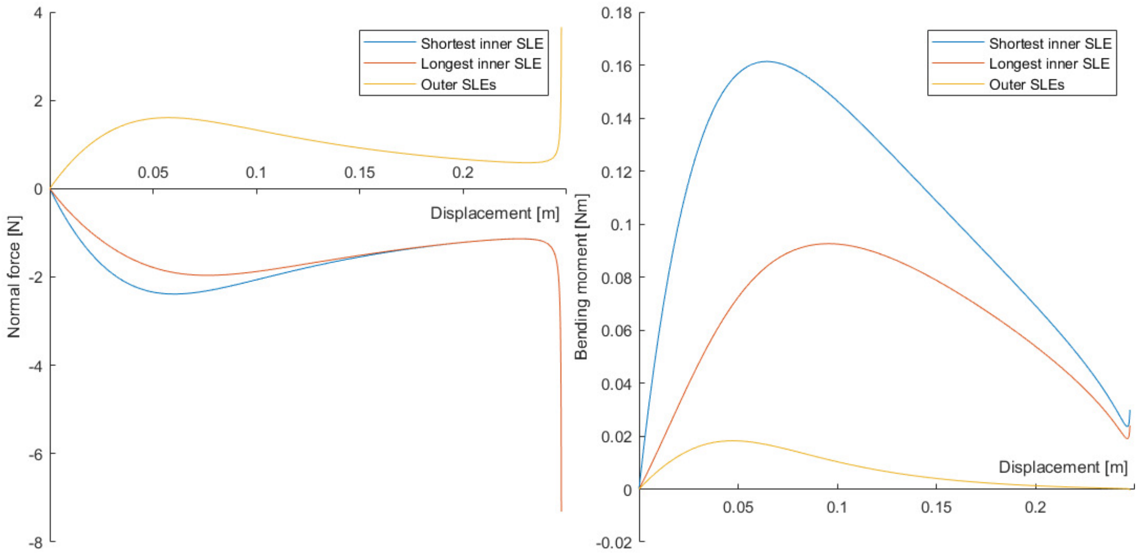

Figure 2.11: Normal force variation (left) and bending moment variation during folding (right).

In Figure 2.11 (left), the variation of the normal force is given. In every element, the normal force first increases and then decreases again until the structure arrives at point E in which the required folding load is zero. After reaching this state, the normal force inside the beams increases tremendously (which will be explained in section 2.1.3). The outer beam elements are in tension during folding, while the inner beam elements are in compression. The magnitude of the normal force is higher for the inner beam elements.

The variation of the bending moment is given in Figure 2.11 (right). The bending moment first increases for all the beams and decreases again until the folded configuration is reached. The highest bending moment occurs in the shortest beam in the inner SLE. Contrary to what was expected, there is also a bending moment in the outer beams although it is small when compared to the bending moment in the inner beams. This bending moment exists to take up a small part of the forces in the inner beams.

In Figure 2.12, the von Mises stress variation during successive folding stages, which is used as a scalar measure of the stress, is displayed in the elements. For the inner beams under bending, this von Mises stress is different in the different fibres of the beams. For metals, a material is said to start yielding when its von Mises stress or equivalent tensile stress reaches a critical value known as the yield strength. For other materials, such as HDPE which is used for the inner elements, this von Mises measure is debatable. In this case, the maximum von Mises stress inside the inner elements is 1.36 MPa, which is way lower than the yield strength of HDPE which is 31.7 MPa. Because the maximum von Mises stress inside the beams is much lower than the yield strength, the use of the von Mises criterion can be justified in this case. The maximum von Mises stress inside the outer elements is only 0.17 MPa, while the yield strength of pure aluminium is between 7 and 11 MPa and of aluminium alloys even between 200 and 600 MPa. Plastic material behaviour is thus avoided in all cases.

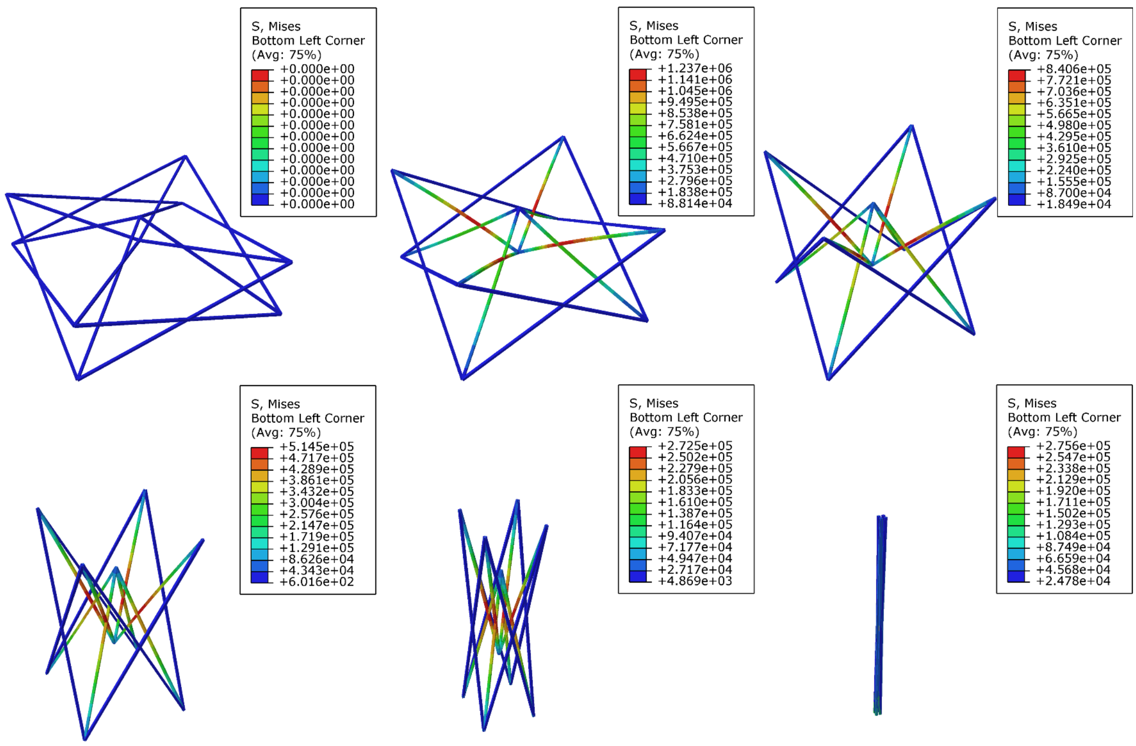

Figure 2.12: Von Mises stress variation during successive folding stages.

2.1.3 Kinematic design versus structural behaviour

In the case presented in Section 2.1.2, the scissor module is incompatible throughout the whole transitional stage. In the ideal situation, the stresses should become zero again in the folded configuration and the required folding load should be zero at the point where the structure is completely folded (i.e. the nodes of the structure are ideally on one line). However, even in this case, in which an idealised structure is investigated without taking imperfections into account, the structure is not completely folded when the required folding load becomes zero again and there are still stresses inside the members, which is actually related to trying to fold the structure using a vertical force on the upper middle point.

In this analysis, a vertical load is again applied on the upper middle node of the structure. When the structure is almost in its folded configuration, a high force will be needed to fold the structure completely, since the driving force is applied in the same direction as the beam axes in the folded configuration. Moreover, the force is applied on the least stiff beams in the structure. Those beams will be deformed during the deployment and they will by then practically lie on a straight line, making it impossible to fold the structure completely. This can be seen in Figure 2.13, which shows that the strain in the outer beams is zero during folding, but on the contrary the strain in the inner beams increases and decreases during folding. In the folded configuration, the strain is still positive, indicating a deformation of these elements at this stage. It could be argued that applying a vertical force on the upper middle point like Gantes did (Gantes, 1991) is not the optimal way to deploy this structure if one wants to implement a stress-free configuration at the end of folding.

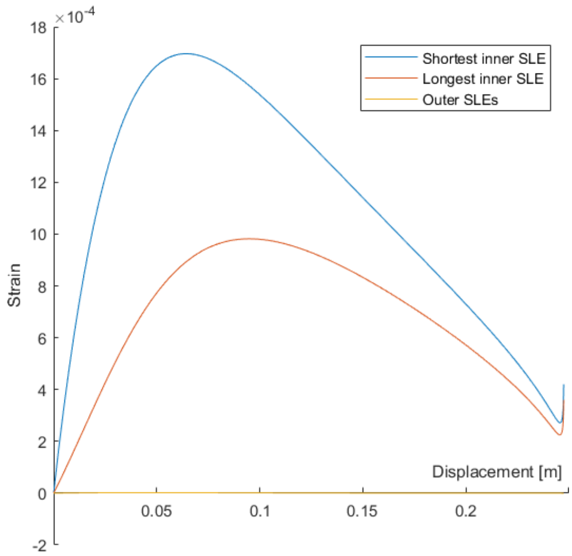

Figure 2.13: Strain variation during folding.

This observation is due to the translation of a kinematic design with rigid elements, in which the geometry is considered without taking statical equilibrium into account, into a structure in which the stiffness and deformability of the beams is taken into account. When a geometry is compatible, it does not directly mean that the structure is stress-free at that compatible state and that no force is required in this state, even when a perfect design geometry is considered, due to the deformation of the structure. It will depend on the relative stiffnesses of the beams in the structure, the boundary conditions and the applied loads. The deployment response is thus not unique for a kinematically designed structure and the kinematic design of compatible configurations furnishes an approximation of the equilibrium configuration obtained using a stress analysis. These compatible configurations can however be approached when an appropriate choice of boundary conditions and applied loads is made.

To support this conclusion, three points were investigated. First, when unfolding a structure from the completely folded configuration, the required folding load is zero in the folded configuration, but then follows almost the same curve as during folding (Figure 2.14). The required folding load is not exactly zero in the unfolded configuration, but it is necessary to remark that an initial imperfection had to be implemented because otherwise the structure would remain in pure compression without deploying. Moreover, real structures cannot be folded on a line anyway. This explains the differences in the load-displacement curve. In the case of folding the structure, the almost vertical line in the folded configuration corresponds to a strain deformation of the beams of the inner SLE's, as can be seen in Figure 3.1 where the strain increases suddenly near the theoretically folded configuration.

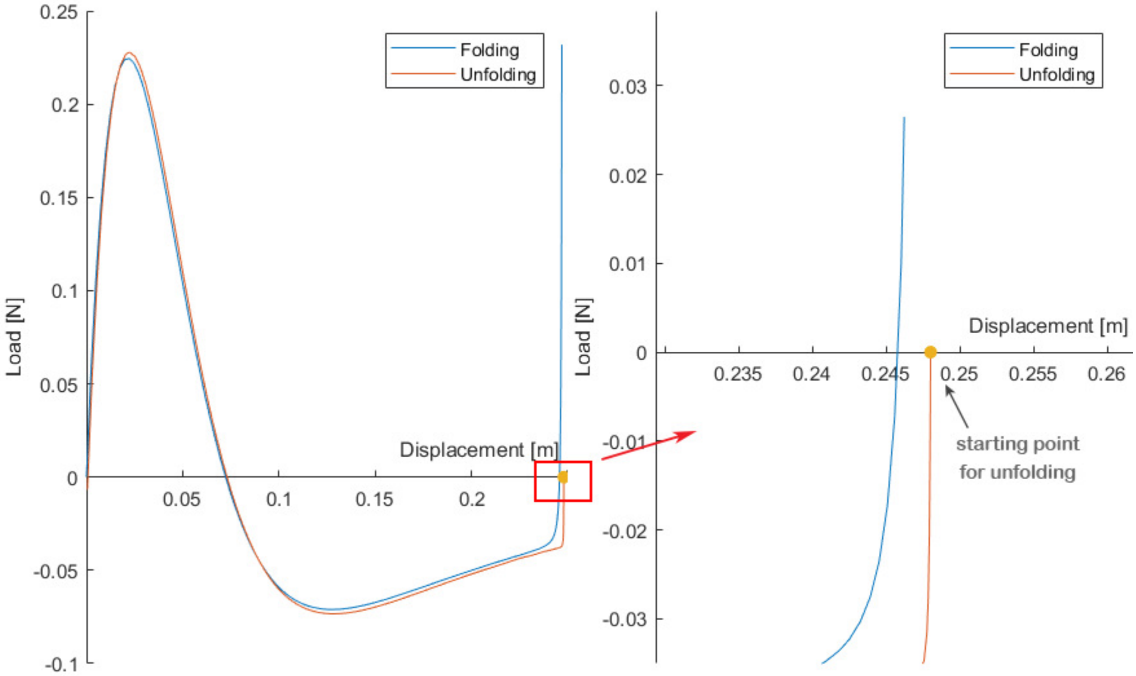

Figure 2.14: Comparison of the load-displacement curves for unfolding and folding (left) and detail of the zero folding forces in the almost folded configuration (right).

Second, when using another set of forces applied at different locations, the deployment behaviour is different (Figure 2.16 left). When pushing horizontally on the corner nodes (Figure 2.15 right), the required folding load is zero when the structure is almost completely folded (Figure 2.16 right). The dot on the figure represents the completely folded configuration (where the nodes lie theoretically on one line). This set of forces yields a more optimal choice regarding the deployment behaviour of the structure. Moreover, when multiple modules are linked, this folding mechanism is more realistic, because it would be practically impossible to fix the lower centre nodes and pull the upper centre nodes of all modules upwards.

In Figure 2.16 (right), the folding force in the case of the horizontal forces at the corner nodes is not zero in the theoretically completely folded configuration as well, although the steep increase of the load near the folded configuration is not as strong as in the case when one vertical load on the central point is used to fold the structure. Using this set of forces, also a small deformation of the inner beam elements takes place during deployment, but it is very limited and thus negligible.

Third, in Figure 2.17, the change of the load-displacement curve is given when increasing the stiffness of the inner beams i.e. reducing their deformation. When increasing the

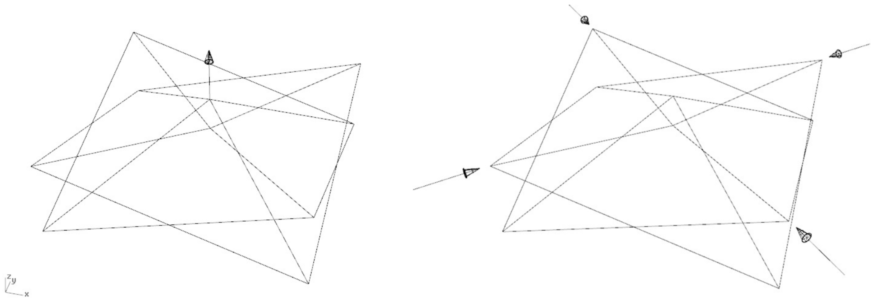

Figure 2.15: Deployment mechanism with one vertical force on the upper centre node (left) and folding mechanism with four horizontal forces on the upper corner nodes (right).

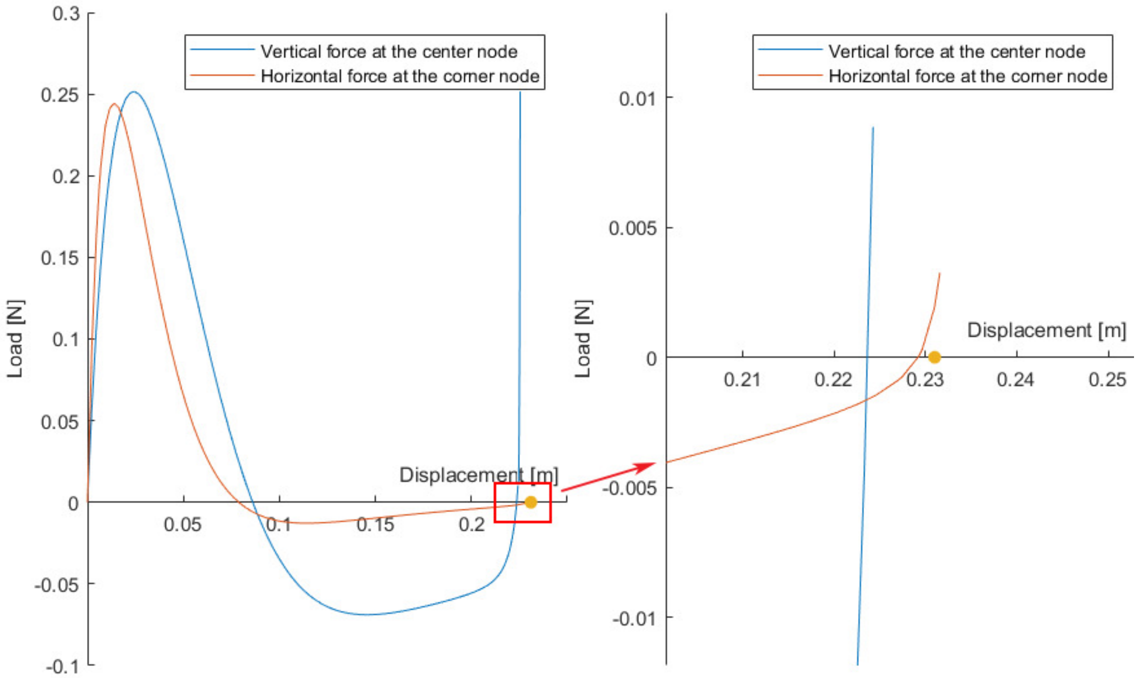

Figure 2.16: Comparison of the load-displacement curves when one vertical force is applied and when four horizontal forces are applied (left) and detail of the zero folding forces in the almost folded configuration (right).

stiffness of the inner elements from 0.5 to 1.5 times the stiffness of HDPE in steps of 0.1, the folded configuration, corresponding to a required folding load which is zero, is a little bit closer to the completely folded configuration, but this variation is so small that it can be neglected.

These three points were investigated to support the conclusion that the deployment response is not unique for a kinematically designed structure and that the kinematic design of compatible configurations furnishes an approximation of the equilibrium configuration obtained using a stress analysis. The three tests show that the relative stiffness of the beams matters, which was to be expected, and they explain the unexpected mismatch with the assumed zero force configuration in the kinematic design.

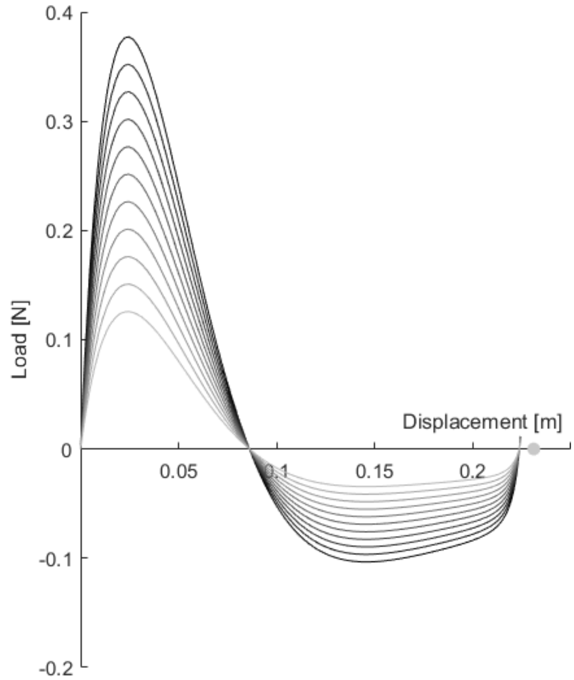

Figure 2.17: Change of the load-displacement curve when the stiffness of the inner beams is altered.

2.2 Parametric study of the design parameters

The designer first has to select the geometry of the structure and the appropriate member properties, and then use numerical models to analyse the structure and evaluate its performance. The design process is intrinsically iterative, due to the interactions between geometric and other design variables on one hand, and the structural behaviour on the other hand. Knowing how the critical structural response quantities are influenced by changes in the main design parameters can be a valuable tool for the structural designer. This is where parametric studies can prove to be very useful (Gantes, 1991; Gantes, Connor, Logcher & Rosenfeld, 1989).

There are two types of design parameters considered. One type consists of the parameters concerning the module geometry, while the other design parameters are related to the stiffness of the structure. The main design parameters of the bistable module of section 2.1 are on the one hand the height of the point in the middle and the height to width ratio of the module which are related to the module geometry, and on the other hand the modulus of elasticity of the beams, the height to width ratio of the cross-section of the beams and the slenderness of the beams which are related to the stiffness of the structure. When altering the geometry of the module, it is expected that the required folding load will change. When making the structure stiffer, it is expected that the required folding load will increase. The quantities of interests studied here are the maximum folding load and the maximum normal stress in the members of inner SLE's (since the stresses in outer SLE's are much smaller).

The geometry of the module can be completely designed in the deployed configuration by knowing the height of the point in the middle of the module for a certain width of the module and by knowing the height to width ratio of the module. That is why these two parameters were chosen. To characterise the stiffness, the modulus of elasticity, the cross-section of the beams and the height to width ratio of the cross-sections are chosen. A higher modulus of elasticity or a larger cross-section will stiffen the structure, while a different height to width ratio of the cross-sections will allow the beams to bend more easily in-plane or out-of-plane of the SLE.

The analyses again represent the folding of one fourth of the structure, with the lower centre node considered fully supported, while the upper centre node is subjected to a vertical concentrated load. Although it was shown that this folding mechanism is a suboptimal case, the trends when changing the design parameters will be the same regardless of the used folding mechanism.

The required peak load and the maximum axial stresses inside the beams during folding are normalised with respect to the previously considered idealised model, to investigate the global trends without taking into account the actual values.

2.2.1 Height to width ratio of the module

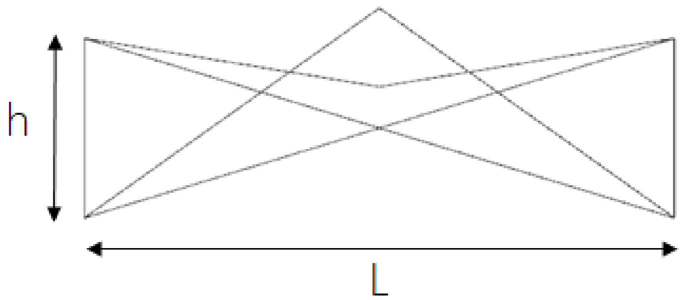

Figure 2.18: The height and the length of the module (side view).

If the height h of the structure decreases while the width L of the module remains the same, there is a stronger snap-through effect and a higher load is required for folding, while the opposite occurs when the height to width ratio of the module increases (Figure 2.19).

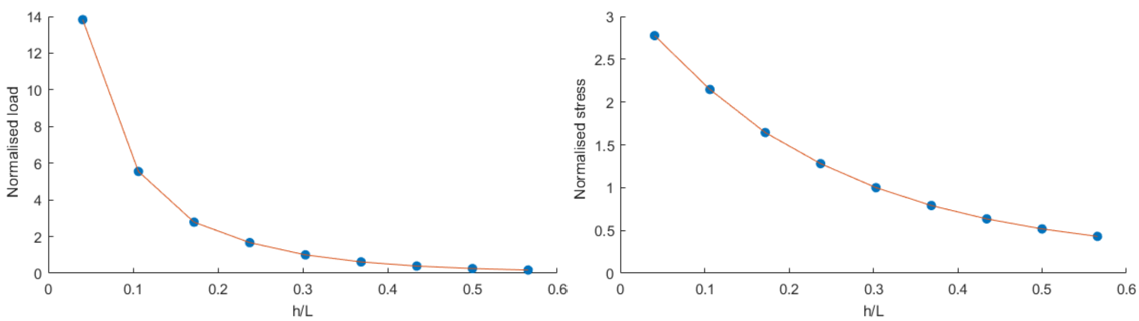

Figure 2.19: Influence of the height to width ratio $\frac{h}{L}$ of the module on the maximum folding load (left) and maximum axial stress (right).

According to Gantes (Gantes, 1991), there is a kind of threshold value of $\frac{h}{L}$ which is critical for the deployment process. For smaller values, the load required for folding increases tremendously. This can be seen in Figure 2.19 (left), where the required folding load for the lowest height to width ratio is almost three times the load of its neighbouring point. The threshold value for the height to width ratio of the module is in this case approximately 0.1. The height to width ratio of the module should thus always be higher than this threshold value. The design of a bistable scissor module will depend on architectural requirements and this 'threshold value'. The chosen value should however be in the neighbourhood of this threshold value, to limit the height to width ratio which is desired architecturally and to limit the folding force.

2.2.2 Height of the point in the middle

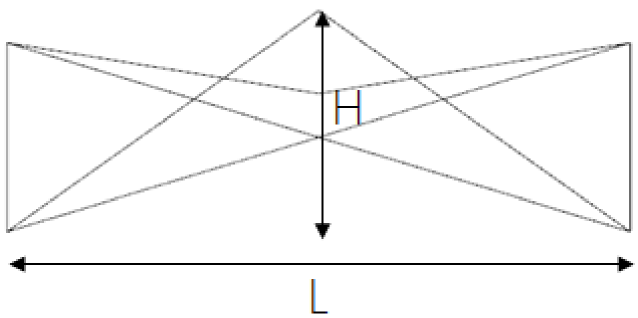

Figure 2.20: The height of the point in the middle and the length of the module (side view).

The next factor investigated is the height of the highest point in the middle of the module, which is a characteristic quantity of the geometry of the module. In most cases, the height should be limited, to have a reasonably small height to width ratio of the module (Gantes, 1991), but it can also be desired by architects to have the middle point higher to alter the required folding load to have a stronger snap-through effect or just to make a pleasing structure. The folding load increases substantially from being 0 (where theoretically the structure behaves like a mechanism) as the height of the point increases (Figure 2.21). To investigate this phenomenon, the ratio $\frac{H}{L}$ is used, with H the height of the upper point in the middle of the module and L the length of the module.

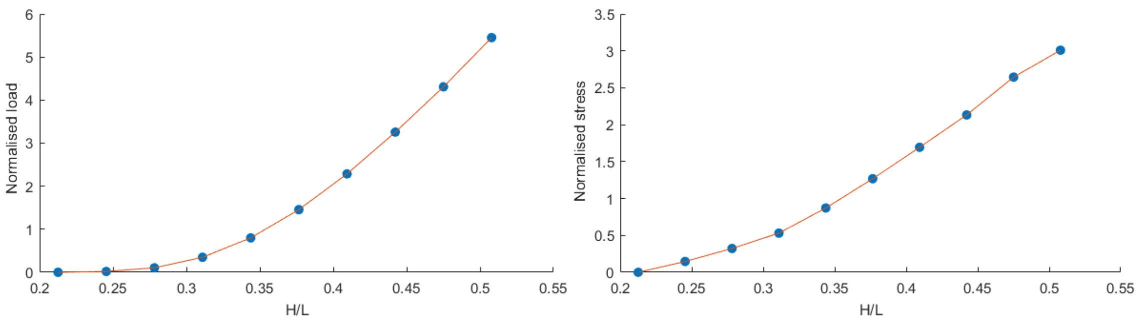

Figure 2.21: Influence of the ratio $\frac{H}{L}$ on the maximum folding load (left) and maximum axial stress (right).

2.2.3 Stiffness of the beams

The next design parameter is the stiffness of the beams of outer and inner SLE's. The influence of the Young's modulus of outer SLE's on the folding load is not very significant (Figure 2.22 left), while an increase of the Young's modulus of inner SLE's results in a linearly proportional stiffening of the response (Figure 2.22 right). This behaviour was expected, since the outer beam elements almost do not bend during the deployment while the inner beam elements do. Yet the outer beam elements are compressed during deployment, which explains the small increase in the required folding force, however their contribution to the folding force is low. Increasing the Young's modulus of the inner SLE's corresponds to making the bending more difficult, which means that the required folding force will also increase.

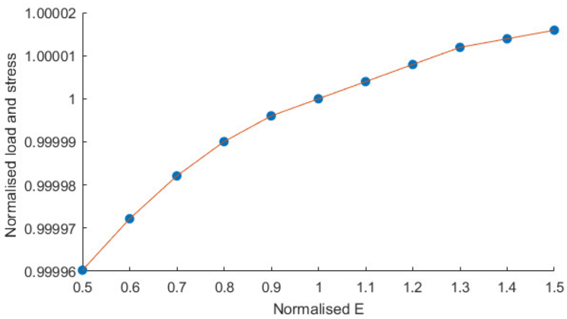

Figure 2.22: Influence of E of outer SLE's (left) and inner SLE's (right) on the maximum folding load and maximum axial stress.

2.2.4 Height to width ratio of the cross-section of the beams

The height to width ratio of the cross-section of the beams is studied in the range from 0.5 to 5, to investigate the effect of this height to width ratio of the cross-sections, but also to investigate when the influence of buckling out of the plane of the SLE becomes important by comparing the behaviour of the idealised structure with a structure with imperfections.

The height to width ratio of the cross-section of the elements in the outer SLE's doesn't have any influence on the snap-through behaviour of the structure. In contrast, the height to width ratio of the cross-sections of the elements in the inner SLE's has a strong influence on the in-plane bending and out-of-plane buckling (Figure 2.23). Without perturbations in the initial node positions (following the fundamental path), only in-plane bending is taken into account. By consequence, a larger height to width ratio leads to a higher force required for folding.

When taking perturbations in the initial node positions into account (i.e. taking the alternative bifurcated path in case of bifurcation), the same trend can be observed, because the influence of the out-of-plane imperfections is small (Gantes, 1991). However, the larger the height to width ratio, the more important the out-of-plane buckling becomes. Perturbations in the initial node positions to obtain out-of-plane buckling as well as in-plane bending should only be taken into account for very large height to width

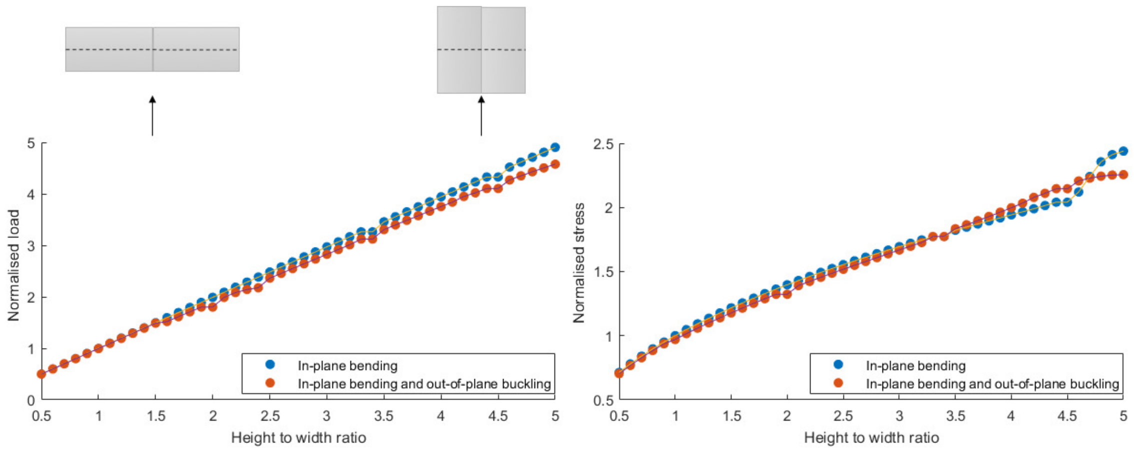

Figure 2.23: Influence of the height to width ratio of the cross-section of inner SLE's on the maximum folding load (left) and maximum axial stress (right).

ratios. It is expected that the out-of-plane buckling will be more important when the stiffness of the hinges is taken into account.

On the one hand, because beams with a smaller height to width ratio accommodate better the bending, such beams seem more appropriate for this module. On the other hand, beams with a larger height to width ratio are easier to assemble. It can be concluded that square cross-sections would be structurally and practically the best choice.

2.2.5 Slenderness of the beams

As was the case with the modulus of elasticity, the cross-sectional area of outer SLE's is of almost no importance for the deployment response (Figure 2.24), while larger cross-sections of inner SLE's stiffen the response (Figure 2.25). Very similar is the influence of the height to width ratio of the cross-sections which is a measure of their bending resistance.

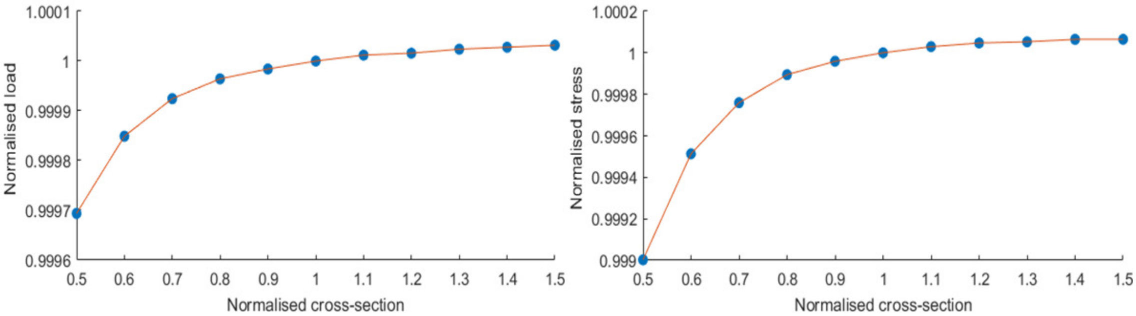

Figure 2.24: Influence of the cross-section of outer SLE's on the maximum folding load (left) and maximum axial stress (right).

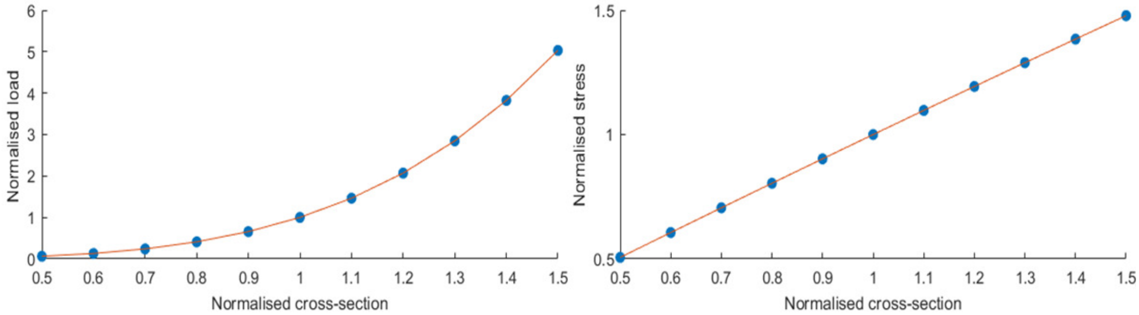

Figure 2.25: Influence of the cross-section of inner SLE's on the maximum folding load (left) and maximum axial stress (right).

2.3 Gravity

The loads required for folding are lower than in reality, which is mainly due to the lack of modelling the gravity in this model. Gravity should be applied on the structure, since it is always present in civil engineering. Gravity is a force that can benefit the deployment process or that has to be overcome by the force required for deployment. Figure 2.26 shows that gravity can have a huge influence on the force needed for the folding of the structure.

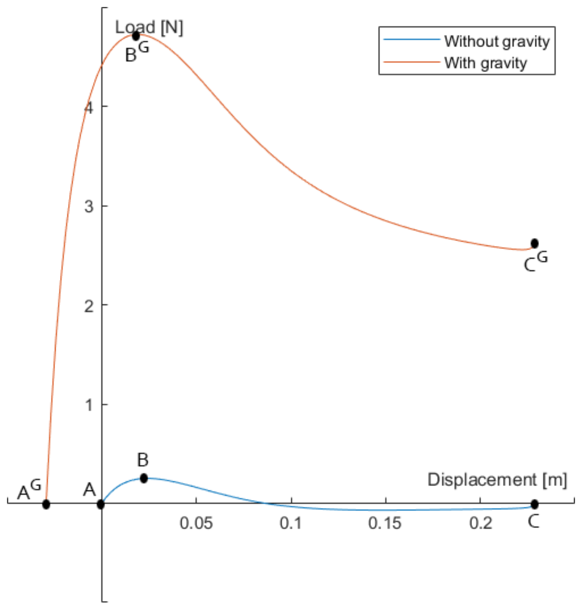

Figure 2.26: Influence of gravity on the folding process.

Point A in Figure 2.26 corresponds to the deployed configuration. When applying gravity, there is an initial deformation of the structure in its deployed state due to the used boundary conditions and materials. That is the reason why the load-displacement curve starts in point A^G at a negative displacement of the upper centre node. This deformation can be seen in Figure 2.27 (left).

For the configuration for which the required folding load is maximum (Figure 2.27 middle) and for the folded configuration (Figure 2.27 right), the difference of the deformed structures is much smaller. This can be explained by B and B^G which occur at the same displacement (Figure 2.26), as is also the case for C and C^G. However, because of the boundary conditions (the fixed lower centre node) and the applied force (the vertical force on the upper centre node), the gravity deforms the structure by pulling the outer beam elements, which are made in aluminium, down.

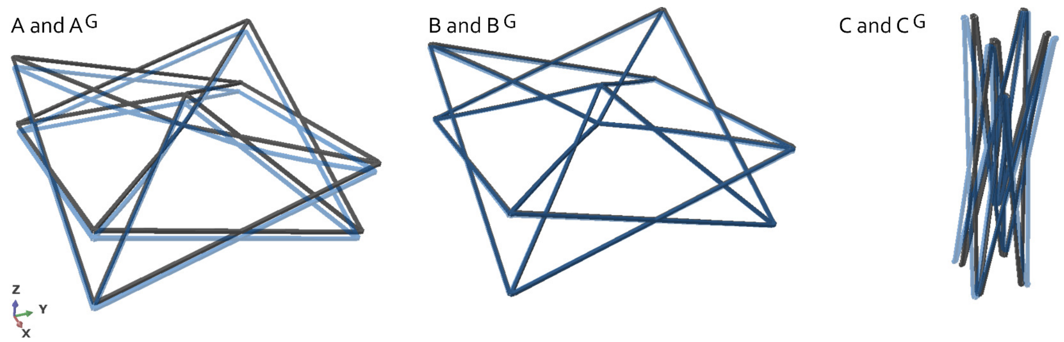

Figure 2.27: Comparison of the deployed configuration (left), the configuration for which the required folding load is maximum (middle) and the folded configuration (right) during the folding process for the analyses with (blue) and without gravity (black).

With gravity, the load required to fold the structure is increased. The force needed to fold the structure is now positive during the whole transitional stage, but there is still a snap-through effect for displacements at which the slope of the curve in Figure 2.26 is negative. In this example, when the required load in the folded configuration is still positive, the structure would move back to the unfolded configuration under its own weight when the load would be released. This means that if the structure has to be folded, the beams have to be kept together or the structure has to be laid down horizontally.

Because the considered structure and its corresponding required folding forces are very small, the influence of the gravity is huge. It is a question of finding the right balance between them. Also, because the considered structure is rather flexible in the deployed configuration due to the choice of the materials and because of the lack of additional stiffening elements, there is a considerable initial deformation of the structure due to the gravity load. The influence of the gravity will largely depend on the dimensions of the structure and the elements, the materials and where the loads are applied. When the force required to fold the structure is higher, the influence of the gravity on the load-displacement curve will be relatively smaller. In this particular case, the peak force is 19 times higher.

When the gravity is applied horizontally, meaning that the orientation of the structure is different during folding, the influence of the gravity is reduced tremendously and the peak force is only 1.25 times higher (Figure 2.28). In this case, the required folding force is not positive any more during the whole transitional stage, which means that the structure will not move back to the unfolded configuration when the load is released. Applying the gravity horizontally on a module corresponds for example to a flat multi-module structure which is used as a wall, or to modules in complex structures which are more horizontal (see Chapter 5).

So far the deployed configuration is used as the initial state to do the analyses, because the geometry is designed in the deployed configuration and because all nodes lie

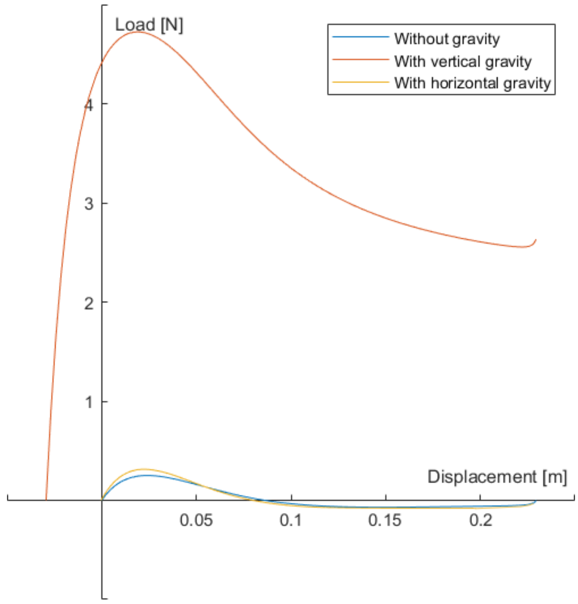

Figure 2.28: Comparison of the influence of vertical and horizontal gravity on the folding process.

theoretically on a straight line in the folded configuration. It is thus very difficult to make a computational model which starts from the folded configuration. Nevertheless, it is important to verify the structural response during unfolding, because the deployment process might not be reversible, in the sense that both the deployment and folding curves are the same, when considering all aspects of the deployment. The structural response during unfolding is modelled in Abaqus as a restart job, starting from the deformed geometry after doing the analysis of the folding.

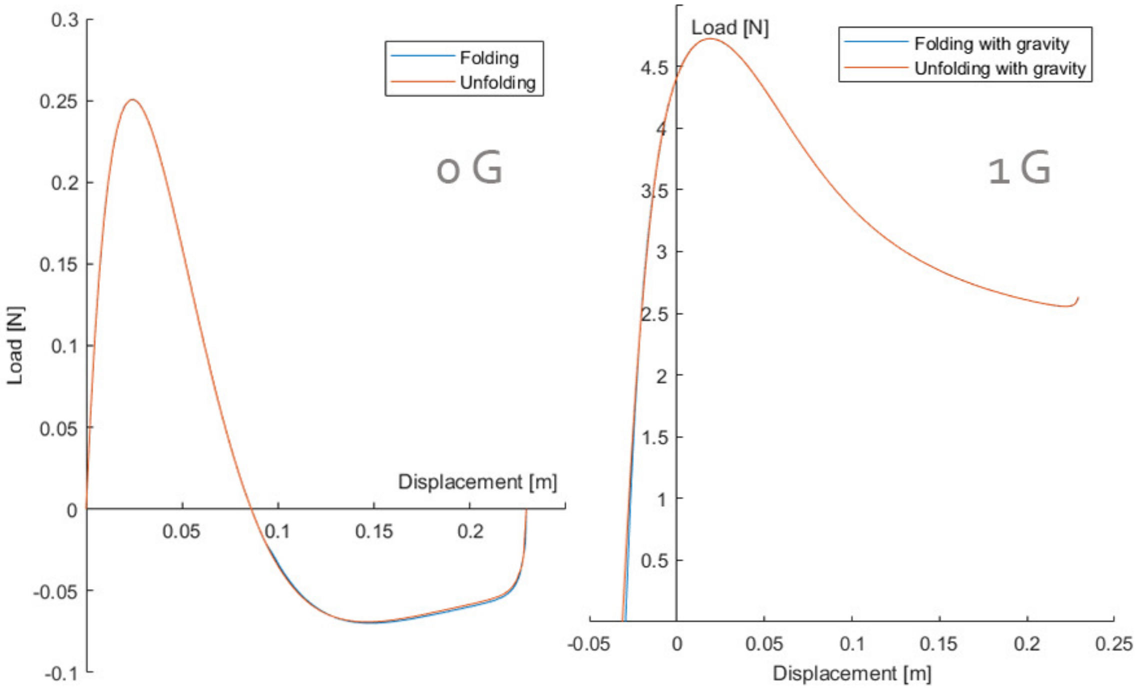

Figure 2.29: Load-displacement curve during folding and unfolding for the simplified model.

Figure 2.29 (right) shows that the folding and unfolding process of a bistable scissor structure is still reversible when considering gravity. During folding the gravity has to be overcome by the force needed for folding, meaning that the required folding force is higher, while during unfolding the gravity benefits the deployment process, with the given orientation of the module.

Gantes tested a curved pentagonal module (Figure 2.30), made of plastic (high density polyethylene). Its folding process was tested in order to obtain its load-displacement curve. Gantes referred to the module as a medium scale module, because the length of one side of the pentagon is only 46 cm and the cross-section of the beams is 6.35x12.7 mm. In the experimental set-up, the lower centre node was fixed, while the upper centre node was attached to the loading piston. A displacement controlled test was carried out. Only approximately the first 80% of the process could be completed due to limitations in the maximum possible deformation of the loading piston (Gantes, 1991).

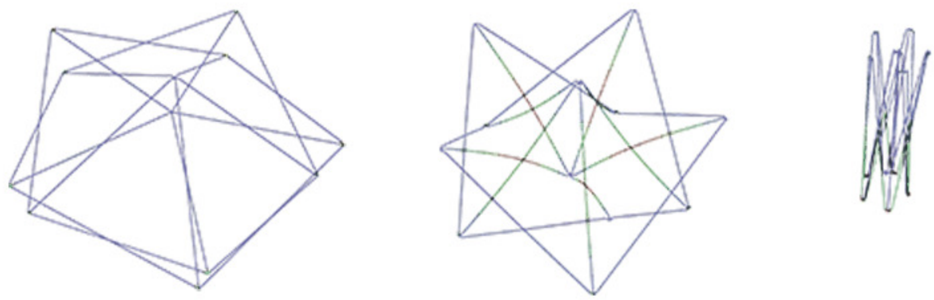

Figure 2.30: Successive folding stages of a curved pentagonal module.

For this analysis, to have comparable results, the finite joint size was also modelled, which will be explained in Chapter 3. Because the exact dimensions of the module and the joints are not known, there are some differences between the curve without gravity (Figure 2.31 right) and Gantes's curve with discrete joints (Figure 2.31 left). This can be due to small differences in the computational model and probably the dimensions of the joints in the experimental model were a bit larger.

The influence of the gravity on this pentagonal module is not as important as it was on the previously investigated square module (Figure 2.26) because the present module is smaller and fully made of plastic, and the snap-through contribution to deploy the structure is of similar magnitude. While Gantes explained the difference between the idealised curve and the experimental data as being the influence of friction at the joints (disregarding gravity completely), a fair agreement is reached here merely considering gravity.

The remaining slight difference between the experimental curve and the curve with gravity obtained in this work can probably be explained by neglecting friction in the computations. This aspect is investigated in Chapter 3 when taking imperfections into account.

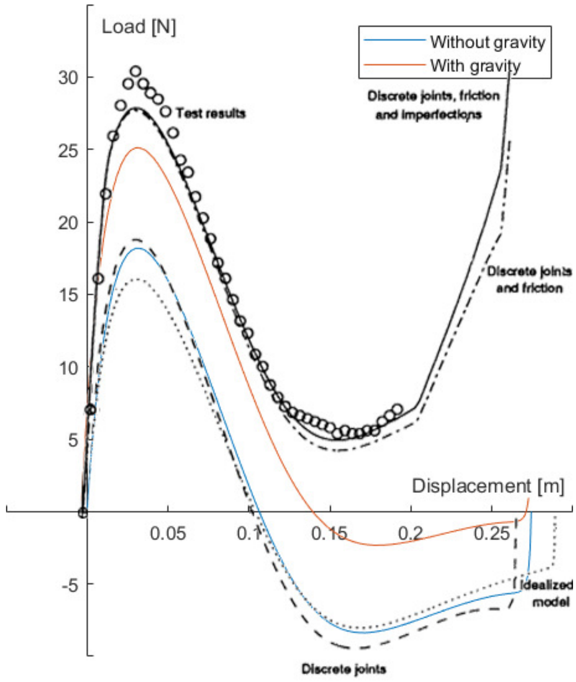

Figure 2.31: Comparison of the idealised model with discrete joint dimensions and the model with gravity with the experimental and numerical load-displacement curves according to Gantes.

2.4 Discussion

A model has been derived that can be used to explore the intensity of the snap-through phenomenon of bistable scissor structures. An initial simplified idealised single square polygonal module was analysed (i.e. corresponding to the design wireframe geometry), which indicated the snap-through effect, but ignores important factors such as joint size and imperfections. The load-displacement curve and the variation of the stress, normal force and bending moment during folding were obtained. The model has been extended to include curved spherical structures as well, for which the type of response is qualitatively the same.

It was observed that when a geometry is kinematically compatible, it does not directly mean that the structure is stress-free exactly at that compatible state and that no force is required in this state. This is due to the problem of translating a kinematic design with rigid elements, in which the geometry is considered without taking statical equilibrium into account, into a structure in which the relative stiffness of the beams is considered. Compatible configurations can be approached by using an appropriate choice of boundary conditions and applied loads.

A parameter study was carried out to give the designer some general guidelines on how to influence the structural response by changing the main design parameters. The main design parameters are related to the module geometry and the stiffness of the elements.

Gravity is included in the computational model because it is always present in civil engineering applications. It has a considerable influence on the load-displacement curve, which will depend on the module geometry and the stiffness of the elements, and should thus certainly be included during the design phase. It has been verified that the snap-through response is reversible, in the sense that the curves for deployment and folding are the same, when an idealised structure is modelled and when gravity is taken into account.

The computational model was verified by comparing the results to the computational and experimental data of Gantes (Gantes, 1991). To do this, a curved pentagonal module was modelled. The results were accurate, bearing in mind that not all dimensions and material characteristics were known exactly. Although the friction in the model of Gantes was used to fit the experimental deployment behaviour, a fair agreement is reached here merely considering gravity.

The initial simplified analysis indicates the snap-through type of behaviour for the structure. However, because an idealised wireframe geometry was used, the obtained results will underestimate the required folding load, because the hinges will stiffen the response when their finite size is considered. Also geometrical imperfections on the beam length, on the position of the pivot point or on the hinge alignment, can alter the folding behaviour. Their influence should be investigated, because imperfections unavoidably take place due to manufacturing defects. Also non perfect hinge behaviour (finite hinge stiffness and friction) should be investigated. When taking all these imperfections into account, the result will be more trustworthy.

Chapter 3

Taking Manufacturing Imperfections into Account on a Single Bistable 3D module

Manufacturing defects are naturally present in all engineered structures. These, together with imperfect hinge behaviour (friction) need thus to be investigated. They are expected to lead to stresses inside the scissor structures and to structures that cannot be entirely folded (Dupont, 2014). Two types of imperfections were identified and are considered in this work, geometrical imperfections (finite hinge size, tolerances on the beam lengths, eccentricity of the pivot points and hinge misalignment) and imperfect hinge behaviour (finite hinge stiffness and friction).

Acceptable tolerances on the position of the centre hole in the beam, which is the point of the hinged connection, and on beam lengths are characterized. Frictional effects that prevent the relative rotation of the beams naturally occur. Their influence on the deployment is quantified. The axis of rotation of the hinges might not coincide with its theoretical direction and in reality, joints have a finite stiffness (i.e. not fully rigid in the constrained direction).

The objective of this chapter is to understand the influence of those imperfections, to identify the most dominant ones and to characterize an acceptable range of geometric tolerances. This range will be based on the maximum folding force, which is a measure of the force that will be needed to fold the structure, the snap-through magnitude, which is a measure of the safety of the folding process, the minimum force required for folding, which will be important when gravity is taken into account and the compactness of the structure in the folded configuration, because the structure should be as compact as possible for storage and transport. This information can be systematically extracted from the load-displacement curve for each simulation. By comparing those curves, the influence of the imperfections can be expressed.

The analyses will be carried out on the idealised model with finite joint dimensions (explained in 3.1.1), while implementing these two classes of imperfections, but not taking gravity into account, because the influence of gravity on the deployment process will always be the same. The complete module will be analysed, because the symmetry of the module is broken when applying imperfections. Again, the initial state is the deployed configuration, because scissor structures are designed and built in this configuration. This means that the structure in the folded state will not be completely folded and stress-free. Including imperfections will make the compactness in the folded state worse.

3.1 Geometrical imperfections

3.1.1 finite hinge size

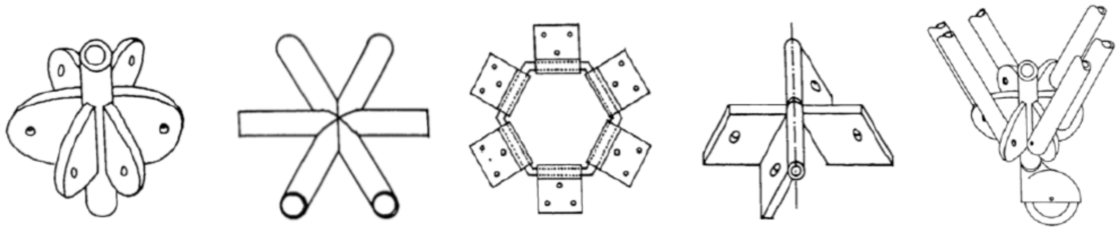

Figure 3.1: Some examples of joints proposed by Escrig (Escrig, 1985).

Crucial to any deployable structure are the joints. In reality, the members and the joints have discrete dimensions, unlike the theoretical geometric line models which have zero thickness. The size of the joint is influenced by the beams it has to connect. The wider the section and the higher the number of beams coming together in one joint, the larger the size of the joint must be, in order to accommodate all elements without interference during deployment (Alegria Mira, 2010). Escrig (1985) proposed some particular solutions for joints (Figure 3.1).

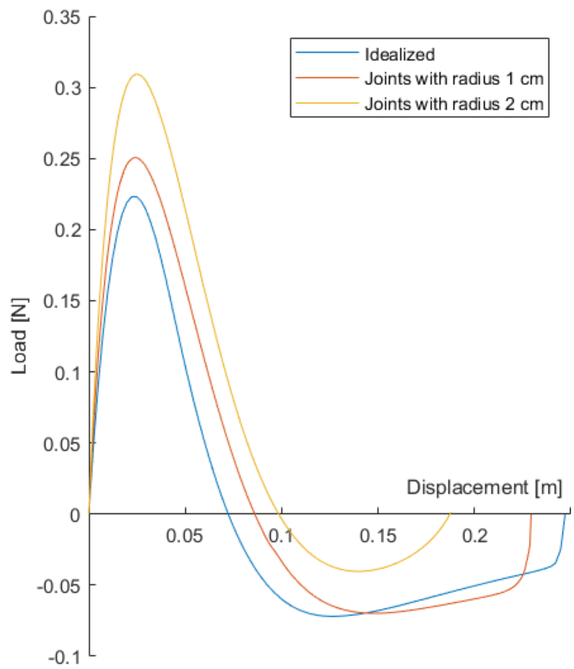

Figure 3.2: Influence of discrete joint size on the load-displacement curve.

The behaviour of deployable structures is very sensitive to member lengths. Hence, the inclusion of the discrete joint dimensions in the numerical model is necessary for an accurate simulation (Gantes, 2001). The hinges are modelled as a stiff grid composed of short beam elements. This stiff grid can represent every type of hinge that can be used for physical models. The connector type hinge in Abaqus is used to model the joints between the beams of the scissor-like elements and the hinges.

Another possible approach is to not draw the joints in the finite element model and to constrain the ends of the members to move simultaneously. This way of modelling reduces the computational time, but the real behaviour of the structure is represented less accurately and the rotation of the beams around the beam axis should be restricted to avoid a non-positive definite stiffness matrix.

Including the discrete joint dimensions in the numerical model has an overall stiffening effect (Figure 3.2). This effect is larger when the dimensions of the joints are larger because larger joints lead to shorter beams. This is related to the fact that the geometry is not perfect any more due to the rotation axes, that were initially in one point, which moved when including the joint dimensions. The final finite element mesh for this initial finite element model is shown in Figure 3.3.

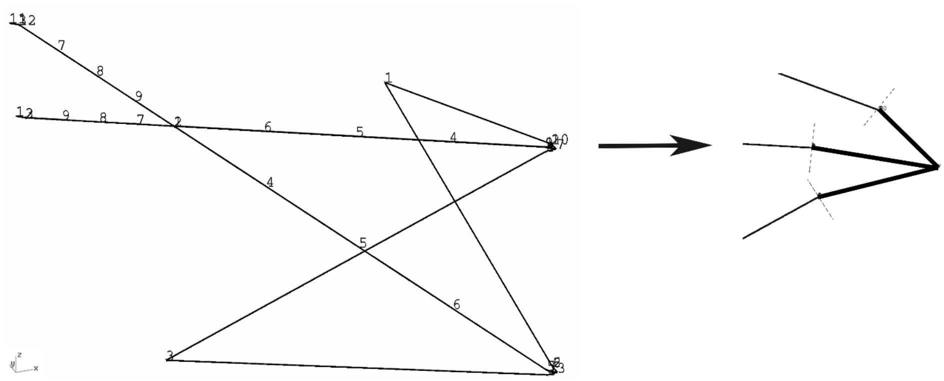

Figure 3.3: Finite element mesh with discrete joint dimensions (left) and detail of the stiff grid of beams that represents the joint and the rotation axes that were initially in one point (right).

Technically, joints are always present and because they have a considerable influence on the deployment behaviour, they are included in all subsequent simulations. For this flat square polygonal modules with a cross-section of the beams of only 9x9 mm, joints with a diameter of 1 cm are used in the following simulations. The larger the joint size, the higher the maximum required folding load and the further the geometry will be from the idealised one, so smaller hinges correspond to the optimal solution.

3.1.2 Tolerances on the beam length

Practically, beam manufacturing companies are delivering a certain standard quality, but geometrical imperfections might occur through the manufacturing assembly process. Two possible imperfections might occur considering the length of the beams: the initial length of the beams can vary or the position of the pivot can vary (Dupont, 2014).

These imperfections are in fact tolerances which have to be defined on a certain basis. The higher the tolerance, the lower the price of the beams will be, but the lower the tolerance, the more the structure will behave like the idealised one. An acceptable range of tolerances will be defined, looking at the maximum required folding force, the snap-through magnitude, the minimum required folding force and the compactness of the structure in the folded configuration.

To do this, imperfections will be introduced on each beam separately to be able to explain what is happening and to investigate within which range the tolerances should be located, in order to be able to investigate realistic tolerances for the beam lengths when modelling them simultaneously. Modelling simultaneous length variations corresponds to the real case.

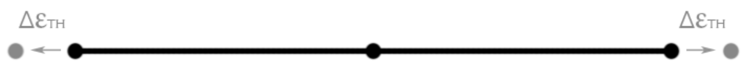

Figure 3.4: Imperfections on the beam length (symmetric length variation from left and right of the middle hinge).

Because of the symmetry of the square module, tolerances on three beams are first investigated separately: an outer SLE, the shortest inner SLE and the longest inner SLE (Figure 3.5). The convoluted effect of imperfections on all of the member lengths is treated afterwards.

To model an increase or decrease in beam lengths, thermal expansion effects are used (Dassault Systèmes Simulia Corp., 2012c). This modelling technique was chosen to represent imperfections on the beam length, instead of changing the nodal coordinates in the model, because the thermal strain is not equal to the mechanical strain due to the interaction with other connected elements. Thermal expansion effects can be defined by specifying thermal expansion coefficients α and a temperature change $\Delta\theta$ according to the formula:

$$\epsilon^{th} = \alpha\Delta\theta \tag{3.1}$$

The thermal effect is thus used to phenomenologically represent length variations inducing stresses in the structures and $\Delta\theta$ is the temperature change. α was taken equal to 1, such that the change in temperature represents directly the imposed strain. The fictitious temperature field is homogeneous for all the elements except for the beam that is investigated.

The tolerances on the beam lengths are investigated for a beam in an outer SLE and a short and a long beam in an inner SLE. To restrict the amount of parameters, the strain in the two semi-lengths of the beam is supposed to be equal (Figure 3.4). The length of the beams is increased/reduced in steps of 0.1% strain. This thermal strain is not equal to mechanical strain because of the interaction with other connected elements. The thermal strain would be the measure of how longer a beam would be with respect to the designed length, if the beam would be free.

When imperfections are taken into account for one beam, the initial node coordinates of the whole bistable scissor module change and at the same time, there are stresses introduced in all the beam elements to accommodate the change in length. This method of using thermal strain is used to model other imperfections as well (i.e. eccentricity of the pivot point and hinge misalignment) because it introduces residual stresses after assembly, which is physically the case.

3.1.2.1 Imperfections on separate beam lengths

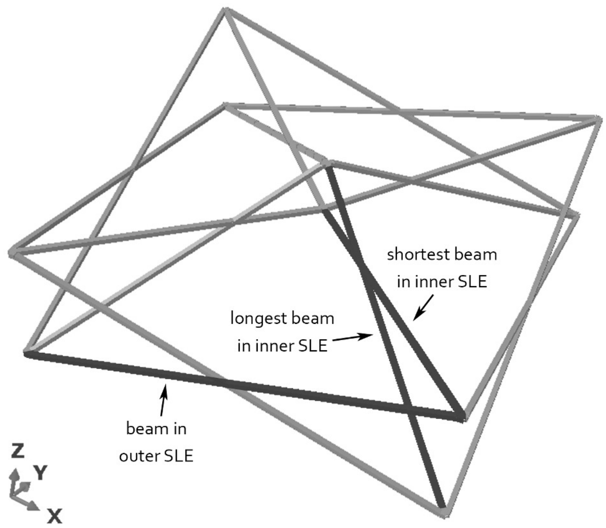

Figure 3.5: Specification of the beam in an outer SLE, the shortest beam in an inner SLE and the longest beam in an inner SLE.

First, the length of a beam in an outer SLE (Figure 3.5) is changed. The darkest curve in Figure 3.6 represents the load-displacement curve of the idealised model. The curves become gradually lighter as the imposed strain increases.

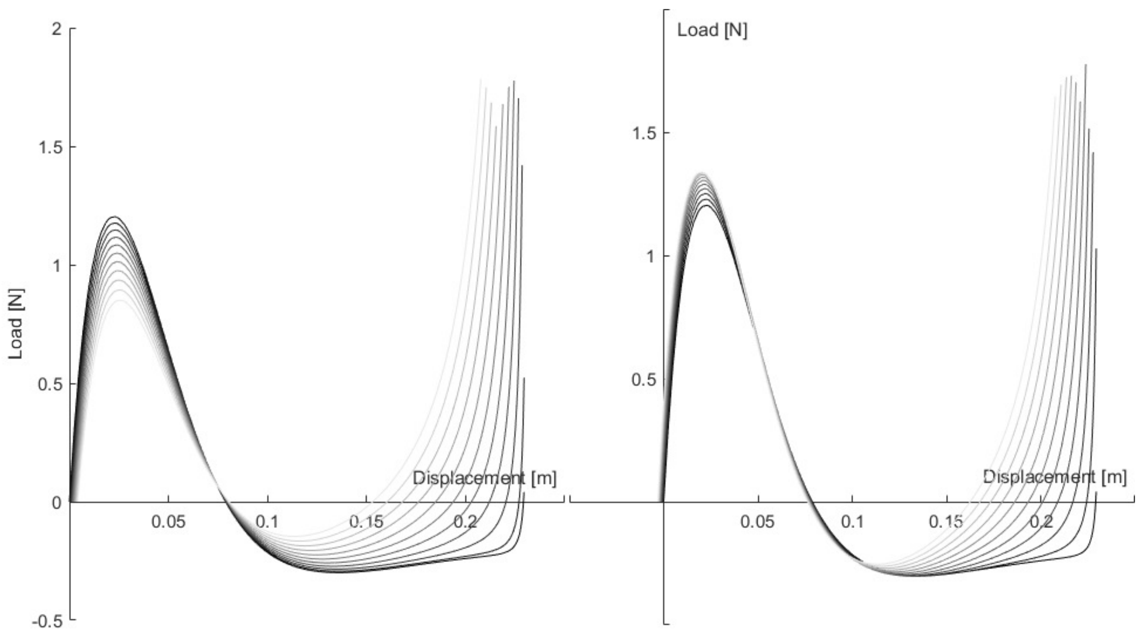

Figure 3.6: Increase (left) and decrease (right) of the beam length in an outer SLE.

When the length of a beam in an aluminium outer SLE is increased, the beam itself will be in compression while putting almost all other outer aluminium beams in tension

(Figure 3.7 left). Increasing the length of this outer beam will force the structure to increase its height to width ratio, which explains the displacement along the positive z-direction of the upper middle point in the initial configuration (Figure 3.6 left). The compression and tension in the inner beams are lower than for the outer beams. For two inner SLE's, the shortest beam is in compression while the longest beam is in tension. For the two other inner SLE's, the opposite occurs. These inner beams thus do not have a lot of influence on the deployment behaviour.

When the length of a beam in an aluminium outer SLE is increased, the magnitude of the snap-through gradually decreases just as the load required to fold the structure. When the initial configuration is changed to a configuration in which the inner deformable beams already start bending in the idealised case, the bending will be less severe. This is the reason why the snap-through effect and the load required for folding drastically decreases when lengthening a beam in an outer SLE.

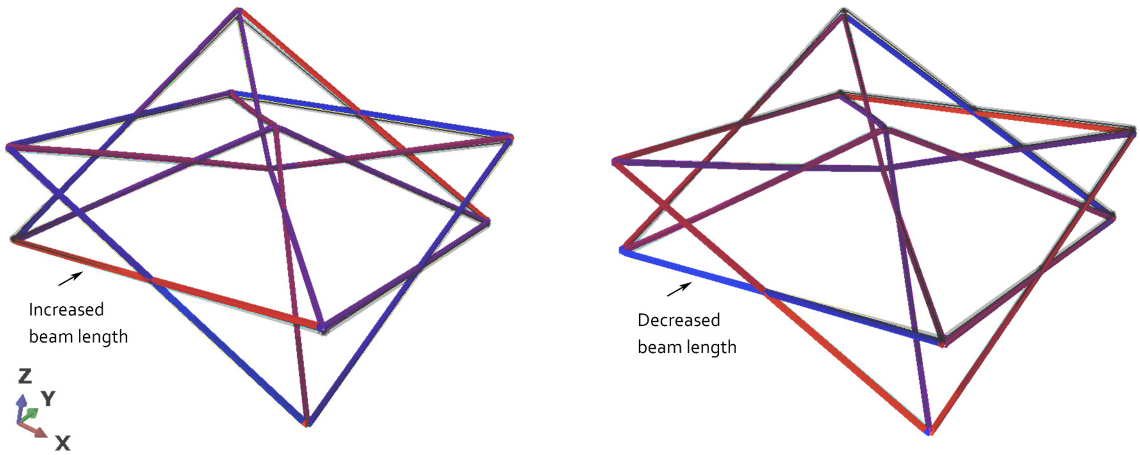

Figure 3.7: Compression (red) and tension (blue) in the beams when increasing (left) and decreasing (right) the length of a beam in an outer SLE.

When the length of the beam is decreased, the beam itself will be in tension while putting almost all other outer aluminium beams in compression (Figure 3.7 right). Decreasing the length of this outer beam will force the structure to decrease its height to width ratio, which explains the displacement along the negative z-direction of the upper middle point in the initial configuration (Figure 3.6 right). The compression and tension in the inner beams is again lower than for the outer beams and these inner beams will thus not change a lot the deployment behaviour.

When the length of the beam is decreased, the load required for folding increases slightly. Note that the variation in the maximum load is smaller than in the case of increasing the length of the outer beam. When the initial configuration is changed to a configuration in which the inner deformable beams do not yet start bending in the idealised case, the bending can be more severe because the bending of the inner deformable beams will start earlier. This is the reason why the snap-through effect and the load required for folding slightly increase when decreasing the length of a beam in an outer SLE.

In Figure 3.8 (left), the load required for folding is given in function of the tolerance on the beam length. When decreasing the length of the beam, the peak load will increase

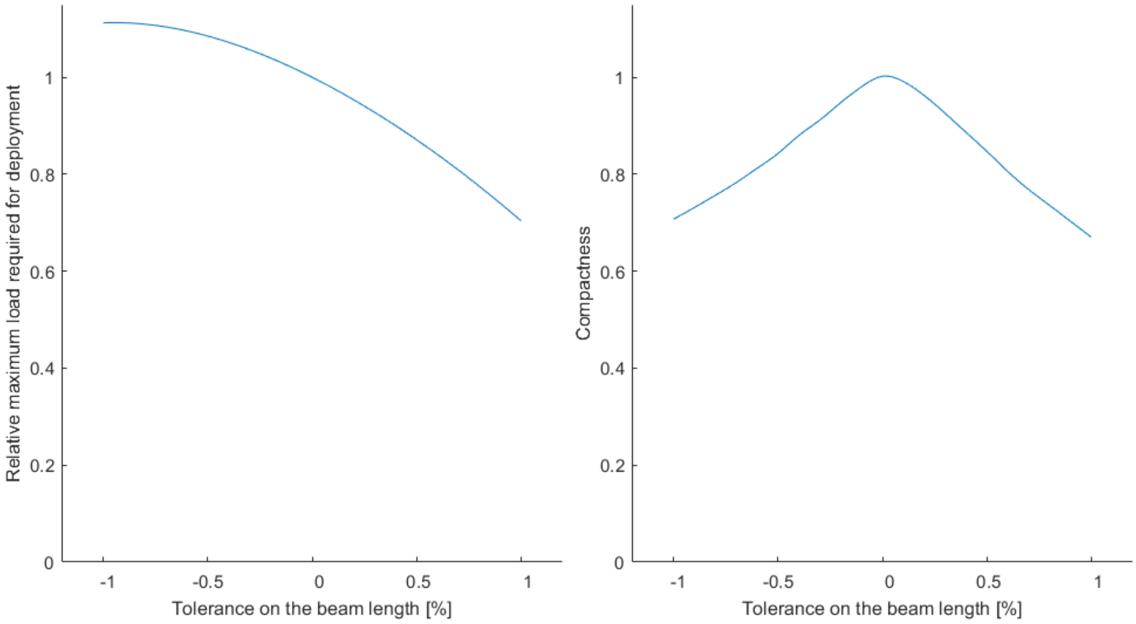

Figure 3.8: The variation of the peak load required for folding when varying the length of a beam in an outer SLE (left) and the compactness of the module (right).

to 110% of the peak load to fold the structure when there are no imperfections in the model. When increasing the length, the peak load decreases rapidly.

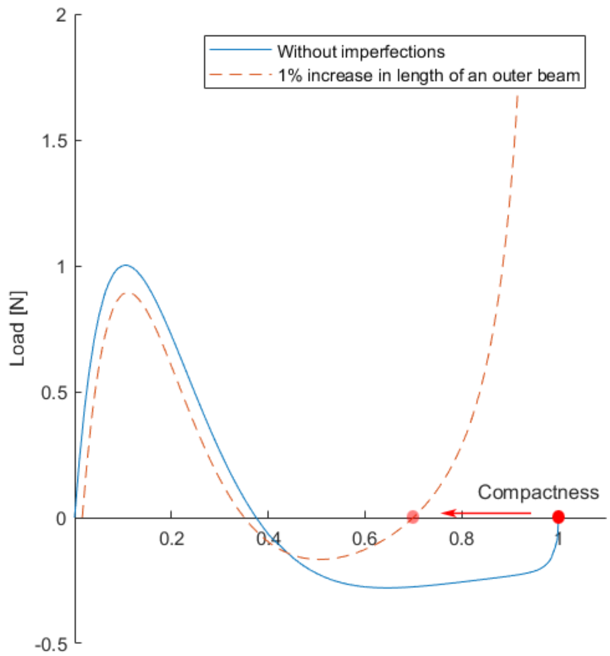

Figure 3.9: The compactness in the folded configuration of a module without imperfections and a module with an increase in an outer beam length of 1%.

When increasing or decreasing the length of a beam, the last part of the load-displacement curve, where the required load is negative for the idealised structure, is strongly affected. The load required for folding will increase tremendously because folding the structure completely is not possible when imperfections are implemented. To measure how far a structure can be folded, the concept of compactness is introduced. A value of 1 for the compactness corresponds to a module that can be folded as compact as an idealised module (Figure 3.9), while a value of 0 corresponds to a module that cannot be folded at all (it is not possible to move the structure from its deployed state). The compactness is deduced from the load-displacement curve, where the force is zero close to the folded configuration (red dot in Figure 3.9).

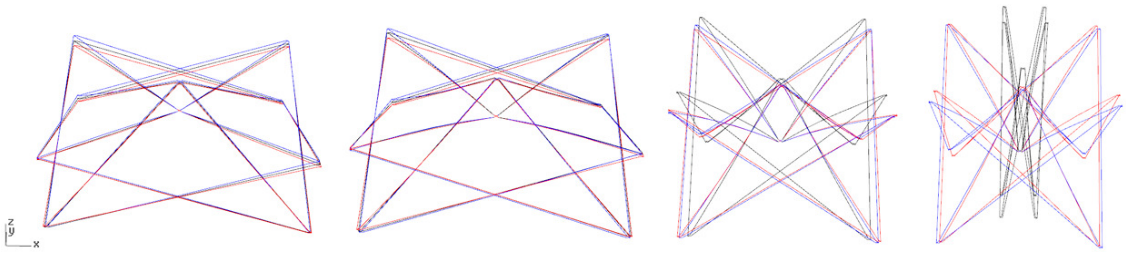

Figure 3.10: From left to right: the initial configuration, the configuration in which the highest load is required, in which the lowest load is required and the final configuration of the module without imperfections (black), with an increase in the beam length of 1% (blue) and a decrease in the beam length of 1% (red).

In Figure 3.8 (right), the compactness of the module is given in function of the strain of a beam in an outer SLE. When the length of the beam is decreased, the compactness rapidly decreases as well. When the length is increased, the compactness also rapidly decreases. This can be seen in Figure 3.10 (right), where the folded configuration for an increase or decrease in the beam length of 1% is not compact at all.

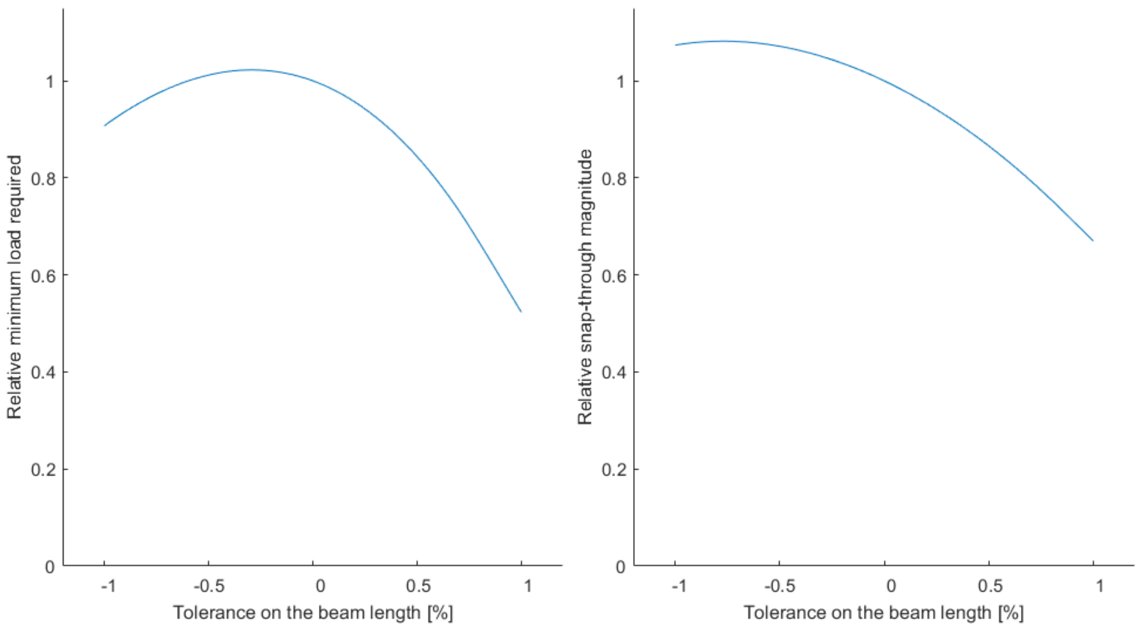

Figure 3.11: The variation of the minimum load required for folding when varying the length of a beam in an outer SLE (left) and the magnitude of the snap-through (right).

As was the case for the peak load, the snap-through magnitude decreases rapidly when the beam length is increased, while it increases to 110% of the snap-through magnitude when there are no imperfections in the model (Figure 3.11 right) when the beam length is decreased.

The maximum negative force is important when considering gravity, because it gives the structure the ability to remain in the folded state without applying loads. In Figure 3.11 (left), this minimum force is given. When increasing the beam length, this maximum negative force decreases rapidly, while when decreasing the beam length, the negative force will only decrease slightly. This will be important when considering gravity, because this maximum negative force will decrease even more when gravity is taken into account, while it is important that the maximum negative force is high enough to give the structure the ability to remain in the folded state under its own weight.

Second, the length of the shortest deformable beam in an inner SLE (Figure 3.5) is changed. Figure 3.12 shows the load-displacement curves for increased strain in this beam. When the length of the beam is increased, the beam itself will be in compression while putting the two connecting outer beam elements in tension (Figure 3.13 left). Because of this configuration, the joint between the beam with the increased length and the outer beams will be forced down, leading to a decrease in the height to width ratio of the structure, which explains the displacement along the negative z-direction of the upper middle point in the initial configuration (Figure 3.12 left). For the same reason as was explained for a decrease in the beam length of an outer SLE, the load required for folding increases slightly.

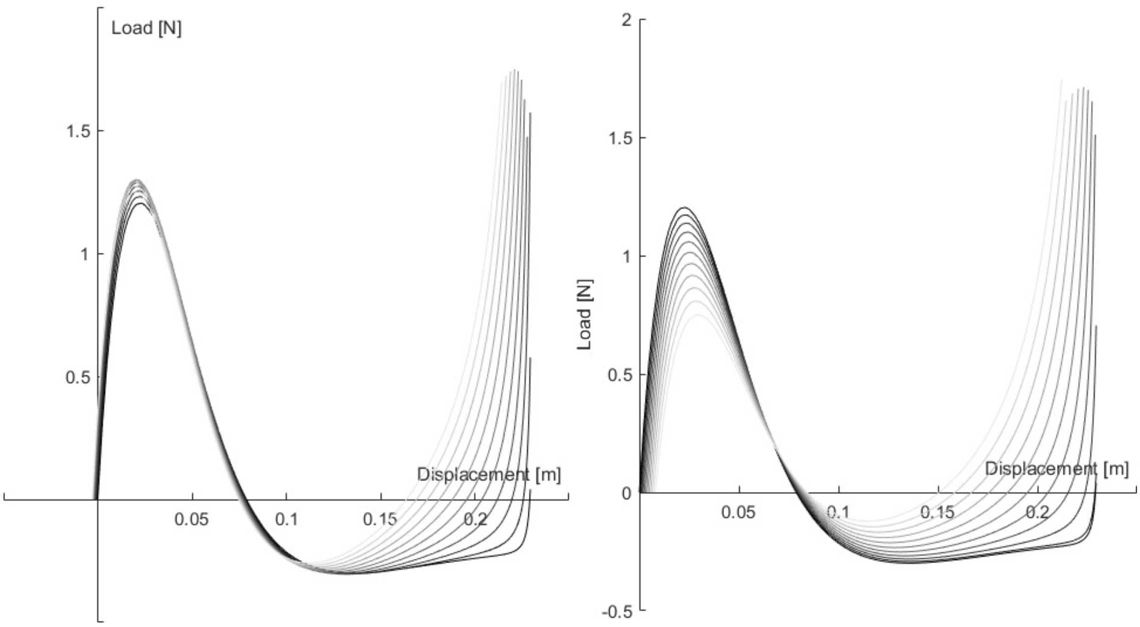

Figure 3.12: Increase (left) and decrease (right) of the length of a short beam element in an inner SLE.

When the length of the beam is decreased, the beam itself will be in tension while putting the two connecting outer beam elements in compression (Figure 3.13 right). Because of this configuration, the joint between the beam with the decreased length and the outer beams will be forced up, leading to an increase in the height to width ratio of the structure, which explains the displacement along the positive z-direction of the upper middle point in the initial configuration (Figure 3.12 right). For the same reason as was explained for an increase in the beam length of an outer SLE, the load required for folding decreases drastically.

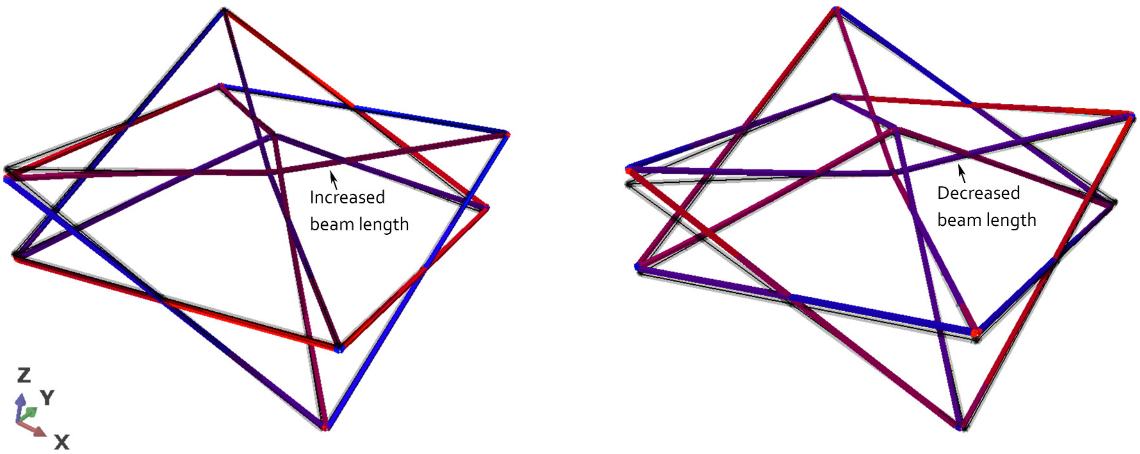

Figure 3.13: Compression (red) and tension (blue) in the beams when increasing (left) and decreasing (right) the length of a short beam element in an inner SLE.

The change in structural response when increasing or decreasing the length of the longest beam in an inner SLE (Figure 3.5), is comparable to the previous case. When increasing or decreasing the length of the longest beam in an inner SLE, the opposite occurs as in Figure 3.13. When increasing the beam length, the beam will be in compression while putting the connecting outer beams in tension. When decreasing the beam length, the opposite will occur.

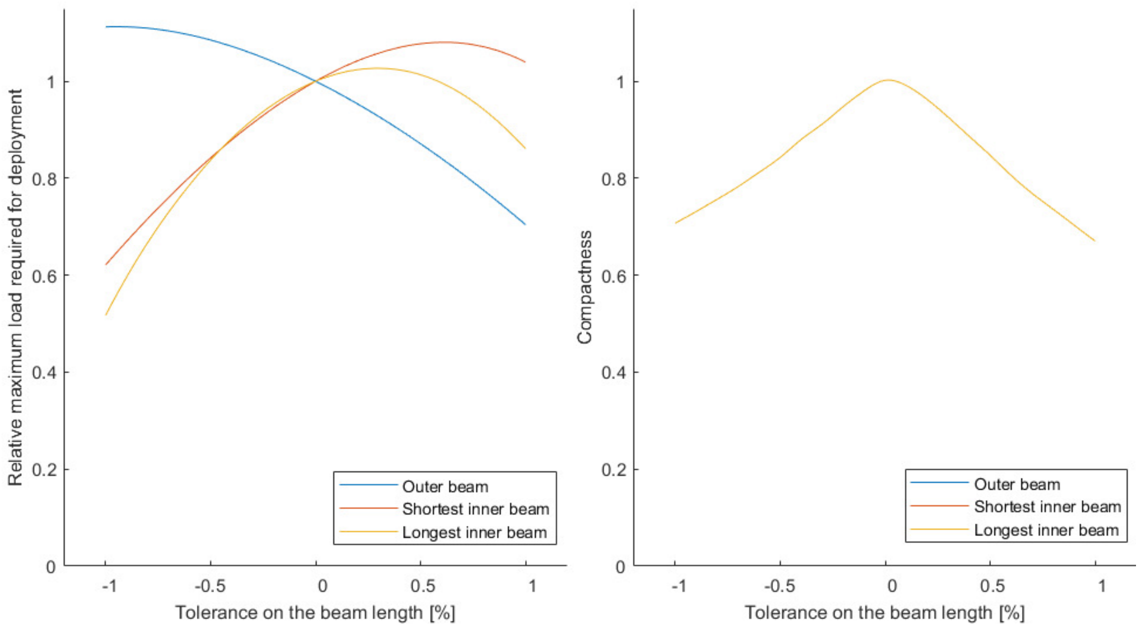

Figure 3.14: The variation of the peak load required for folding (left) and the compactness of the module (right).

In Figure 3.14 (left), the comparison is shown between imperfections on the three different beams separately for the variation of the peak load. As was explained, the influence of imperfections on the outer beam is the opposite as imperfections on the inner beams. The difference between imperfections on the beam length of a short and a long beam in an inner SLE is a stronger sensitivity for imperfections on the longest beam, which can be explained by the higher sensitivity to bending and buckling for longer beams.

In Figure 3.14 (right), the compactness of the module is given for the three different beams. Decreasing or increasing the length of a beam has the same effect on the compactness, which is decreased tremendously by the imperfections. For the three beams, the effect of increasing or decreasing the beam length on the compactness is exactly the same.

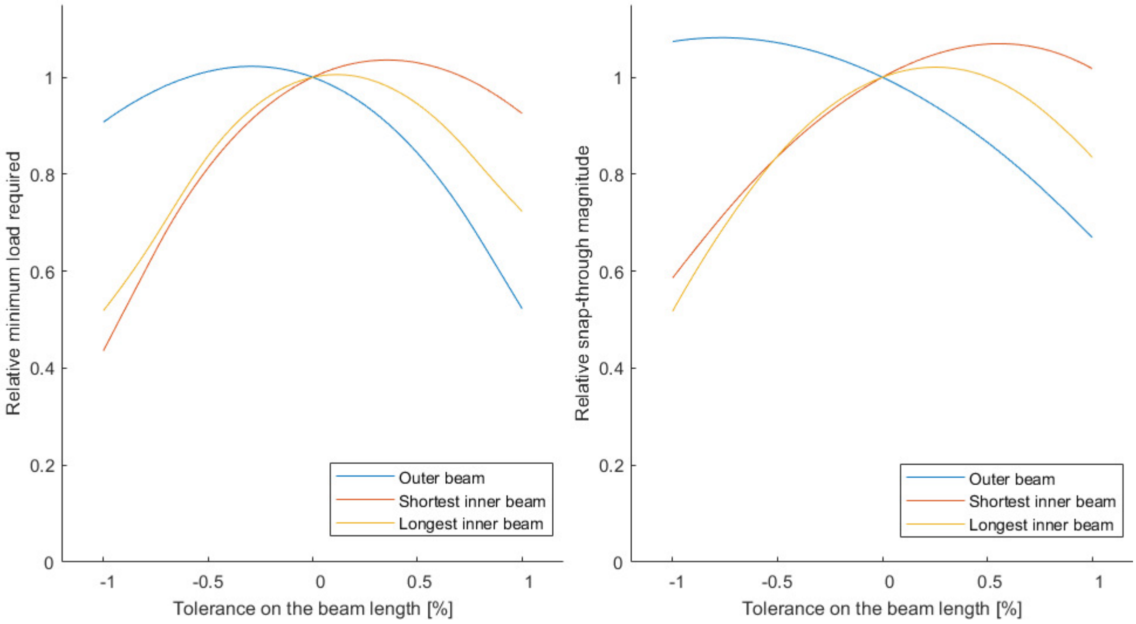

Figure 3.15: The variation of the minimum load required for folding (left) and the magnitude of the snap-through (right).

For the variation of the minimum load required for folding (Figure 3.15 left), and for the variation of the magnitude of the snap-through (Figure 3.15 right), the same conclusions can be drawn as for the variation of the required peak load (Figure 3.14 left). The influence of imperfections on the outer beam is the opposite to the influence of imperfections on the inner beams and the difference between imperfections on the beam length of a short and a long beam in an inner SLE is a stronger sensitivity for imperfections on the longest beam.

3.1.2.2 Simultaneous imperfections on all of the beam lengths of the module

In order to investigate realistic tolerances for the beam lengths, these have to be modelled simultaneously. In order to stay consistent with the model to be developed, the tolerances have to be defined so that the values for each module are not too different through a complete structure and on a large number of computations. Therefore, a random distribution has been introduced in order to define the tolerances accordingly (Dupont, 2014). The mean value is 0 and the standard deviation is defined as the strain in the beams.

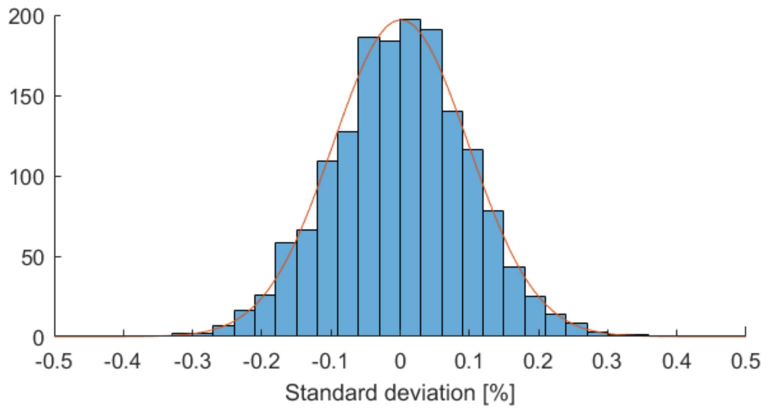

Figure 3.16: Histogram of the random values for the strain and probability density function with a mean value of 0 and a standard deviation of 0.1%.

Practically values between 0.001 and 0.01 are the most realistic, as is found by Dupont (2014). An imperfection of 1 cm on 1 m already seems huge. When looking at the compactness of the module for the imperfections on the separate beam lengths, tolerances of 1% indeed are not acceptable because the compactness is only 0.7, as can be seen of Figure 3.14 (right). This compactness of 0.7 corresponds to a 'folded' configuration as shown in Figure 3.10 (right).

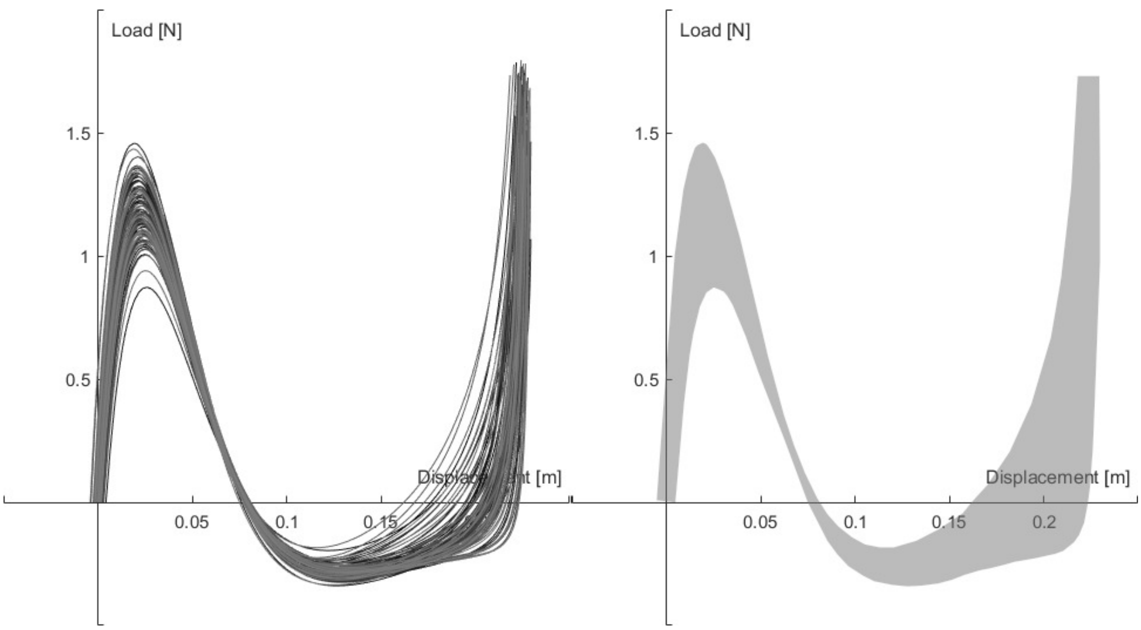

Figure 3.17: Load-displacement curves for 100 simulations with random values for the tolerances on all of the beam lengths of the module with a standard deviation of 0.1% (left) and the range of the load-displacement curves (right).

100 modules are modelled with strains derived from a random distribution with a standard deviation of 0.1%, which means that 99.7% of the values are within the range of -0.3% to 0.3%. Using 100 simulations (Figure 3.16), the probability distribution function can be approached decently (a random distribution with mean value 0.00004 and a

standard deviation of 0.098% is obtained), which is relevant if one random variable would be associated for all the beams. However, this initial assumption is not physical, and that is why the random variables are associated to each member separately (i.e. each beam has a different imperfection on the beam length). This ensures full randomness, even though some correlations on the imperfections might be missing. In this case, 100 simulations do not sample completely the space, but they are chosen to limit the time to perform the analyses (all of them are nonlinear) and yet to get an idea about the range in which the maximum and minimum load will be, as well as the snap-through magnitude and the compactness.

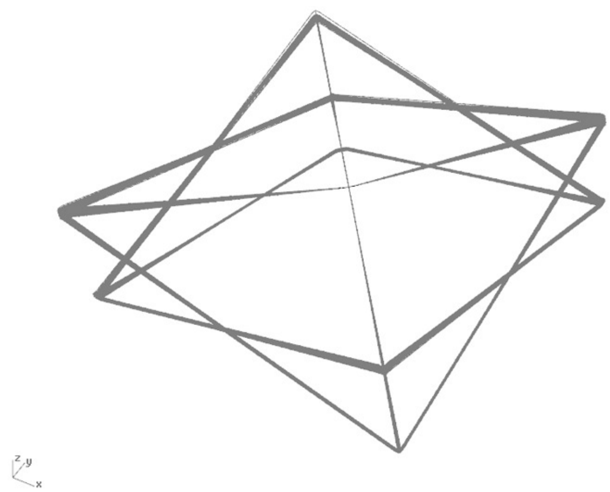

Figure 3.18: Initial configurations of the 100 simulations after applying random imperfections with a standard deviation of 0.1% on the beam lengths.

The results of these 100 simulations are given in Figure 3.17 (left). The range of the load displacement curves is given in Figure 3.17 (right) and the initial configurations of the 100 simulations after applying random imperfections on the beam lengths are given in Figure 3.18.

In Figure 3.19 and 3.20, the frequency is given for the relative peak force, the compactness, the relative minimum load and the relative snap-through magnitude. Looking at the histograms, it is clear that 100 simulations do not cover completely the space of the normal distribution. Probability density functions are fitted on the histograms to show the trend of what will happen if the space would be covered more completely.

Other simulations with a standard deviation of 0.2% and 0.3% are performed to obtain the maximum standard deviation that is acceptable. Because tolerances of 1% are not acceptable (because of the limited compactness of 0.7), a maximum standard deviation of 0.3% is chosen, which means that 99.7% of the values are within a range of -0.9% to 0.9%. The results of 100 simulations with a standard deviation of 0.3% are given in Figure 3.21, to denote the difference of the range of the load-displacement curves with the 100 simulations with a standard deviation of 0.1% (Figure 3.17). The range of the load-displacement curves of the simulations with a standard deviation of 0.2% is between those two ranges.

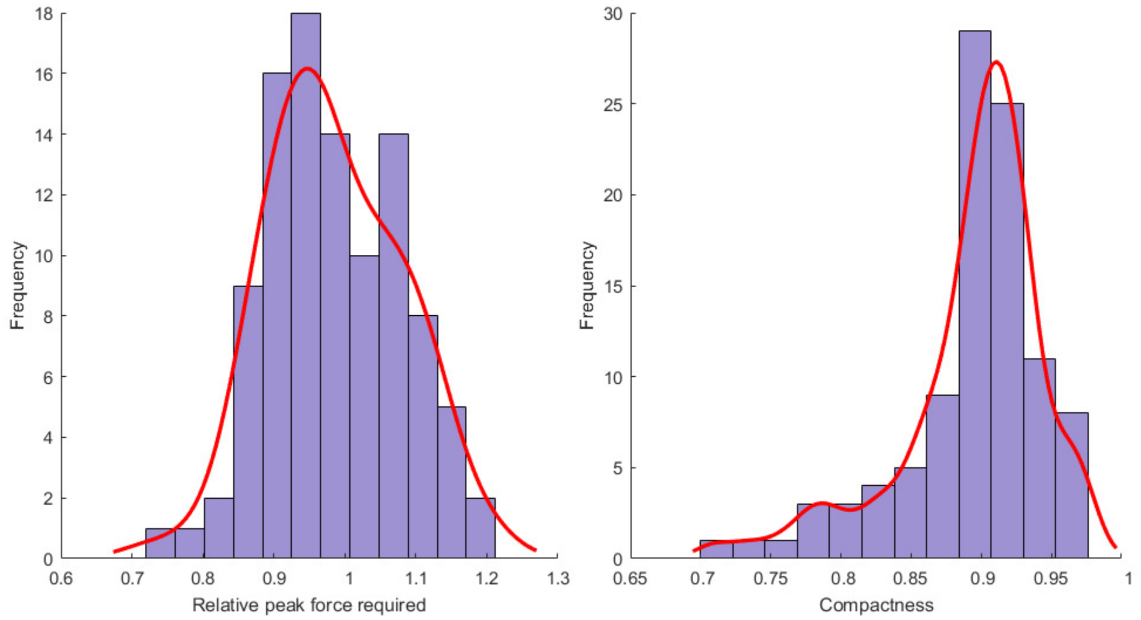

Figure 3.19: The variation of the peak load for 100 simulations with random values for the tolerances on all of the beam lengths of the module with a standard deviation of 0.1% (left) and the compactness of the module (right).

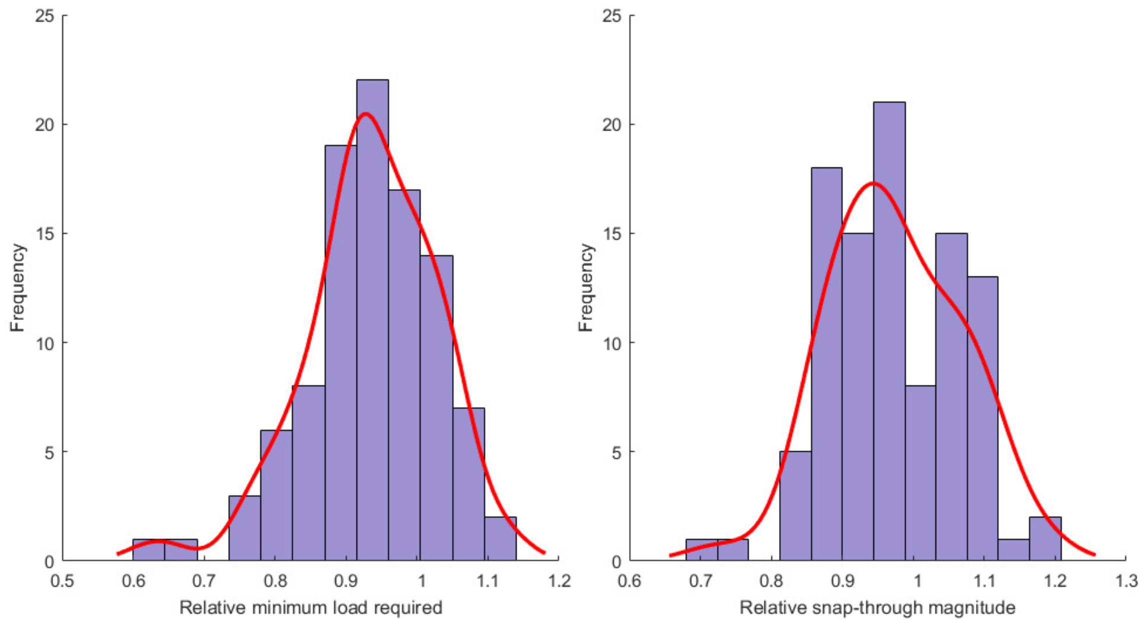

Figure 3.20: The variation of the minimum load required for 100 simulations with random values for the tolerances on all of the beam lengths of the module with a standard deviation of 0.1% (left) and the magnitude of the snap-through (right).

In Figure 3.22 and 3.23, the comparison of the 100 simulations with a standard deviation of 0.1%, 0.2% and 0.3% is given by comparing the probability density functions for the peak load, the compactness, the minimum load required and the snap-through magnitude. With a standard deviation of 0.1%, the peak force is between 70% and 125% of the peak force for the structure without imperfections. The average compactness is 0.9 and the minimum compactness is 0.7. The minimum force required is between 60% and 120% of the minimum force required for the structure without imperfections and

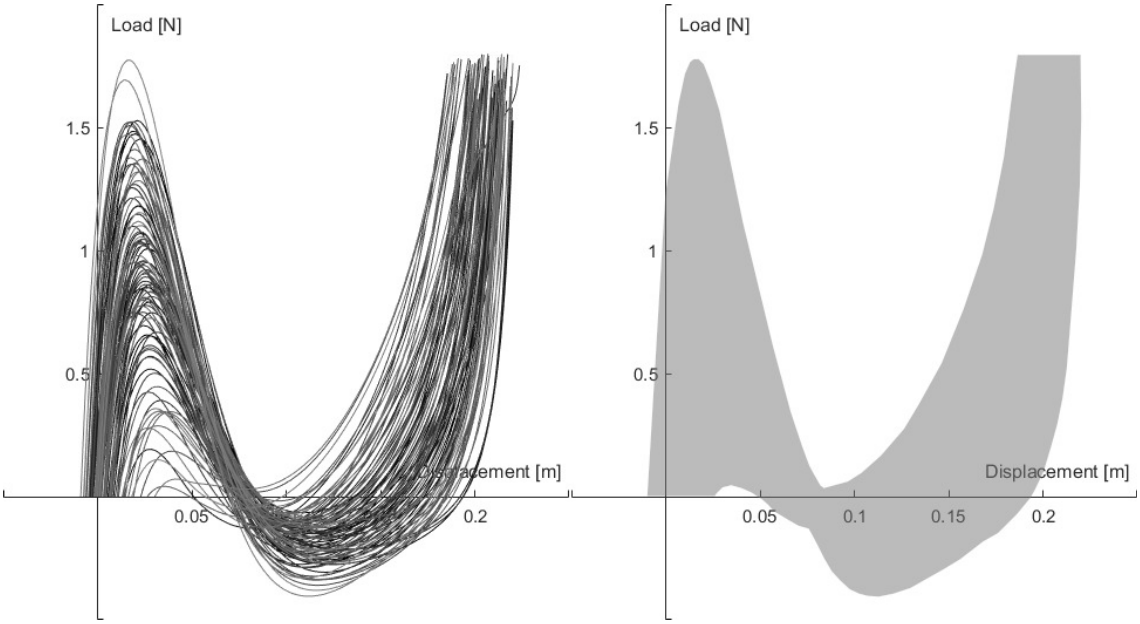

Figure 3.21: Load-displacement curves for 100 simulations with random values for the tolerances on the beam lengths with a standard deviation of 0.3% (left) and the range of the load-displacement curves (right).

the snap-through magnitude is between 70% and 125% of the snap-through magnitude for the structure without imperfections.

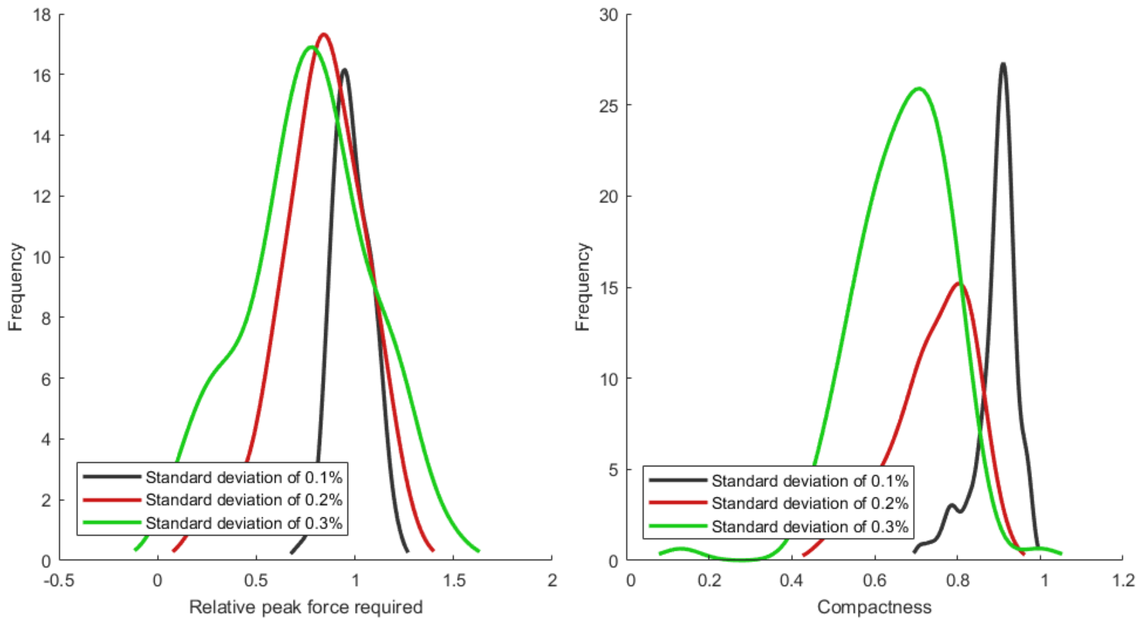

Figure 3.22: Comparison of the probability density functions for the peak load (left) and the compactness (right) for 100 simulations with random values for the tolerances on all of the beam lengths of the module with a standard deviation of 0.1%, 0.2% and 0.3%.

The results of the 100 simulations with a standard deviation of 0.2% are not acceptable because the differences in the peak force required for folding (between 10% and 140% of the structure without imperfections) are too high as is the compactness (between 0.4

and 1 with an average of 0.8). A compactness of 0.4 means that the structure cannot even be folded halfway, which is totally unacceptable. In this case, the minimum force required is between 0% and 130% and the snap-through magnitude is between 10% and 140% of the structure without imperfections.

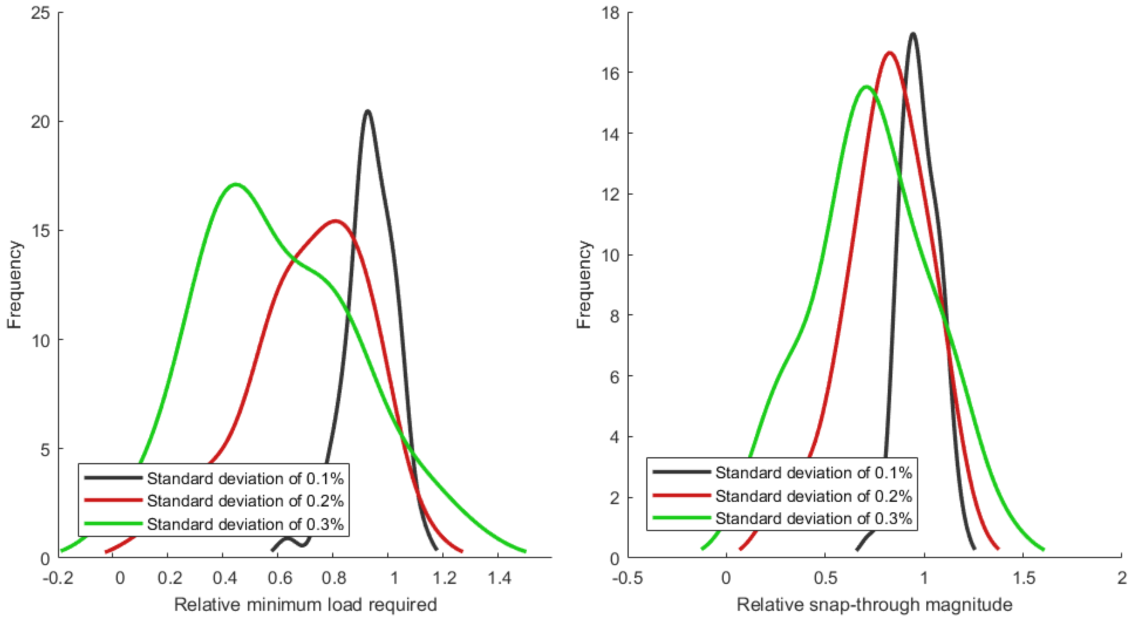

Figure 3.23: Comparison of the probability density functions for the minimum load required (left) and the snap-through magnitude (right) for 100 simulations with random values for the tolerances on all of the beam lengths of the module with a standard deviation of 0.1%, 0.2% and 0.3%.

The results of the 100 simulations with a standard deviation of 0.3% are given in Figure 3.21. As expected, the results are even less acceptable. The peak force is between -10% and 160%, the minimum force between -20% and 150% and the snap-through magnitude between -10% and 160% of the structure without imperfections, while the compactness is between 0.1 and 1 with an average of 0.6.

3.1.3 Eccentricity of the SLE pivot point

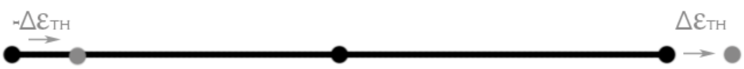

Figure 3.24: Antisymmetric length variation on the left and right from the midpoint.

The position of the hole which will be bored after manufacturing also has a limited accuracy, which is modelled here by imposing an opposite strain for the two semi-lengths of the beam. The thermal strain does not cause a variation in the total free length, as was the case in 3.1.2. It represents a strain on a semi-length of the beam and an opposite strain on the other semi-length.

3.1.3.1 Imperfections on separate pivot points

Figure 3.26 represents a shift in the position of the pivot point along the beam axis of a beam in an outer SLE (Figure 3.25). The darkest curve again represents the load-displacement curve of the idealised model. The curves become gradually lighter as the imposed eccentricity of the pivot point increases. In Figure 3.26 (left), the hole is shifted downwards in steps of 0.2% strain of a semi-length of the beam. To make it comparable to the previous case, the results are expressed as a function of the full length of the beam, which means that the hole is shifted in steps of 0.1% strain of the full length of the beam. In Figure 3.26 (right), the hole is shifted upwards (Figure 3.25).

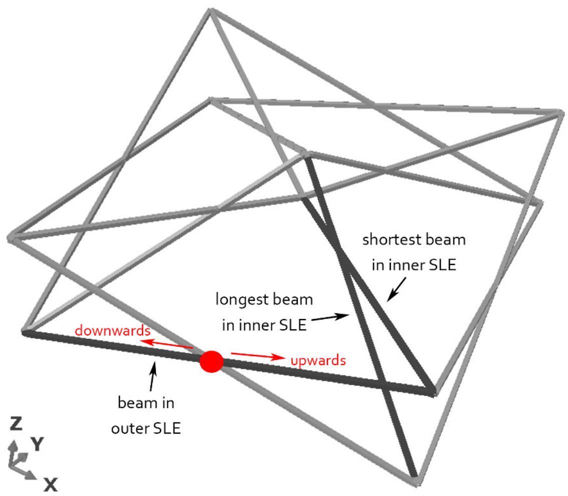

Figure 3.25: Specification of the beam in an outer SLE, the shortest beam in an inner SLE and the longest beam in an inner SLE, with the shift in position of the pivot on a beam in an outer SLE highlighted.

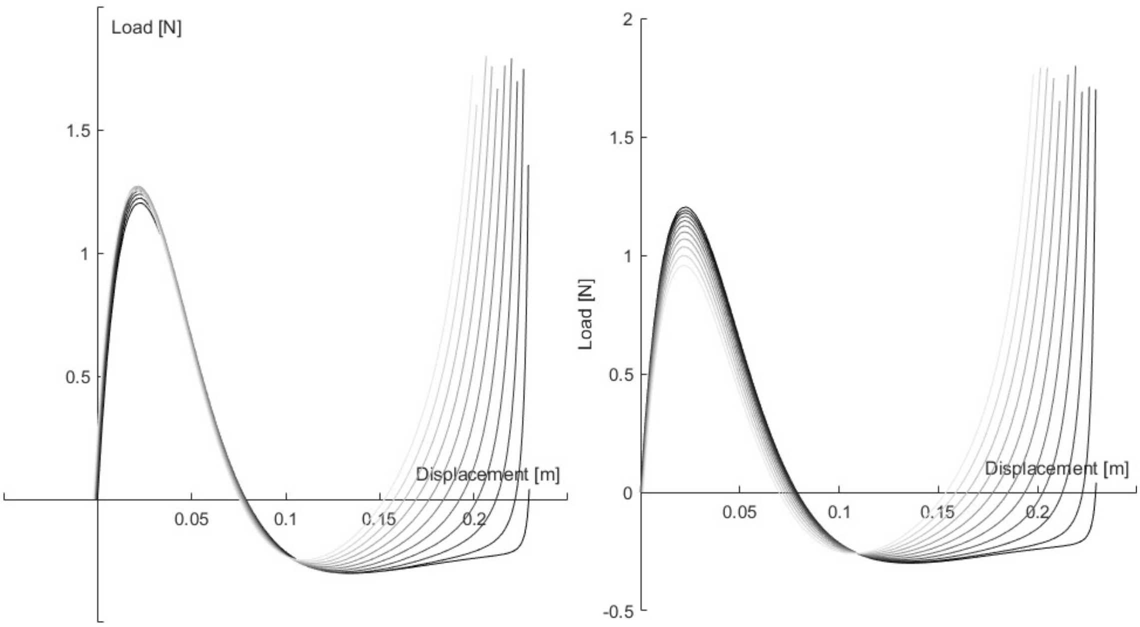

Figure 3.26: Eccentricity to one side (left) and to the other (right) of the pivot on a beam in an outer SLE.

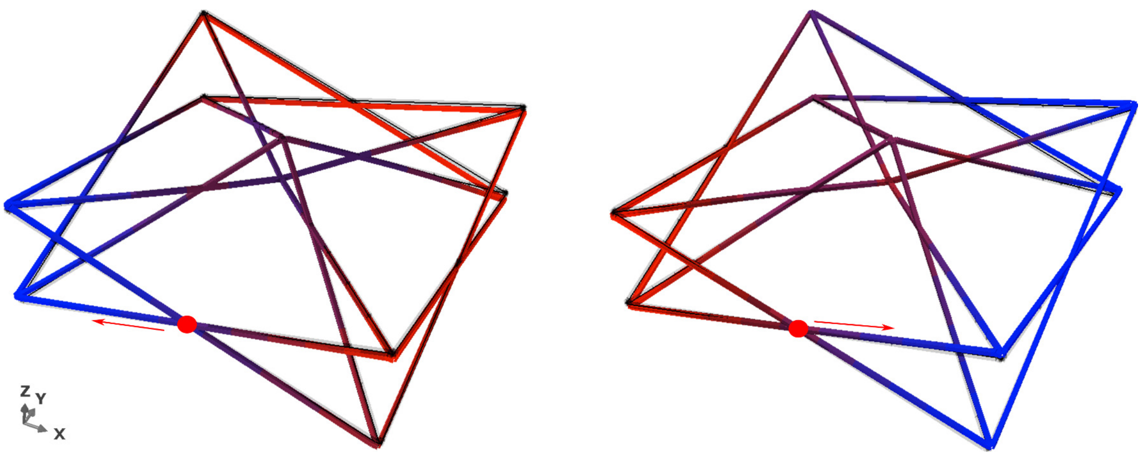

Figure 3.27: Displacement in the z-direction (blue is positive, red is negative) when there is a shift downwards (left) and upwards (right) of the pivot point on a beam in an outer SLE.

When increasing the eccentricity of the pivot downwards (Figure 3.26 left), the required folding load only slightly increases and then slightly decreases again. When increasing the eccentricity upwards (Figure 3.26 right), the required folding load decreases. This is due to the initial configuration of the module after applying the shift of the pivot point. When shifting the pivot point downwards to the left side of the SLE (Figure 3.27 left), the left side of the SLE will be forced upwards along the positive z-direction, while the right side is forced downwards. The upper centre node will also shift a little bit downwards, leading to a slight increase in the peak load required for folding, as was explained in the previous section.

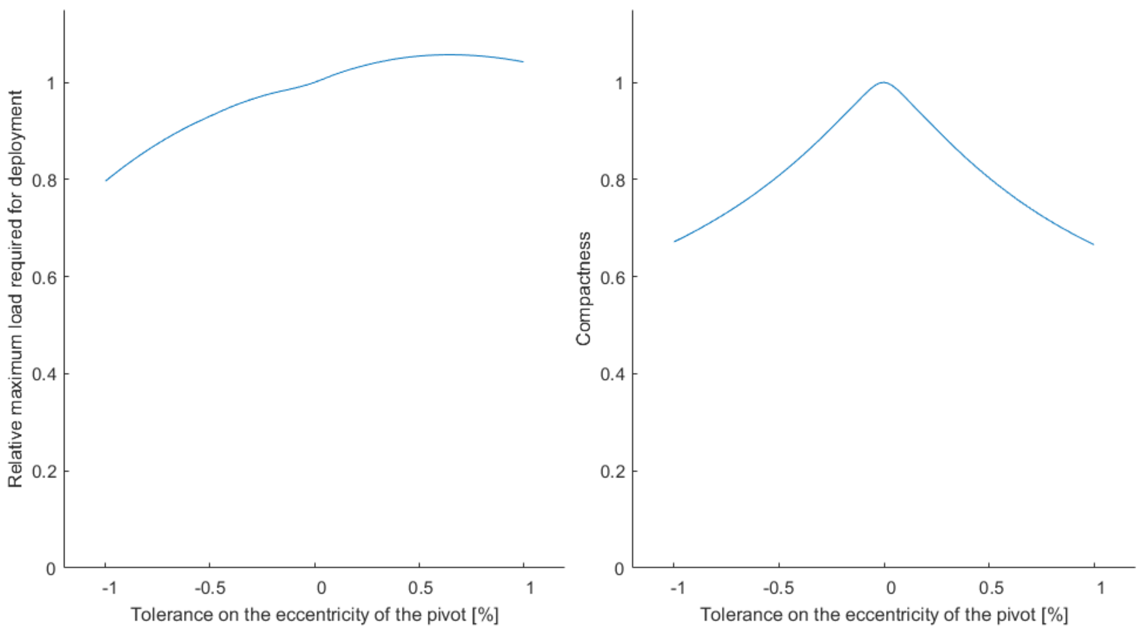

Figure 3.28: The variation of the peak load required for folding when varying the position of the hole in a beam in an outer SLE (left) and the compactness of the module (right).

When shifting the pivot point upwards to the right side of the SLE (Figure 3.27 right), the right side of the SLE will be forced upwards along the positive z-direction, while the left side is forced downwards. The upper centre node will shift upwards, leading to a decrease in the peak load required for folding, as was explained in the previous section.

In Figure 3.28 (left), the load required for folding is given in function of the value on the eccentricity of the pivot point. A positive value corresponds to a downward shift of the hole, while a negative value corresponds to an upward shift. In Figure 3.28 (right), the compactness of the module is given as a function of the position of the pivot point. A value of 1 again corresponds to the folded configuration of a module without imperfections, while a value of 0 corresponds to a module that cannot be folded. When the eccentricity of the pivot point is increased, the compactness rapidly decreases.

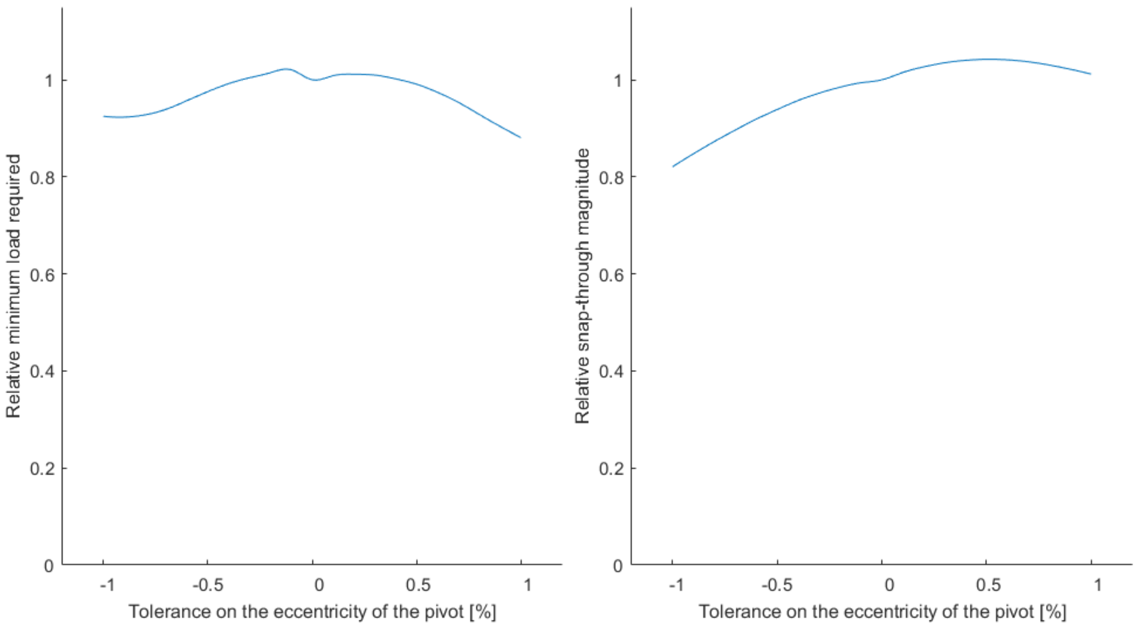

Figure 3.29: The variation of the minimum load required for folding when varying the position of the hole in a beam in an outer SLE (left) and the magnitude of the snap-through (right).

As was the case for the peak load, the snap-through magnitude decreases rapidly when the pivot point is shifted upwards, while it increases only slightly when the pivot point is shifted downwards (Figure 3.29 right). In Figure 3.29 (left), the minimum load required for folding is given as a function of the imperfection on the eccentricity of the pivot point. This minimum force is not much altered when changing the position of the pivot point.

Figure 3.30 represents a shift in the position of the pivot point along the beam axis of a short beam in an inner SLE. In Figure 3.31 (left), the hole is shifted to the outside of the module while in Figure 3.31 (right), the hole is shifted to the inside of the module.

When increasing the eccentricity of the pivot to the outside of the module (Figure 3.31 left), the required folding load decreases slightly. When increasing the eccentricity of the pivot to the inside of the module (Figure 3.31 left), the required folding load increases. Again, this is due to the initial configuration of the module after applying the shift of the pivot point. When shifting the pivot point to the outside of the module (Figure 3.32

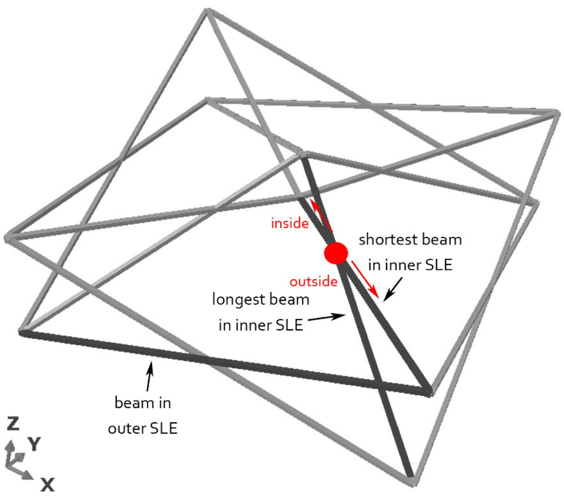

Figure 3.30: Specification of the beam in an outer SLE, the shortest beam in an inner SLE and the longest beam in an inner SLE, with the shift in position of the pivot on the shortest beam in an inner SLE highlighted.

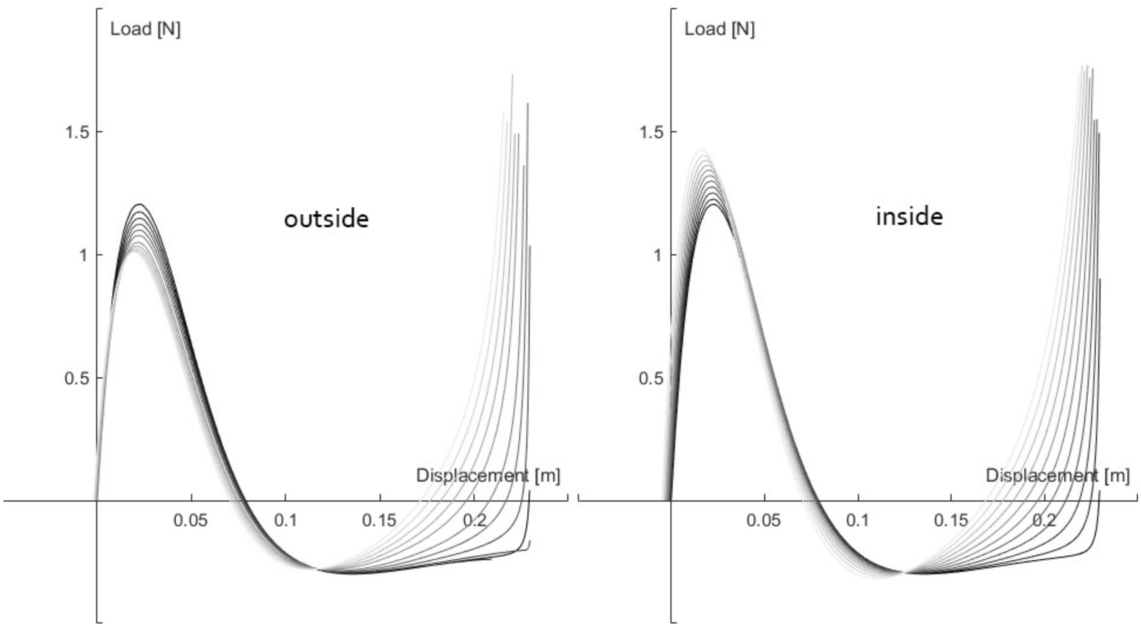

Figure 3.31: Eccentricity to outside (left) and to the inside (right) of the module of the pivot on the short beam element in an inner SLE.

left), the outer beams that are connected to the considered SLE are forced downwards, while the opposite side of the module is forced upwards. The upper centre node is forced a little bit upwards. For the same reason as in the previous cases, the peak load is decreased.

When shifting the pivot point to the inside of the module (Figure 3.32 left), the outer beams that are connected to the considered SLE are forced upwards, while the opposite side of the module is forced dowwards. The upper centre node is forced a little bit downwards. Again, for the same reason as in previous cases, the peak load is increased.

The change in structural response when shifting the pivot point along the longest beam in

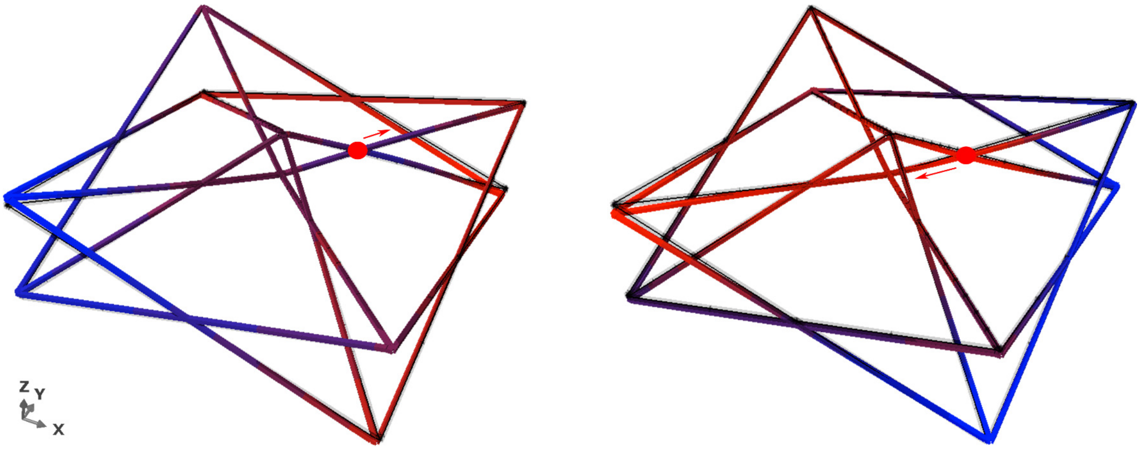

Figure 3.32: Displacement in the z-direction (blue is positive, red is negative) when there is a shift to the outside (left) and to the inside (right) of the module of the pivot point on a short beam in an inner SLE.

an inner SLE (Figure 3.33), is comparable to the previous case. When shifting the pivot point to the outside or to the inside of the module, the opposite occurs as in Figure 3.32.

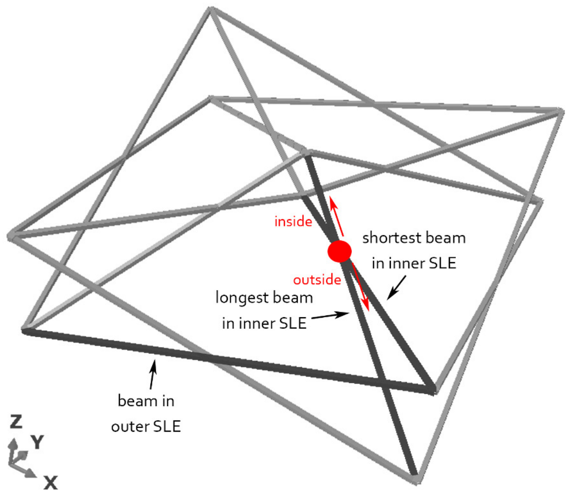

Figure 3.33: Specification of the beam in an outer SLE, the shortest beam in an inner SLE and the longest beam in an inner SLE, with the shift in position of the pivot on the longest beam in an inner SLE highlighted.

In Figure 3.34 and 3.35, the comparison between the imperfections on the beam length and the imperfections on the position of the pivot point is given for imperfections on an outer beam, the short beam of an inner SLE and the long beam of an inner SLE. The variation of the peak load is given, as well as the compactness, the minimum load required for folding and the snap-through magnitude.

For the variation of the peak force (Figure 3.34 left), the influence of imperfections on the beam length of the beams in an inner SLE is the most considerable.

When the imperfection increases, the compactness rapidly decreases 3.34 (right). The compactness is a little bit less influenced by a shift of the pivot along the axis of a beam

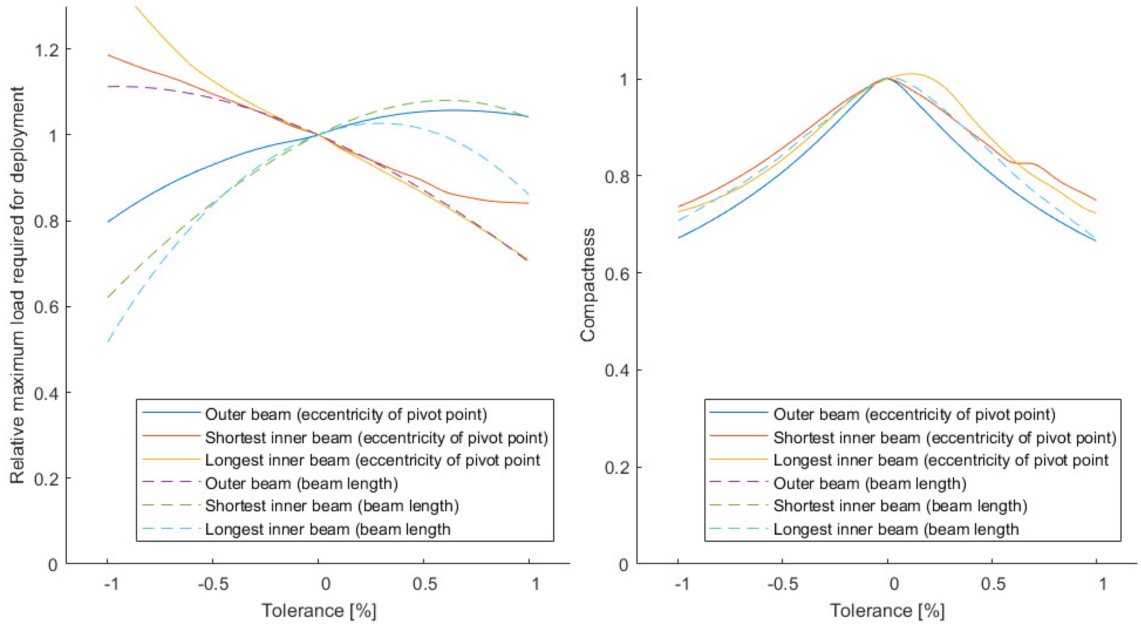

Figure 3.34: Comparison of the imperfections on the beam length and on the position of the pivot point for the variation of the peak load required for folding (left) and the compactness of the module (right).

in an inner SLE in comparison to a shift along the axis of a beam in an outer SLE. The compactness decreases comparably for imperfections on the beam length as for a shift of the pivot point.

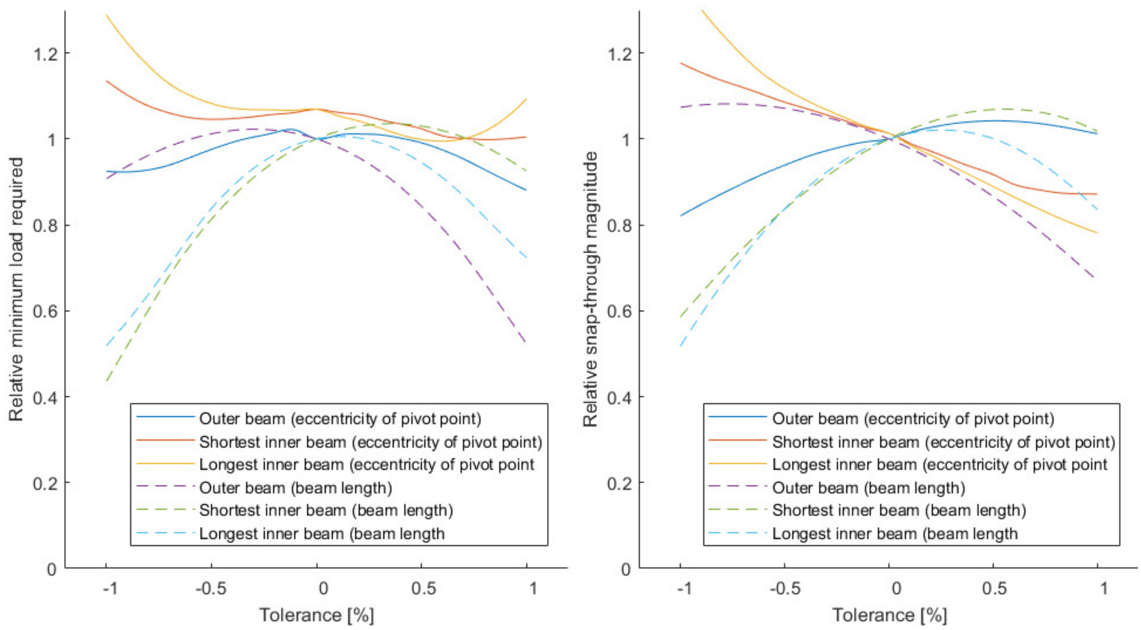

Figure 3.35: Comparison of the imperfections on the beam length and on the position of the pivot point for the variation of the minimum load required for folding (left) and the magnitude of the snap-through (right).

For the variation of the minimum load required for folding (Figure 3.35 left) and the snap-through magnitude (3.35 right), the influence of imperfections on the beam length of the beams in an inner SLE is again the most considerable. In general, the imperfections on the beam lengths seem to be a slightly more important than a shift of the pivot point, but the influence of the tolerances is more or less comparable.

3.1.3.2 Simultaneous imperfections on the eccentricity of all the pivot points in the module

In order to investigate realistic tolerances for the eccentricity of the pivot points, they have to be modelled simultaneously. To define the tolerances, a random distribution has been introduced. Again, practically values between 0.1% and 1% are the most realistic and tolerances of 1% are not acceptable because of the low compactness of 0.7 which is not acceptable. Because the imperfections on the position of the pivot points seem to be comparable to the imperfections on the beam lengths, it is expected that a standard deviation larger than 0.2% will not be acceptable, as was the case for the imperfections on the beam lengths. 100 simulations are performed with a standard deviation of 0.05%, 0.1% and 0.15%. For the largest value (0.15%), 99.7% of the values will be within a range of -0.45% and 0.45%.

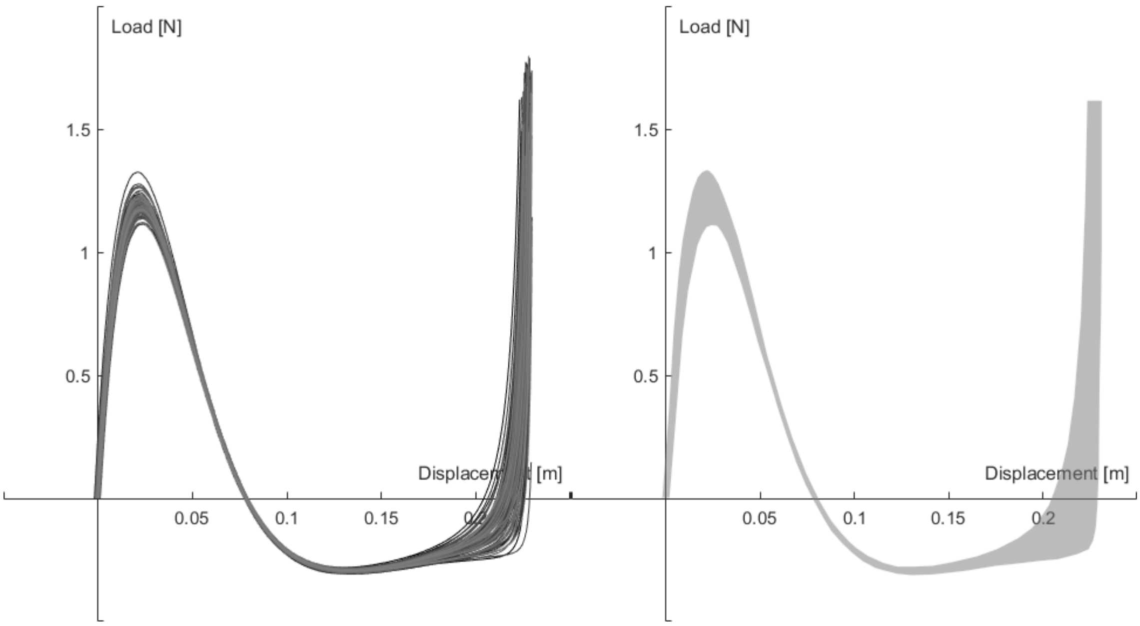

Figure 3.36: Load-displacement curves for 100 simulations with random values for the tolerances on the eccentricity of the pivot with a standard deviation of 0.05% (left) and the range of the load-displacement curves (right).

The results of 100 simulations with a standard deviation of 0.05% are given in Figure 3.36 (left). The range of the load-displacement curves is given in Figure 3.36 (right). All the load-displacement curves lie within a very close distance to the load-displacement curve of the structure without imperfections.

To compare the results of the imperfections on the position of the pivot points with the imperfections on the beam lengths, Figure 3.37 and 3.38 show the comparison between the probability density functions for the peak load, the compactness, the minimum load and the snap-through magnitude for 100 simulations with a standard deviation of 0.1%

for the imperfections on the beam lengths and on the position of the pivot points.

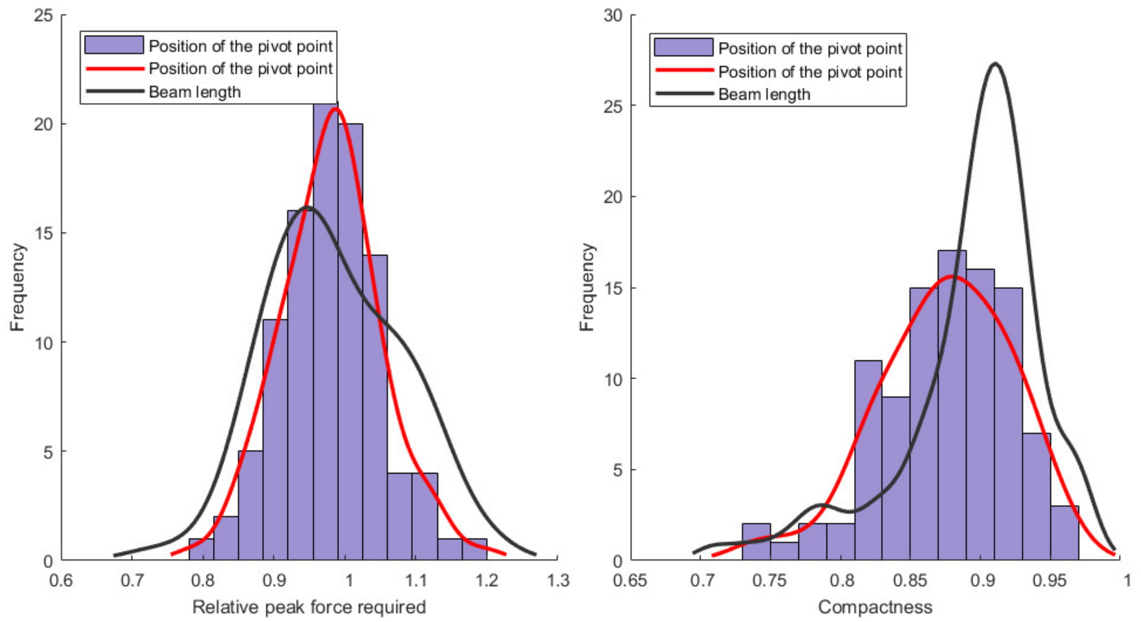

Figure 3.37: Comparison of the probability density functions for the peak load (left) and the compactness (right) for 100 simulations with a standard deviation of 0.1% for the imperfections on the beam lengths and on the position of the pivot points.

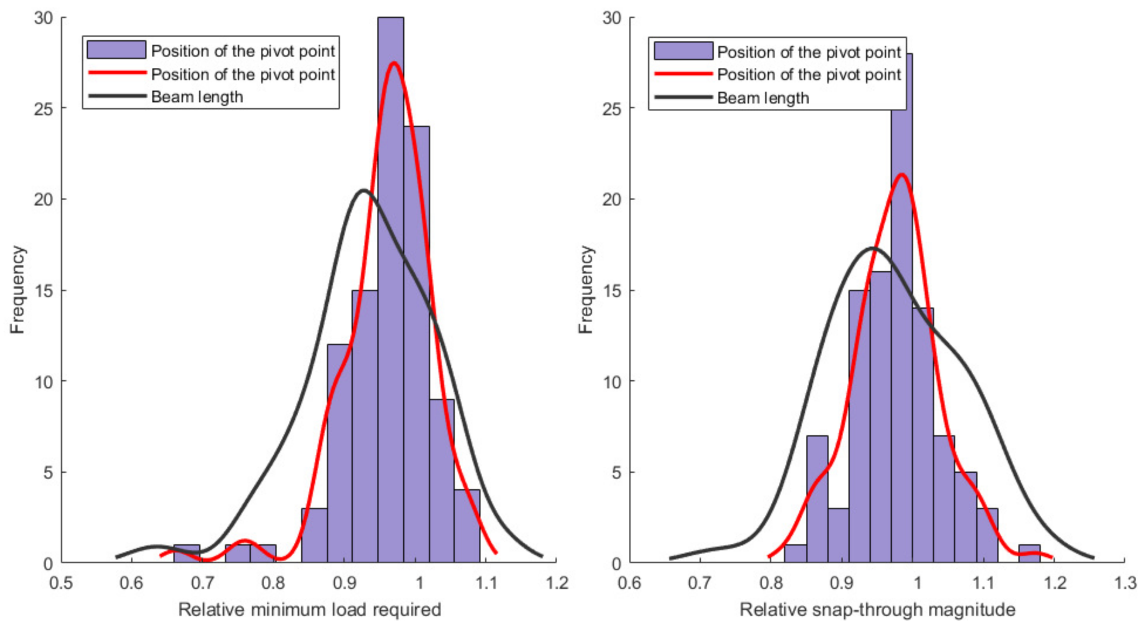

Figure 3.38: Comparison of the probability density functions for the minimum load required (left) and the snap-through magnitude (right) for 100 simulations with a standard deviation of 0.1% for the imperfections on the beam lengths and on the position of the pivot points.

For the peak force (Figure 3.37 left), the imperfections on the beam lengths are more considerable, since they cover a larger range. For the compactness (Figure 3.37 right), the results are comparable, but the average value is a little bit better for the imperfections on the beam lengths, although this can be due to the incomplete covering of the space with 100 simulations.

For the minimum force required for folding (Figure 3.38 left) and for the snap-through magnitude (Figure 3.38 right), the imperfections on the beam lengths are again more considerable because they cover a larger range.

The results of 100 simulations with a standard deviation of 0.15% are given in Figure 3.39, to be able to compare the results with the results of 100 simulations with a standard deviation of 0.05% (Figure 3.36).

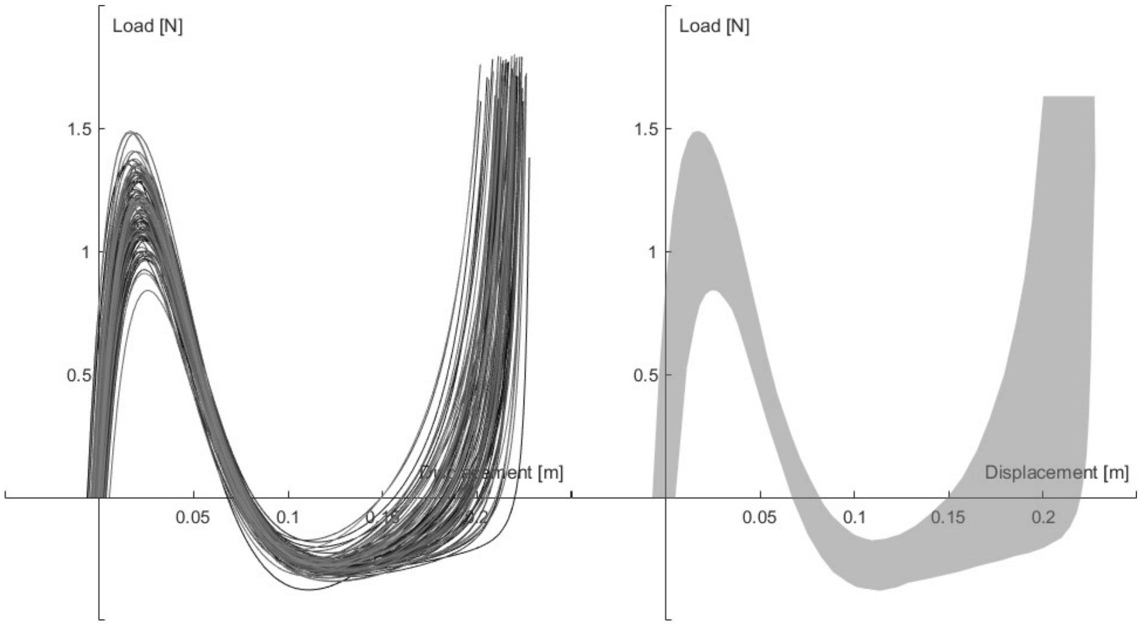

Figure 3.39: Load-displacement curves for 100 simulations with random values for the tolerances on the eccentricity of the pivot with a standard deviation of 0.15% (left) and the range of the load-displacement curves (right).

In Figure 3.40 and 3.41, the comparison of 100 simulations with a standard deviation of 0.05%, 0.1% and 0.15% is given by comparing the probability density functions for the peak load, the compactness, the minimum load required and the snap-through magnitude. With a standard deviation of 0.05%, the peak force is between 90% and 110% of the peak force for the structure without imperfections. The average compactness is 0.95 and the minimum compactness is 0.9. The minimum force required is between 90% and 105% of the minimum force for the structure without imperfections and the snap-through magnitude is between 90% and 110% of the snap-through magnitude for the structure without imperfections.

The results of the 100 simulations with a standard deviation of 0.1% are still acceptable because of the minimum compactness of 0.7 (with an average of 0.9). The peak force is between 75% and 120% of the peak force for the structure without imperfections. The minimum force required is between 65% and 110% and the snap-through magnitude is between 80% and 120% of the structure without imperfections.

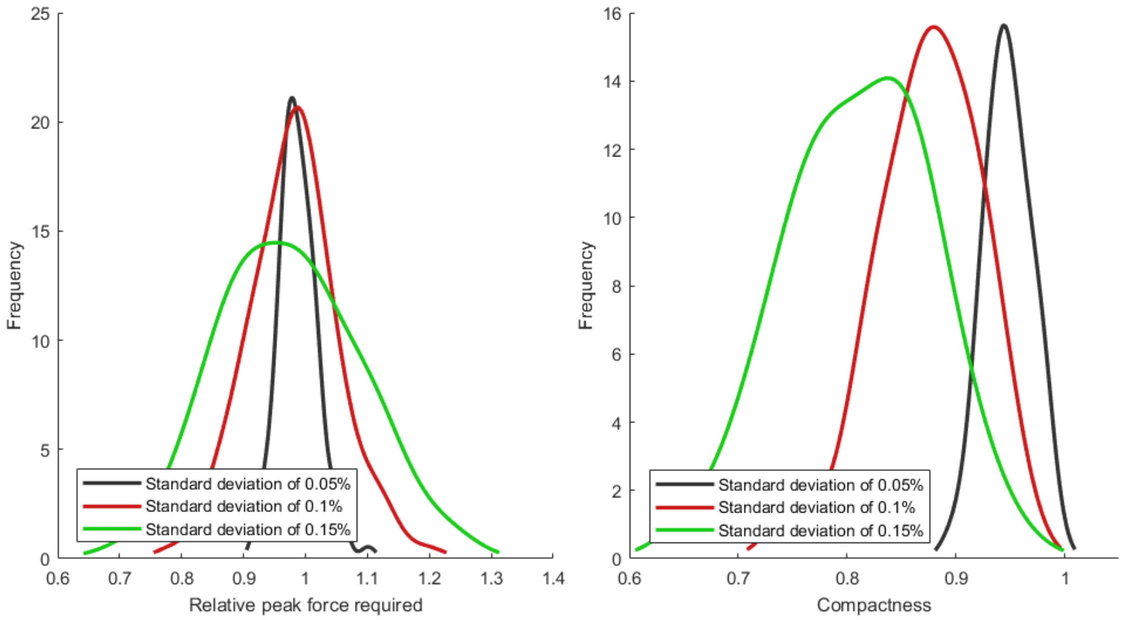

Figure 3.40: Comparison of the probability density functions for the peak load (left) and the compactness (right) for 100 simulations with random values for the tolerances on all of the beam lengths of the module with a standard deviation of 0.05%, 0.1% and 0.15%.

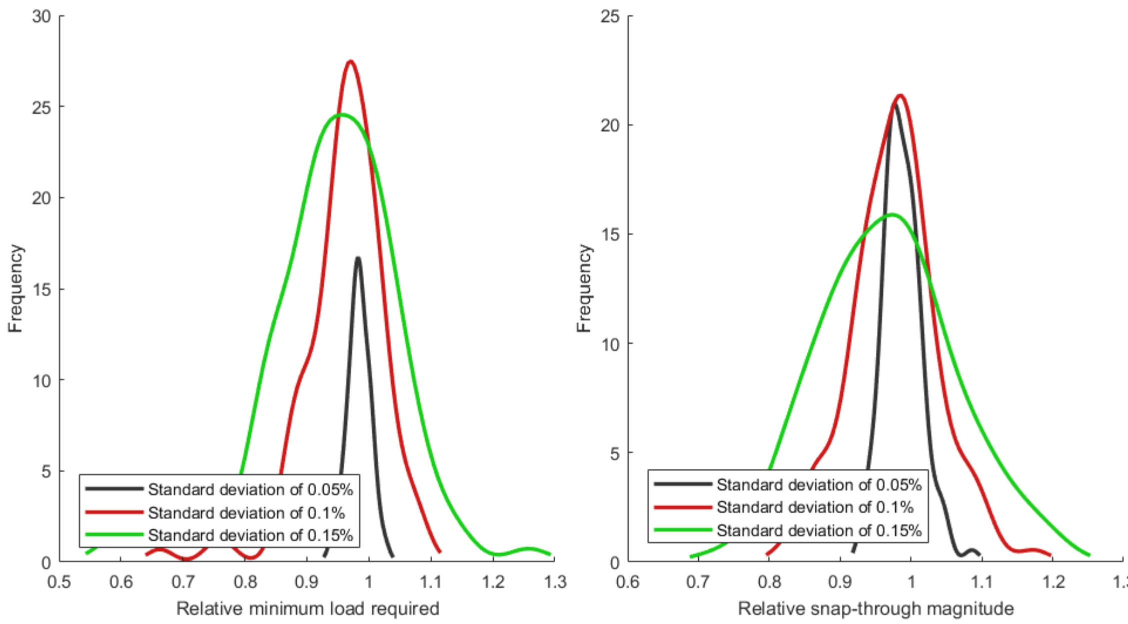

Figure 3.41: Comparison of the probability density functions for the minimum load required (left) and the snap-through magnitude (right) for 100 simulations with random values for the tolerances on all of the beam lengths of the module with a standard deviation of 0.05%, 0.1% and 0.15%.

The results of the 100 simulations with a standard deviation of 0.15% are not acceptable, since the minimum compactness is only 0.6 (which means that the structure can be folded a bit more than halfway) with an average of 0.8. The peak force is between 65% and

130%, the minimum force between 55% and 130% and the snap-through magnitude between 70% and 125% of the structure without imperfections.

3.1.4 Hinge misalignment

The hinges are a crucial part during the deployment of a scissor structure. Ideally, the rotation of the members is perpendicular to the plane of the SLE. Because of manufacturing imperfections, this hinge axis can be misaligned.

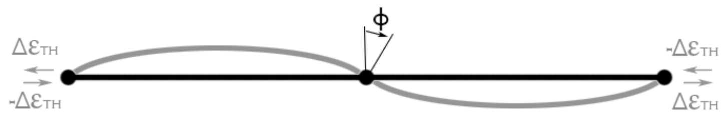

Figure 3.42: Imperfections on the hinge axis misalignment.

Normally, the rotation of an SLE should be around the axis perpendicular to the plane of the SLE. A hinge misalignment originates from a hole in a beam that is not bored perfectly perpendicular to the beam axis during manufacturing. This implies that the hole has to be forced to become straight when introducing the pivot, resulting in initial stress in the beam. If we take into account tolerances on the orientation of the axis of rotation, parasitic values of the rotation of the other components will appear and therefore the resultant axis of rotation will be misaligned creating a deviation of the rotation (Dupont, 2014). This effect introduces an out-of-plane displacement of the scissor-like element or introduces stresses inside the members when the displacement is prevented by the elements in the module.

The misalignment of the hinge axis is modelled by using a thermal strain gradient in the cross-section of the beam, which leads to a pre-bent beam when it is assembled to the other members in the structure (Figure 3.43). The beam dimensions and the hinge positions remain the same while modelling the hinge misalignment.

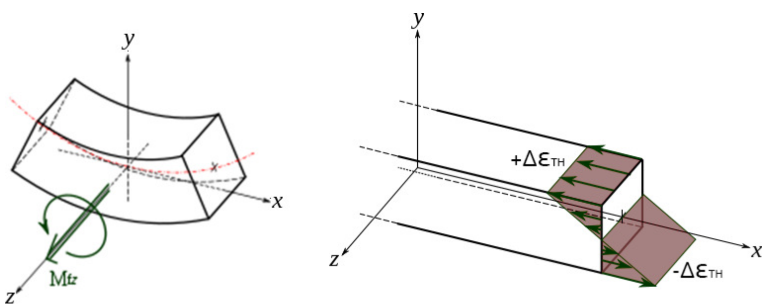

Figure 3.43: Pre-bent beam by a thermal strain gradient in the cross-section.

Only the pivot points will be considered (i.e. the intermediate hinges in the SLE's). The initial stress is modelled by using a gradient of thermal strain in the cross-section of the beam. The temperature in equation 3.1 is defined as:

$$\theta = \bar{\theta} + \frac{\partial \theta}{\partial x_1} x_1 + \frac{\partial \theta}{\partial x_2} x_2 \tag{3.2}$$

with $\bar{\theta}$ the temperature of the beam axis and $\frac{\partial\theta}{\partial x_1}$ and $\frac{\partial\theta}{\partial x_2}$ the gradients of temperature with respect to the local x_1 and x_2 axes (Dassault Systèmes Simulia Corp., 2012c).

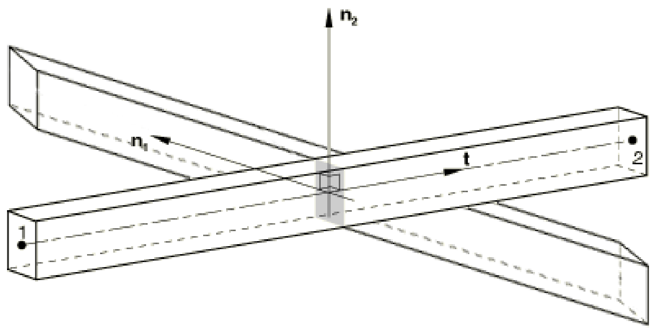

Figure 3.44: Local axis definition for a beam in an SLE.

Only the thermal gradient along the local axis perpendicular to the SLE plane is considered (n_1 in Figure 3.44), since this causes the hinge axis to not be perpendicular to the SLE plane any more. A thermal gradient along the local axis in the SLE plane (n_2 in Figure 3.44) would not cause bending of the beam, because the hinge axis would remain perpendicular to the SLE plane. The misalignment angle ϕ is linked to the thermal strain gradient as follows:

$$\phi = \arctan \frac{\Delta\epsilon_{TH} l}{t} \tag{3.3}$$

with l the length of the beam with the thermal gradient and t the thickness of this beam along the considered local axis.

3.1.4.1 Imperfections on separate hinges

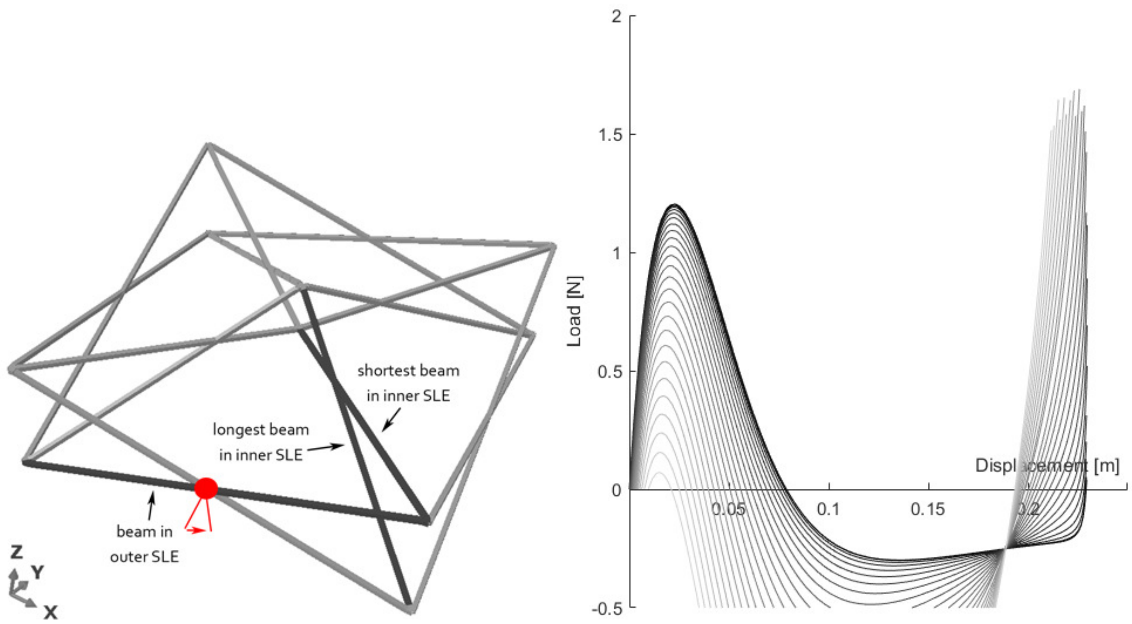

Figure 3.45: Hinge misalignment in an outer SLE (left) and the variation of the load required for folding (right).

Figure 3.45 represents the change in the load-displacement curve when there is a misalignment of the hinge axis in a beam element of an outer SLE. The darkest curve represents the load-displacement curve of the idealised model. The curves become gradually lighter as the imposed misalignment of the hinge axis increases. For each step, the strain of the semi-lengths of the beam is increased with a gradient from -0.01% to 0.01%. In this case, the semi-length of the beam is 38.9 cm. One side of the cross-section is elongated with 0.0389 mm in each step while the other side is shortened with 0.0389 mm. One side of the hinge will thus be 0.0778 mm misaligned with the other side. The cross-section of the beam has a width of 9 mm. This means that the hinge misalignment is 0.5°. This way of thinking is translated in formula 3.3.

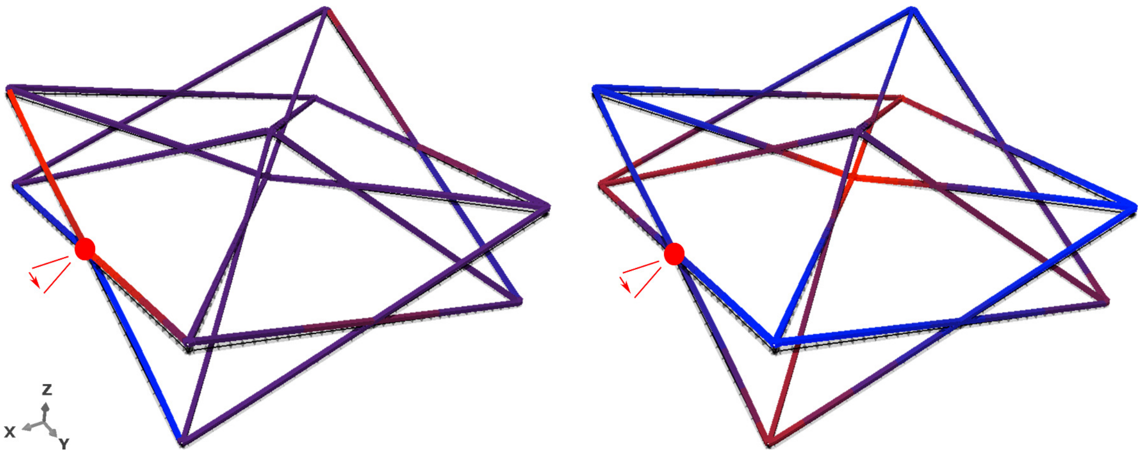

Figure 3.46: Bending moments (blue is positive, red is negative) in the initial configuration when there is hinge misalignment in an outer SLE (left) and displacements (blue is the largest displacement, red is zero) of the nodes (right).

In this case, the misalignment of the hinge to one side or the other has the same influence on the deployment behaviour of the module (Figure 3.45). When the thermal gradient in the cross-section of the beam is increased, the beam is forced to bend in the initial configuration (Figure 3.46 left). Because of the misalignment of the axis, the other beam in the outer SLE will also be forced to bend. Because of these introduced incompatibilities, the corners of the module will be forced upwards, as is the upper centre node. For the same reason as in previous cases, the peak load will decrease.

In Figure 3.47 (left), the peak load is given in function of the misalignment angle of the hinge. When increasing the hinge misalignment, the required folding load decreases rapidly.

In Figure 3.47 (right), the compactness of the module is given. A value of 1 corresponds again to the folded configuration of a module without imperfections, while a value of 0 corresponds again to a module that cannot be folded. When the hinge misalignment increases, the compactness decreases, but it stabilises at a value of 0.8.

In Figure 3.48 (left), the minimum load required for folding is given as a function of the hinge misalignment. When the hinge misalignment is increased, the negative loads become more dominant, which will be dangerous when folding the structure. The change in this minimum load is huge, for a misalignment of 10° (which is the maximum considered

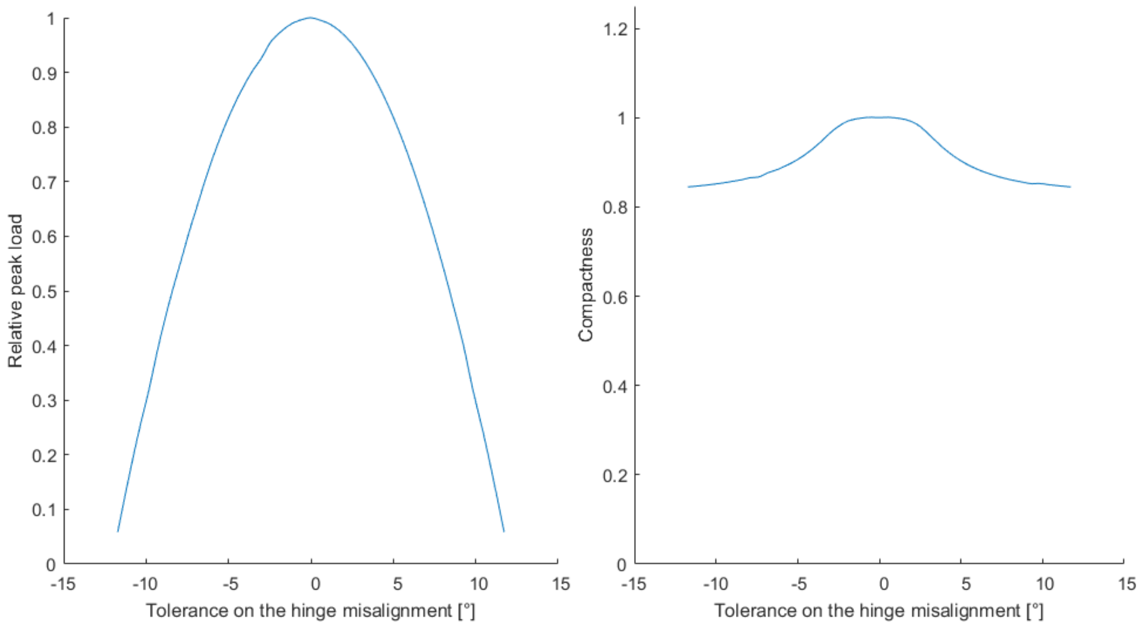

Figure 3.47: The variation of the peak load required for folding when there is hinge misalignment in an outer SLE (left) and the compactness of the module (right).

misalignment, and which is not realistic), the minimum load is 7 times the minimum load for the structure without imperfections. By consequence, the snap-through magnitude also increases when increasing the misalignment of the hinge. For a misalignment of 10°, the snap-through magnitude is 1.5 times the snap-through magnitude of the structure without imperfections.

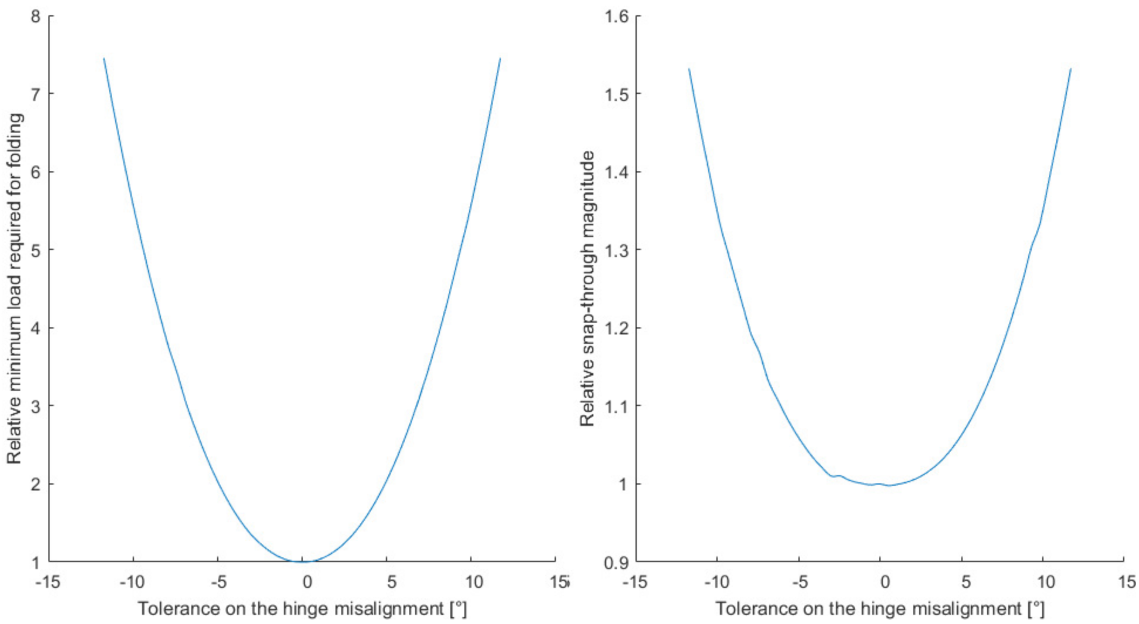

Figure 3.48: The variation of the minimum load required for folding when there is hinge misalignment in an outer SLE (left) and the magnitude of the snap-through (right).

Figure 3.49 represents the change in the load-displacement curve when there is a misalignment of the hinge axis in the shortest beam element of an inner SLE. Again, the

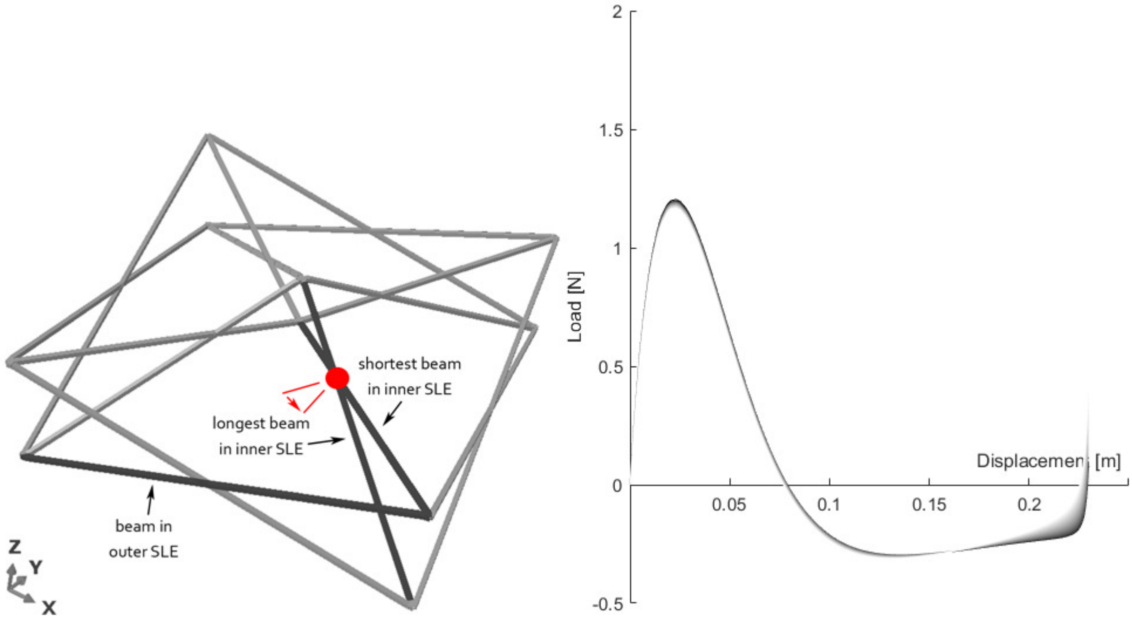

Figure 3.49: Hinge misalignment along the shortest beam in an inner SLE (left) and the variation of the load required for folding (right).

influence is the same whether the misalignment is to one side or the other. When increasing the axis misalignment, the required folding load only slightly decreases. This is due to the fact that the inner beams bend during deployment. For the deployment process, it does not matter if the beams bend in-plane or buckle out-of-plane, so a misalignment of the hinge forces the beams to bend in a certain direction without altering the deployment response a lot.

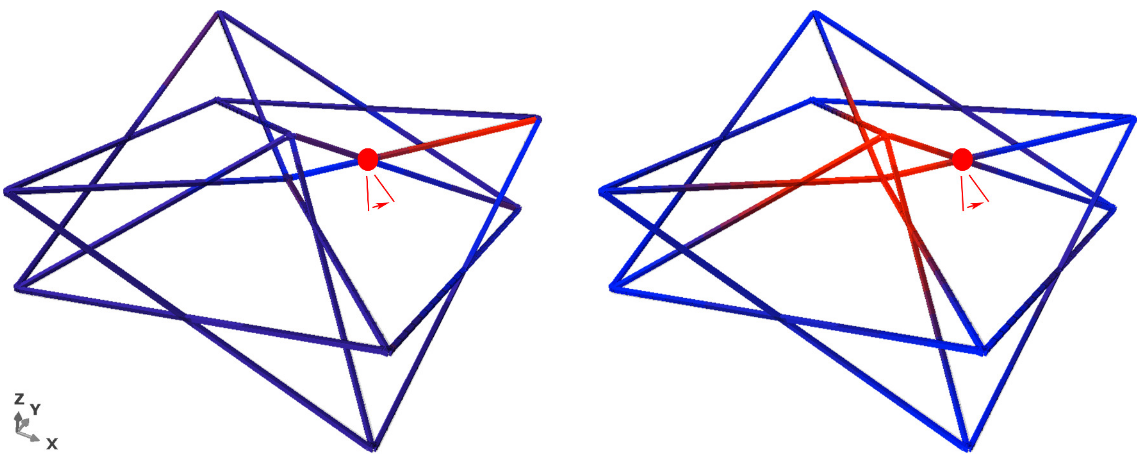

Figure 3.50: Bending moments (blue is positive, red is negative) in the initial configuration when there is hinge misalignment in an inner SLE (left) and displacements (blue is the largest displacement, red is zero) of the nodes (right).

When the thermal gradient in the cross-section of the shortest beam in an inner SLE is increased, the beam is forced to bend in the initial configuration (Figure 3.50 left). Because of the misalignment of the axis, the longest beam in the inner SLE will also be forced to bend. Because of these introduced incompatibilities, the corners of the module will be forced upwards, as is the upper centre node. For the same reason as in previous cases, the peak load will decrease, but in this case, the influence of the misalignment of the hinge can be ignored because it forces the beams to bend in a certain way without altering the deployment response.

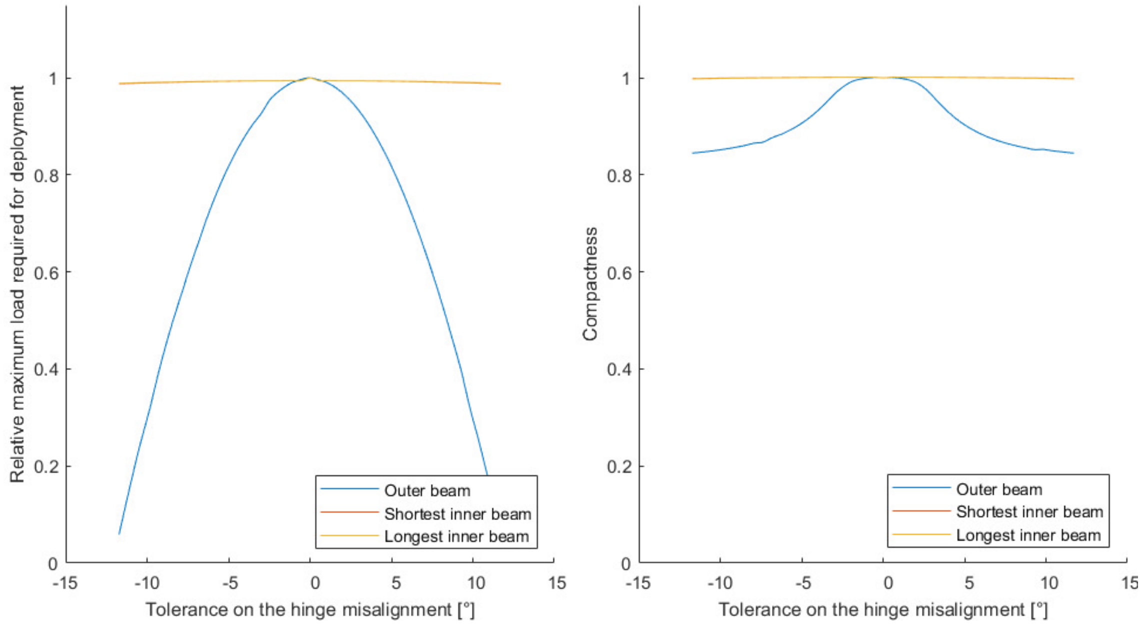

Figure 3.51: The variation of the peak load required for folding (left) and the compactness of the module (right).

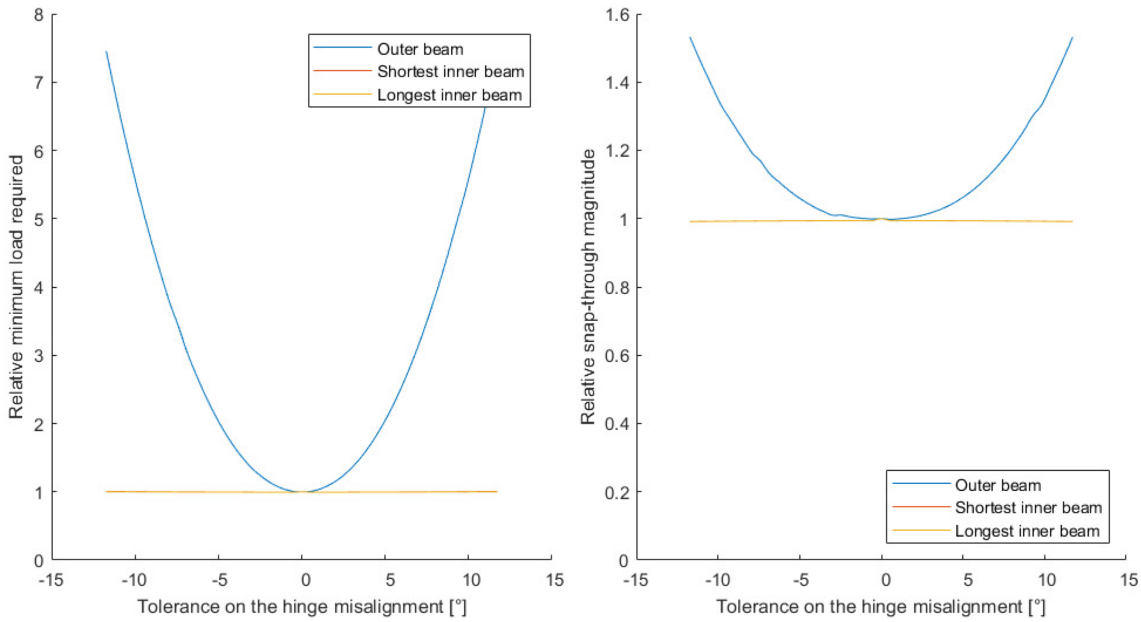

Figure 3.52: The variation of the minimum load required for folding (left) and the magnitude of the snap-through (right).

When there is a misalignment of the hinge axis in the longest beam of an inner SLE, again, the influence is the same whether the misalignment is to one side or the other and again, when the axis misalignment is increased, the required folding load only slightly decreases. The influence is exactly the same as the influence of the misalignment of the hinge axis in the shortest beam of an inner SLE.

In this case, hinge misalignment mainly has an influence on the deployment behaviour of this bistable scissor module when there is a misalignment of the hinge axis in beam elements in outer SLE's. The difference is not due to the stiffness contrast between inner and outer SLE's, which is verified by doing the same simulations for inner SLE's with a comparable stiffness to the outer ones. The results were quantitatively exactly the same.

In Figure 3.51 and 3.52, the comparison is shown between misalignment of the hinge on the three different beams separately for the peak load, the compactness, the minimum load required for folding and the magnitude of the snap-through.

3.1.4.2 Simultaneous imperfections in outer SLE hinge misalignment

In order to investigate realistic tolerances for the misalignment of the hinge axes, they have to be modelled simultaneously. To define the tolerances on the hinge misalignment, a random distribution has been introduced with mean value 0 and the standard deviation is defined as the angle of misalignment of the hinge. 100 simulations are performed with a standard deviation of 0.5°, 1.5° and 2.5°. For the largest value (2.5°), 99.7% of the values for the misalignment will be lower than 7.5°, which implies already a minimum force that is almost 4 times the minimum force for the structure without imperfections (Figure 3.52 left).

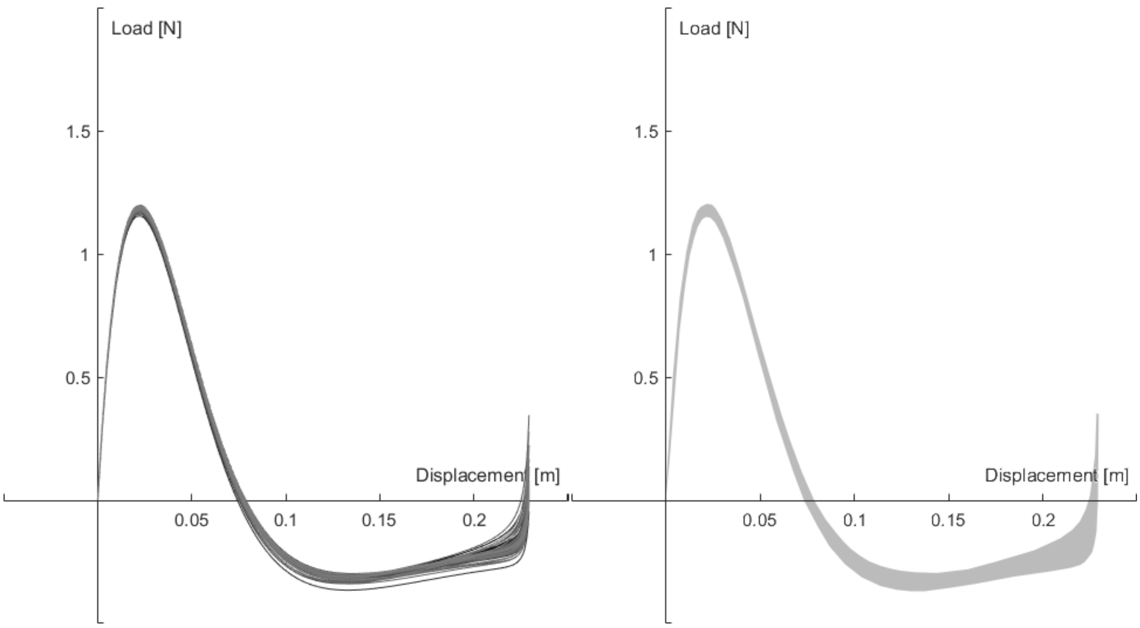

Figure 3.53: Load-displacement curves for 100 simulations with random values for the tolerances on the hinge misalignment with a standard deviation of 0.5° (left) and the range of the load-displacement curves (right).

The results of 100 simulations with a standard deviation of 0.5° are given in Figure 3.53 (left). The range of the load-displacement curves is given in Figure 3.53 (right).

In Figure 3.54 and 3.55, the frequency is given for the relative peak force, the compactness, the relative minimum load and the relative snap-through magnitude.

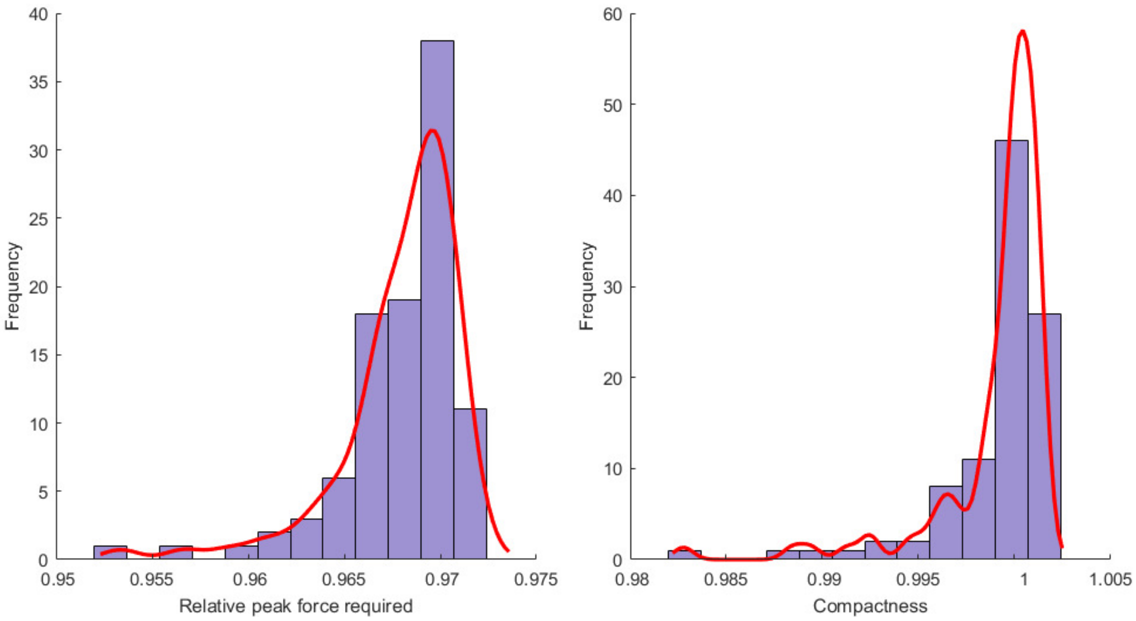

Figure 3.54: Frequency of the peak load (left) and the compactness (right) for 100 simulations with a standard deviation of 0.5° for the misalignment of the hinge.

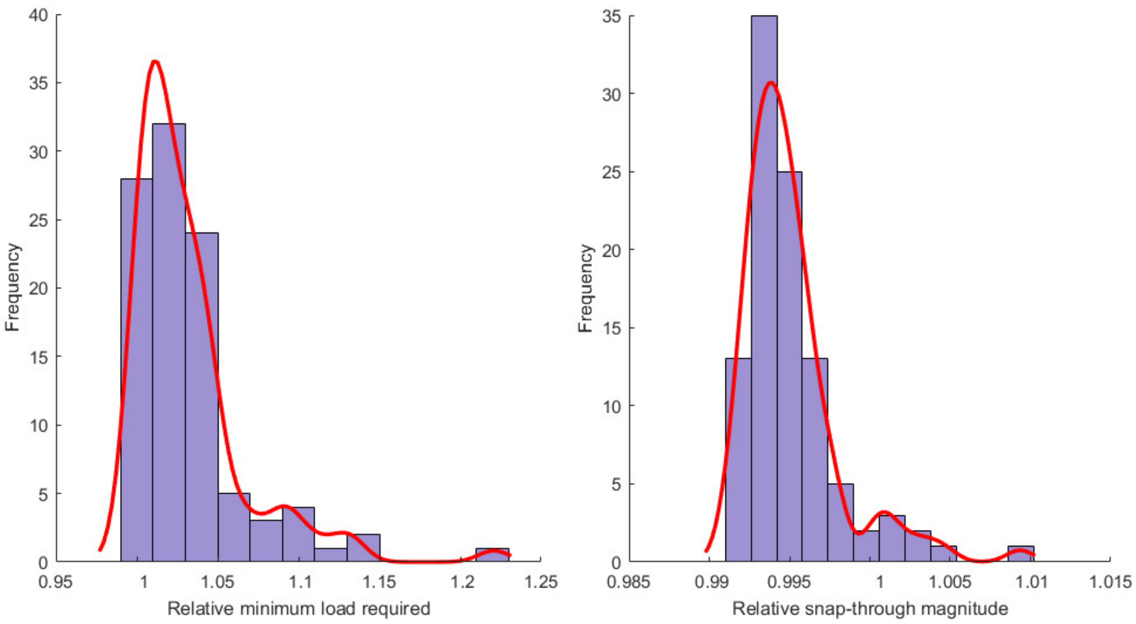

Figure 3.55: Frequency of the minimum load required (left) and the snap-through magnitude (right) for 100 simulations with a standard deviation of 0.5° for the misalignment of the hinge.

As can be seen in Figure 3.54 (right), the compactness will not be the limiting factor in this case, as was the case for the imperfections on the beam lengths and the imperfections on the position of the pivot points. The limiting factor will be the minimum load required for folding and, by consequence, the snap-through magnitude.

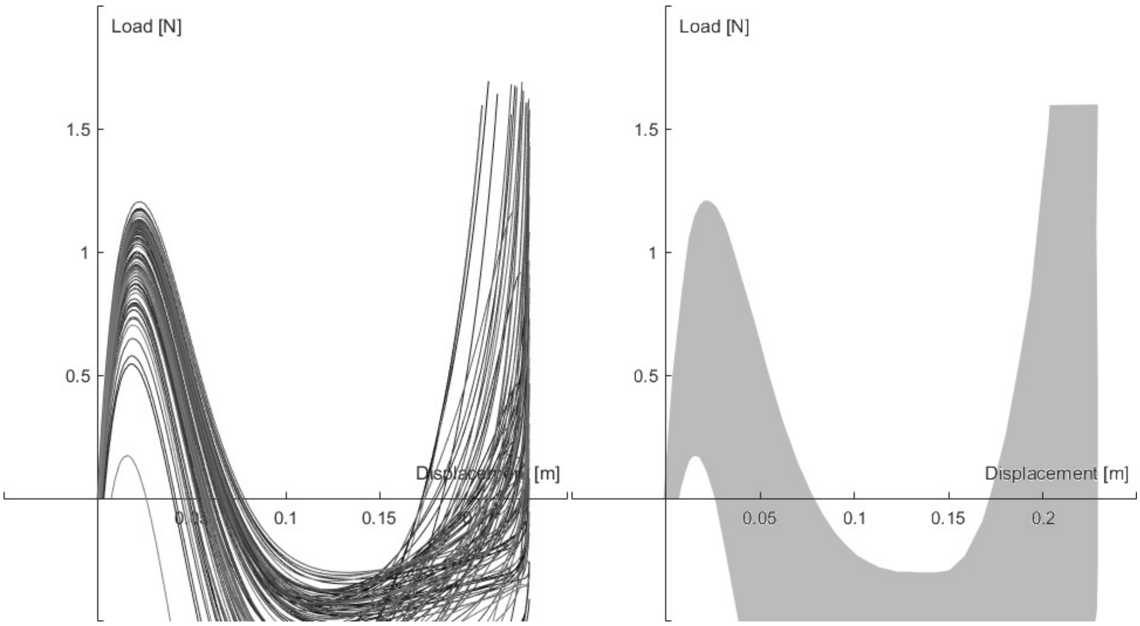

Figure 3.56: Load-displacement curves for 100 simulations with random values for the tolerances on the hinge misalignment with a standard deviation of 2.5° (left) and the range of the load-displacement curves (right).

To compare, the load-displacement curves of 100 simulations with a standard deviation of 2.5° are given in Figure 3.56 (left) and their range is given in Figure 3.56 (right).

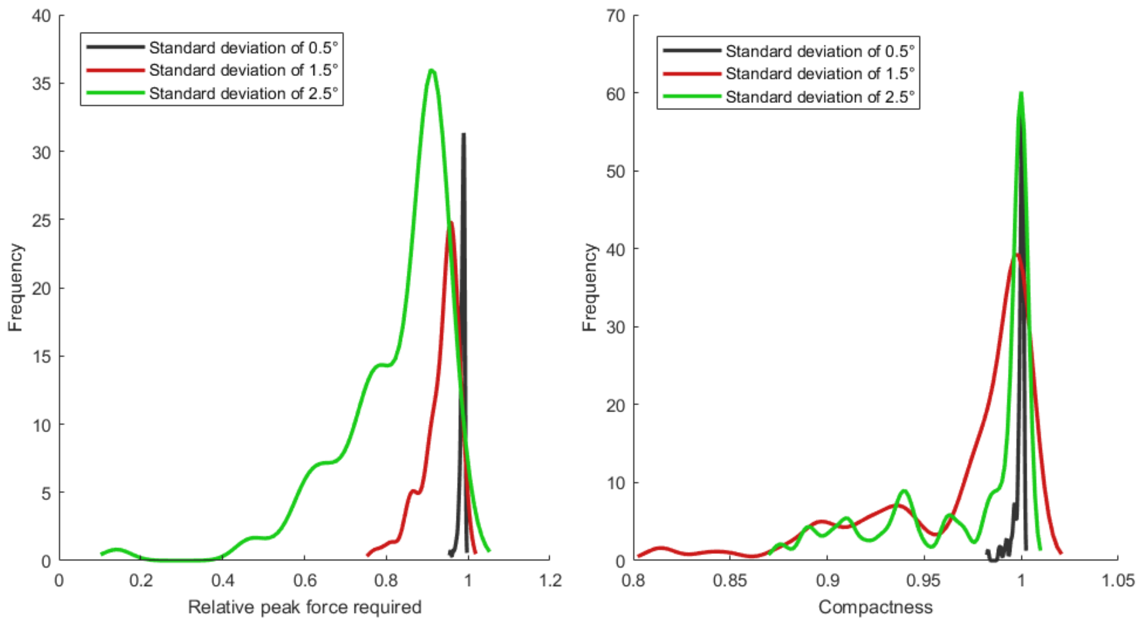

Figure 3.57: Comparison of the probability density functions for the peak load (left) and the compactness (right) for 100 simulations with random values for the tolerances on the misalignment of all the hinges of the module with a standard deviation of 0.5°, 1.5° and 2.5°.

In Figure 3.57 and 3.58, the comparison of the 100 simulations with a standard deviation of 0.5°, 1.5° and 2.5° is given by comparing the probability density functions for the peak load, the compactness, the minimum load required for folding and the snap-through magnitude.

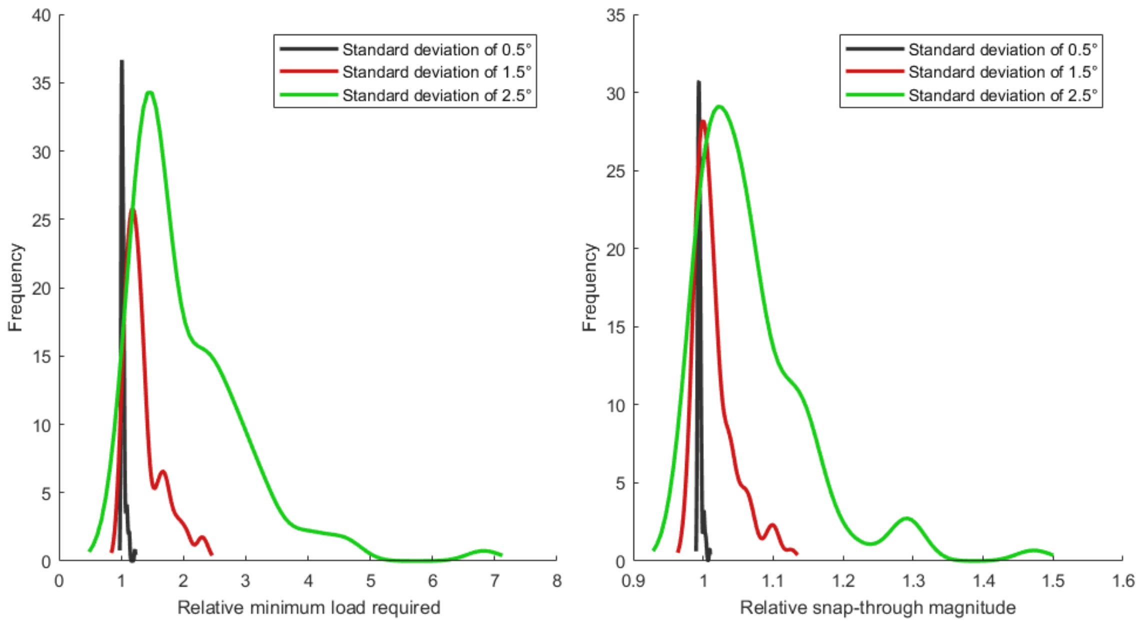

Figure 3.58: Comparison of the probability density functions for the minimum load required (left) and the snap-through magnitude (right) for 100 simulations with random values for the tolerances on the misalignment of all the hinges of the module with a standard deviation of 0.5°, 1.5° and 2.5°.

With a deviation of 0.5°, the peak force is between 95% and 100% of the peak force for the structure without imperfections. The minimum compactness is 0.98, the minimum force required is between 95% and 120% and the snap-through magnitude is between 98% and 100% of the snap-through magnitude for the structure without imperfections.

The results of the 100 simulations with a standard deviation of 1.5° are not acceptable because the differences in the minimum force required for folding are too high (between 85% and 250% of the structure without imperfections), which leads to a dangerous deployment. The peak force is between 75% and 100% of the peak force for the structure without imperfections, the minimum compactness is 0.87 and the snap-through magnitude is between 90% and 150% of the structure without imperfections.

The results of the 100 simulations with a standard deviation of 2.5° (Figure 3.56) are even less acceptable, as expected. The minimum force is between 50% and 700% of the structure without imperfections, which is a huge difference. The peak force is between 10% and 105%, the minimum compactness 0.98 and the snap-through magnitude between 90% and 150% of the structure without imperfections.

To conclude, misalignment of the hinge axes is acceptable when the standard deviation is below 0.5°. This allowable tolerance is rather limited, which is a motivation to investigate the influence of flexible hinges to correct the influence of hinge misalignment.

3.2 Non perfect hinge behaviour

3.2.1 Flexible hinges

In the previous analyses, the mid beam joints had a theoretical perfect rigidity for all translations and rotations except for one released rotation to simulate a scissor mechanism. However, in reality the stiffness of the connections is finite, allowing for some flexibility. A variation in joint stiffness is examined by allowing additional rotations in the joints or misalignment of the hinge axis. Allowing additional rotations represents a rubber bearing around the pin in the hole which connects the two beams of an SLE.

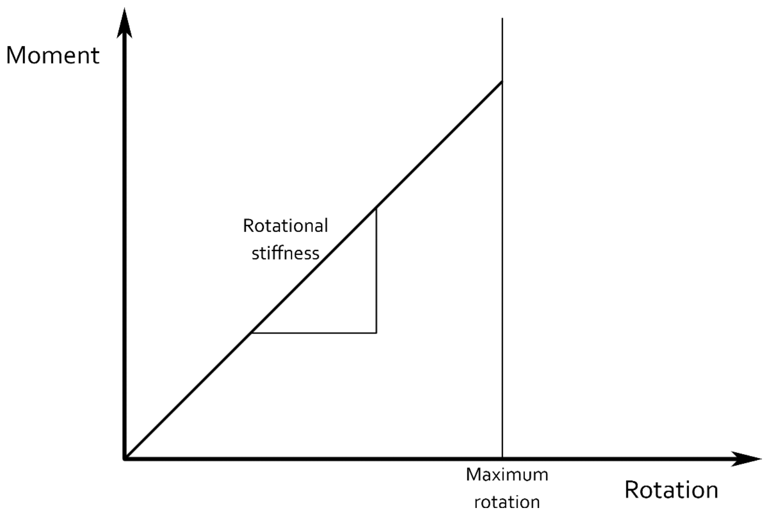

Figure 3.59: Principle of the additional allowable rotations around the other axes.

It is realistic to define a maximum allowable rotation around the axes other than the hinge axis, which corresponds to the tolerance on the difference between the hole and the pin radius. For the additional rotations, a rotational stiffness should be defined (Figure 3.59). A certain value can be taken for this rotational stiffness corresponding to a rubber bearing for example, which can be placed around the pin in the hole (Figure 3.60). To take into account a more realistic approach for this hinge stiffness, a non linear rotational stiffness can be considered in the future.

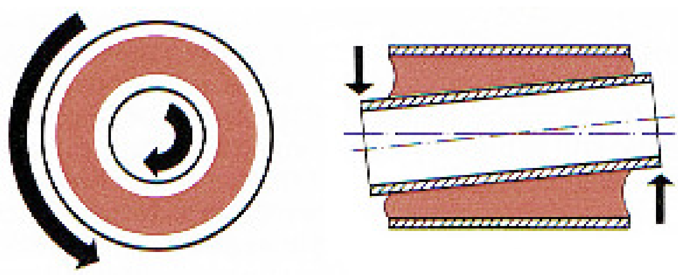

Figure 3.60: Front view of the torque on a pin in a hole with rubber bearing (left) and side view of the additional rotational freedom of this pin (right) (Euro-bearings Ltd., 2016).

When allowing additional rotations around the other axes of 17° (which approximately corresponds to the dimensions of Figure 3.60) and having a rotational stiffness of 200

Nm/°, the deployment behaviour of the idealised module is almost not altered, except for the last part of the load-displacement curve (Figure 3.61 left). Allowing additional rotations during deployment allows the structure to be a little bit more compact in the folded state.

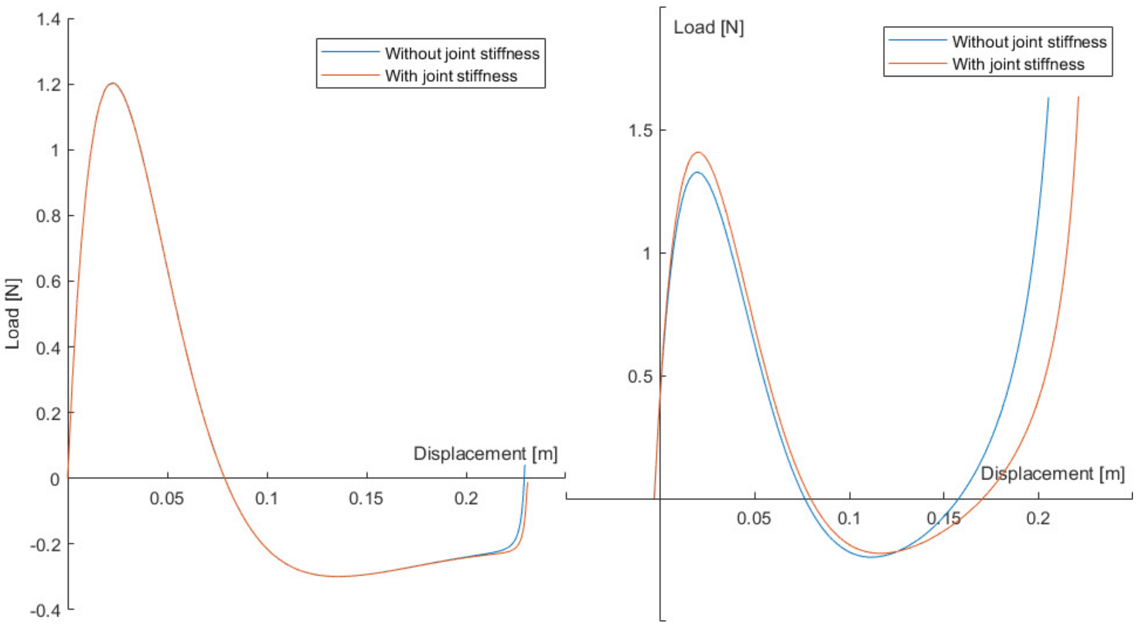

Figure 3.61: Load-displacement curves for the model without imperfections and for a model where additional rotations of 17° are allowed (left) and the comparison of the load-displacement curves with an imperfection of 1% on the beam length without and with finite hinge stiffness (right).

The influence of the finite hinge stiffness will be more important when combining imperfections. To investigate the effect of hinge stiffness on a module with imperfections on the beam lengths, a module with an imperfection of 1% on the beam length is modelled without allowing additional rotations and compared with a module where additional rotations were allowed (Figure 3.61 right). In this example, including the finite hinge stiffness is beneficial, because the compactness in the folded state is increased.

Allowing additional rotations together with imperfections on the misalignment of hinges will be even more important. These additional rotations counteract the influence of hinge misalignment on the deployment behaviour and the problem encountered when investigating the influence of hinge misalignment will be smoother. This is very beneficial, since hinge misalignment was only acceptable when the standard deviation of the misalignment was below 0.5°, which is very limiting.

To verify this statement, 100 simulations were run with imperfections on the hinge misalignment with a standard deviation of 1.5°, which was not acceptable, while additional rotations were allowed of 17° with a rotational stiffness of 200 Nm/°, 20 Nm/° and 2 Nm/° (Figure 3.62). The results are given in Figure 3.63 and 3.64.

With a rotational stiffness of 200 Nm/°, the results are already better than for the case without flexible hinges, but the smaller the rotational stiffness, the better the results and

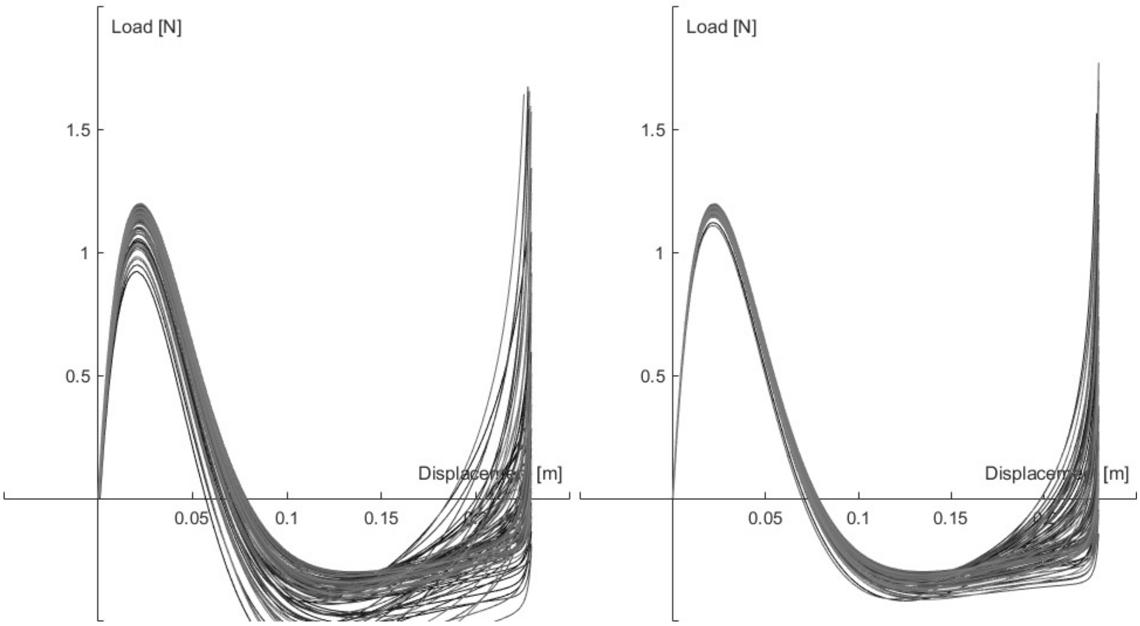

Figure 3.62: Load-displacement curves for 100 simulations with random values for the tolerances on the misalignment of all the hinges of the module with a standard deviation of 1.5°, for the structure without flexible hinges (left) and with flexible hinges with a rotational stiffness of 2 Nm/° (right).

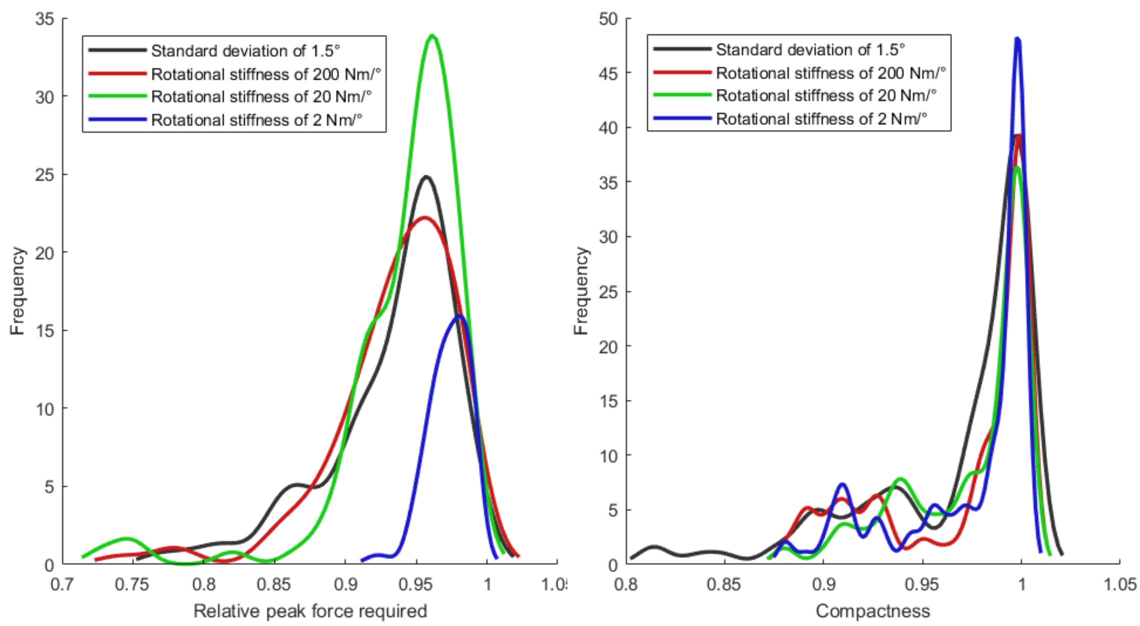

Figure 3.63: Comparison of the probability density functions for the peak load (left) and the compactness (right) for 100 simulations with random values for the tolerances on the misalignment of all the hinges of the module with a standard deviation of 1.5°, for the structure without flexible hinges, with flexible hinges with a rotational stiffness of 200 Nm/°, 20 Nm/° and 2 Nm/°.

the smaller the range for the peak load, compactness, minimum force and snap-through magnitude.

The finite hinge stiffness does have a very small influence on the deployment behaviour

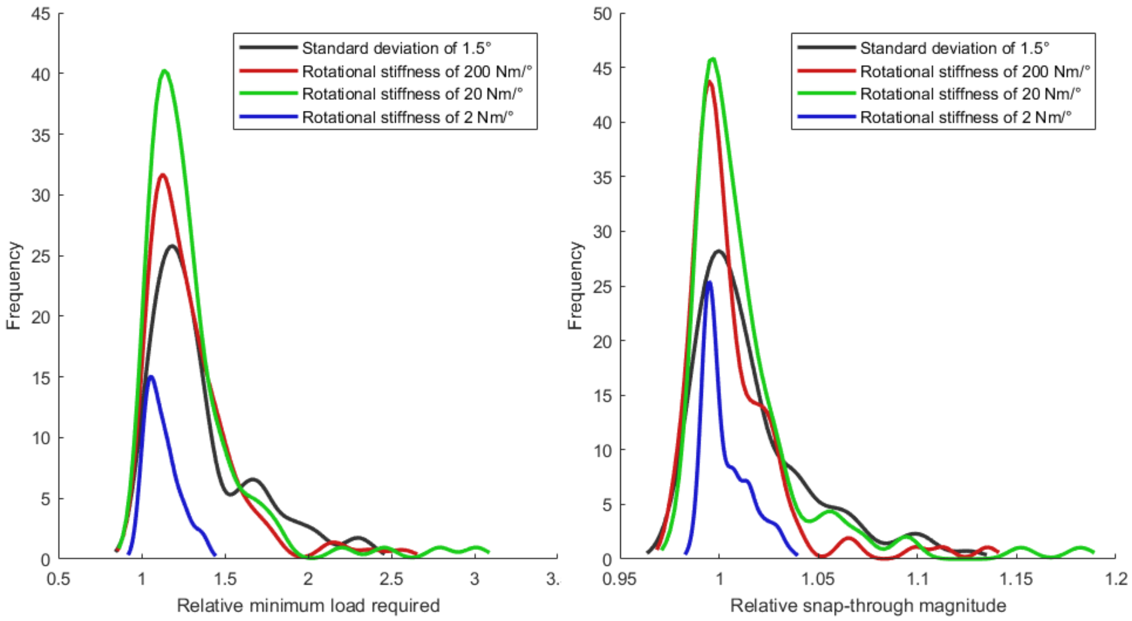

Figure 3.64: Comparison of the probability density functions for the minimum load required (left) and the snap-through magnitude (right) for 100 simulations with random values for the tolerances on the misalignment of all the hinges of the module with a standard deviation of 1.5°, for the structure without flexible hinges, with flexible hinges with a rotational stiffness of 200 Nm/°, 20 Nm/° and 2 Nm/°.

of bistable scissor structures. The higher the rotational stiffness of the rubber bearings, the smaller the influence of the flexible hinges, because the rotational stiffness is higher and the additional rotations are retarded. In the considered case, additional rotations of 17° were allowed, which can counteract the influence of hinge misalignment.

3.2.2 Friction in the hinges

Friction is always present and it is difficult to control, although it can be changed by the choice of the hinges and by tightening them. Friction is not desired, since additional loads are necessary in order to overcome the friction (Gantes, 2001). There exists a friction model that Gantes has derived (appendix C), but it overestimates the friction significantly, because the end nodes of the beams of a scissor-like element are forced to be in a common plane, which causes deformation of the beams. Because of this deformation, forces between the beams are generated which add up to a frictional moment that resists rotation. This permanent bending of the beams is not desired, to avoid permanent residual stresses inside the elements. Better solutions exist in which the beams do not lie in one plane and in practice, friction is often designed to be reduced. For planar scissor structures, Dupont found that the influence of friction is small in comparison to other imperfections such as tolerances on the beam lengths (Dupont, 2014).

The Coulomb friction model is useful in many applications in spite of its simplicity, while it can still explain several phenomena associated with friction. The friction force F_f acts as internal force in the tangential direction of the contacting surfaces. Below a critical value it is a reaction force causing no relative motion between the contacting surfaces. At a critical value μF_N, where F_N is the normal force exerted by each surface on the other, perpendicular to the surface and with μ the friction coefficient, the force obeys a constitutive equation such as Coulomb's law and acts in a direction opposite to the relative velocity (Gaul & Nitsche, 2001).

The most frequently used model is Coulomb's law. The friction force is given by

$$F_f \leq \mu F_N \tag{3.4}$$

In the case of the joints used in scissor modules, the friction force represents the friction moment in the hinges. The friction moment is derived from the coulomb friction moment as in Figure 3.65. k is a function of μ and F_N. The contact force F_N is automatically generated by Abaqus based on the connection type. To calculate this contact force, the resultant of the forces which produce the moment between the two beams, as well as an optional tightening force of the hinge is taken into account.

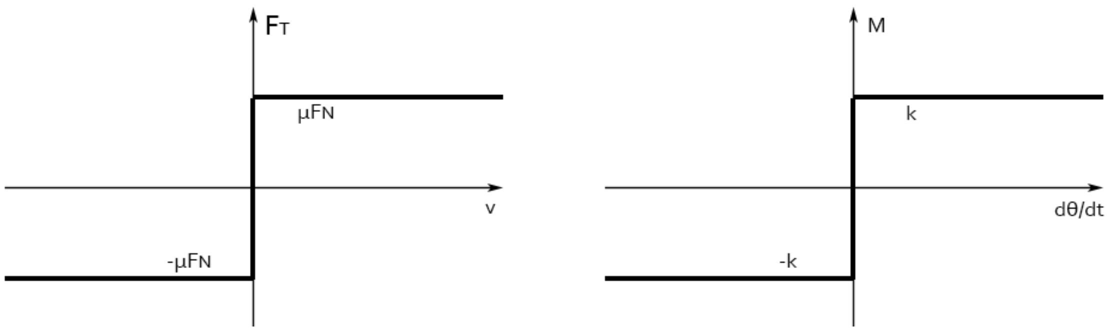

Figure 3.65: The coulomb friction force (left) and the derived coulomb friction moment (right).

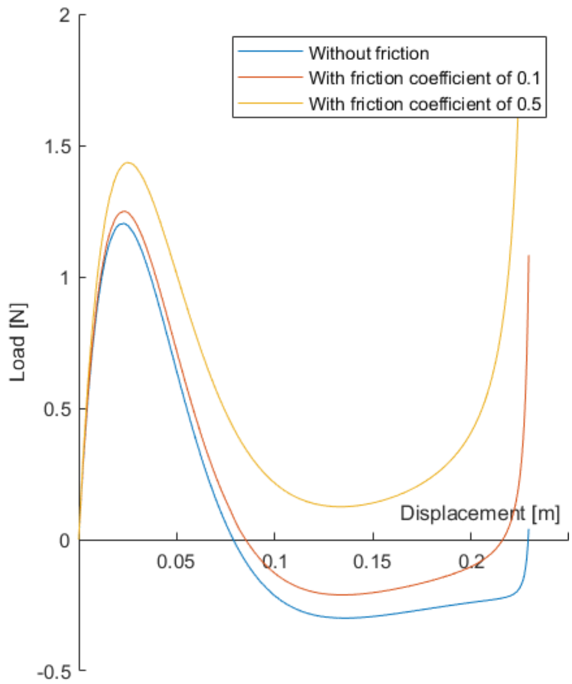

Figure 3.66: Comparison of the load-displacement curves without friction, with a friction coefficient of 0.1 and with a friction coefficient of 0.5.

The friction is implemented in the model for two values of the friction coefficient: 0.1 and 0.5, which is the range described by Gantes (Gantes, 2001) and Dupont (Dupont, 2014). The results are given in Figure 3.66.

When taking into account friction, the force required for folding will always be higher than in the idealised case because of frictional dissipation.

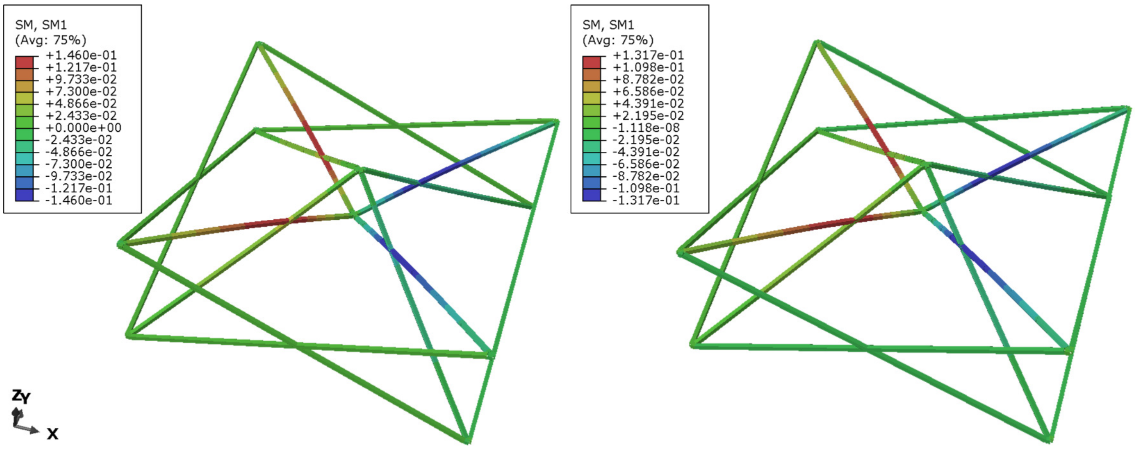

Figure 3.67: Comparison of the bending moment for the configuration for which the maximum load is needed for folding without friction (left) and with friction (right) with a friction coefficient of 0.5.

In Figure 3.67 and 3.68, the bending moments in the structure with and without friction are compared for the configuration for which the maximum and minimum load is required for folding. For the configuration in which the maximum force is required (Figure 3.67), the bending moment is higher for the structure without friction. This is due to the bending which is retarded because of the friction.

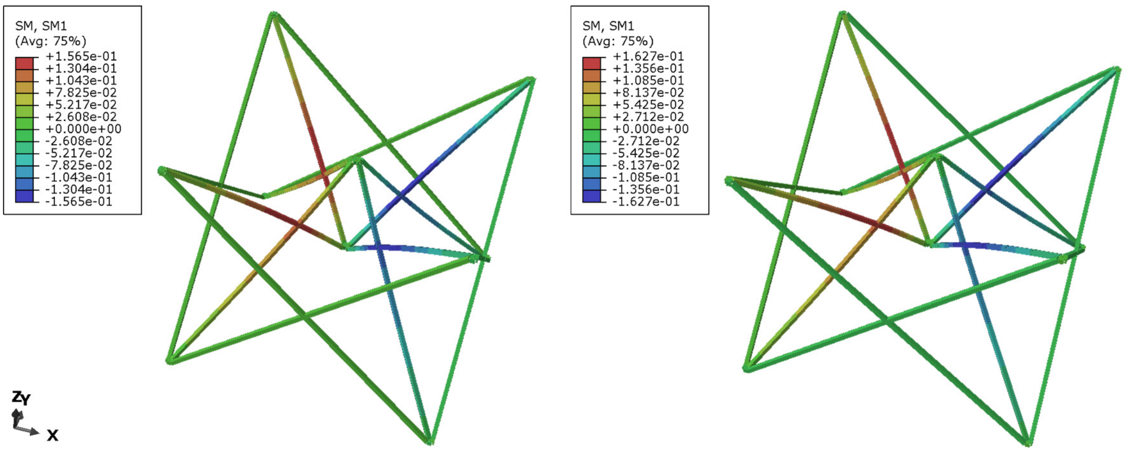

Figure 3.68: Comparison of the bending moment for the configuration for which the minimum load is needed for folding without friction (left) and with friction (right) with a friction coefficient of 0.5.

For the configuration in which the maximum force is required (Figure 3.68), the bending moment is higher for the structure with friction. This is because for the structure without friction, the beams already become straight again after the snap-through, while for the structure with friction, the beams are still more bent because the folding is retarded.

3.3 Discussion

Manufacturing defects and imperfect hinge behaviour are naturally present in all engineered structures and were investigated in this chapter. Two types of imperfections were identified, geometrical imperfections (finite hinge size, tolerances on the beam lengths, eccentricity of the pivot points and hinge misalignment) and imperfect hinge behaviour (finite hinge stiffness and friction).

Joint are technically always present and including their dimensions in the numerical model has an overall stiffening effect, which is larger when the joint dimensions are larger.

When introducing tolerances on the beam lengths, the peak force changes as well as the minimum force and the snap-through magnitude because the initial configuration changes. The higher the imperfection, the lower the compactness of the structure in the folded state. The influence of imperfections on an outer beam is the opposite as imperfections on an inner beam and there is a bigger sensitivity for imperfections on the longest beam in an inner SLE. When introducing random imperfections, values for the strain on the beam length with a standard deviation of 0.1% are acceptable (which means that 99.7% of the values of within a range of -0.3% to 0.3%).

When introducing imperfections on the position of the SLE pivot points, again the initial configuration changes, leading to a change in the peak force, minimum force and the snap-through magnitude and a decrease of the compactness. The compactness decreases comparably for imperfections on the beam length as for a shift of the pivot point. For the peak force, the minimum force and the snap-through magnitude, the imperfections on the beam lengths seem to be slightly more important than a shift of the pivot points. As was the case for random imperfections on the beam lengths, values for the strain on the beam lengths with a standard deviation of 0.1% are acceptable.

The influence of a misalignment of a hinge in an outer SLE is huge for the peak load, minimum load and snap-through magnitude, but less important for the compactness. A misalignment of a hinge in an inner SLE almost has no influence on the deployment response. When introducing random imperfections, only the results of simulations with a standard deviation of 0.5° are acceptable. The structure is thus most sensitive to the variation of this parameter.

When using flexible hinges and allowing additional rotations around the other axes, the deployment behaviour of the idealised module is almost not altered, but flexible hinges can counteract the effect of imperfections, for example imperfections on the beam length and more important, it will counteract the influence of hinge misalignment, allowing a higher tolerance for imperfections on the hinge misalignment.

To model friction, which is always present, the Coulomb friction model is used. To calculate the friction, a friction coefficient, a tightening force and the resultant forces from the rotation are taken into account. The higher the friction coefficient, the higher will be the peak force as well as the minimum force.

Chapter 4

Numerical Analysis on Multi-Module Structures During Deployment

In this chapter, the numerical model developed for a single module was applied for the deployment analysis of structures consisting of many modules in order to investigate the effect of the increase in the complexity of the structure, as well as the influence of imperfections on their deployment behaviour.

Three structures were therefore selected. The first one is a flat multi-module structure consisting of 3 by 3 flat square polygonal modules (Figure 4.1 left), for example a roof. The second one is an arch, which is a curved multi-module structure consisting of 5 curved square modules (Figure 4.1 middle) that could be used for example to construct a cylindrical roof. The last one is a dome which consists of 4 square modules, 4 hexagonal modules and 1 octagonal module (Figure 4.1 right) e.g. an emergency shelter.

These structures are chosen to be able to compare the results for a simple flat structure, a curved structure composed of identical modules and a more complex structure composed of several different modules, all with practical relevance. The flat structure folds and unfolds in one plane, corresponding to a 1D deployment, the arch folds and unfolds while creating a single curvature in the structure, corresponding to a 2D deployment and the dome folds and unfolds while creating a double curvature in the structure, corresponding to a 3D deployment.

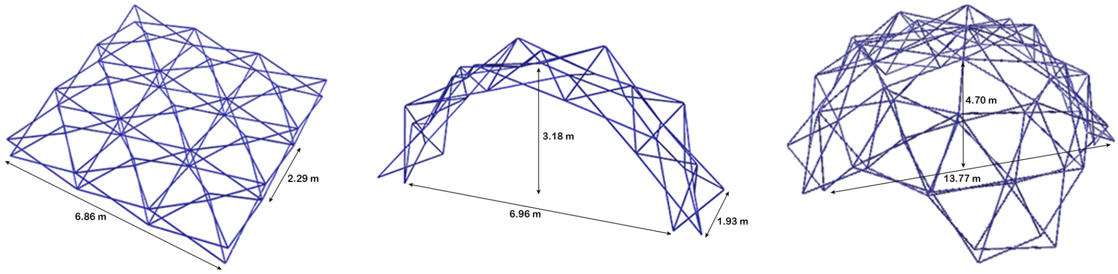

Figure 4.1: The flat multi-module structure (left), the arch (middle) and the dome (right).

To examine realistic structures, realistic dimensions were chosen for the modules (as opposed to the reduced scale models investigated previously). The current modules are chosen to be 3 times larger than the previously investigated module, resulting in beams between 1.5 and 2.5 meters for the flat roof and the arch. For the dome, the length of the beams is between 2 and 4.5 meters.

Square cross-sections are chosen over circular tubes because they are easier to connect to a joint in practice. Square cross-sections are chosen over rectangular ones for the sake of simplicity.

When assigning sections to the beams the following condition (Alegria Mira, 2010) about the ratio between the thickness t and the size of the square cross-section d is taken into account:

$$0.02 < \frac{t}{d} < 0.15 \tag{4.1}$$

The lower value is the minimum bound preventing local buckling phenomena (Eurocode 9, 2007), while the upper bound is set as commercially available; larger ratios are less structural efficient (Latteur, 2000). For this structure, beams with a hollow cross-section of 50x50x3 mm are chosen to start with, which corresponds to realistic values for cross-sections of beams in scissor structures (Gantes, 2001; De Temmerman, 2007; Alegria Mira, 2014).

Aluminium is chosen as the material for the beams because of its low density (2700 kg/m^3) and high relative strength (E = 70 GPa, σ_y = 600 MPa). Additionally, it is resistant to corrosion and recyclable, designating it as a sustainable material (Alegria Mira, 2014). HDPE is chosen as material for the beams that bend during deployment. It has a high strength-to-density ratio and is commonly recycled (ρ = 940 kg/m^3, E = 0.8 GPa, σ_y = 31.7 MPa). During deployment, it is checked under gravity loads that the stresses remain below the yielding strength for the chosen cross-sections.

The complete structures are analysed, because the symmetry of the structures is broken when applying imperfections. The initial state is the deployed configuration, because scissor structures are designed and built in this configuration. First, the folding of the idealised models with finite joint dimensions is investigated, with and without taking gravity into account. Gravity was included in the structural model and led to formulate the fundamental question of how to adjust the snap-through magnitude with respect to the gravity loads.

Realistic imperfections of all of the previously investigated types were introduced simultaneously in the multi-module models, to assess the global behaviour with and without these imperfections. Random imperfections of the beam lengths, on the position of the pivot point and on the hinge alignment are implemented together in the model, because it is realistic to consider these imperfections at the same time. The deployment behaviour of the idealised model is compared with the deployment behaviour when imperfections and gravity are taken into account.

The values for the imperfections are chosen according to the imperfections that were acceptable for the single bistable module in chapter 3. Random values for the imperfections on the beam lengths are modelled with a standard deviation of 0.1% of the total beam length. The random values for the position of the pivot point are also defined with a standard deviation of 0.1% of the total beam length and the random values for the misalignment of the hinge axes are defined with a standard deviation of 0.5° misalignment.

4.1 Flat multi-module structures

The folding/deployment load was adapted to the geometry: diagonal horizontal loads (i.e. in the direction of the inner SLE's in the modules) at the upper corner nodes were applied while the lower corner nodes were supported against vertical displacements (Figure 4.2). This set of forces is chosen because it makes practically more sense and because diagonal horizontal loads are exerted on the hinges of a module when several modules are assembled.

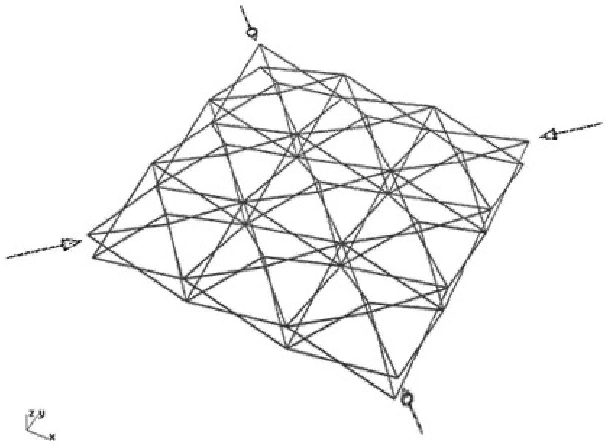

Figure 4.2: The folding loads for a multi-module flat structure. The nodes in the bottom plane are constrained to remain in this plane during transformation.

Aluminium is used as material for the beams because of its low density (2700 kg/m^3) and high relative strength (E = 70 GPa, σ_y = 600 MPa). HDPE (ρ = 940 kg/m^3, E = 0.8 GPa, σ_y = 31.7 MPa) is chosen as material for the beams that bend during deployment, to accommodate better the snap-through behaviour.

The deployment for the idealised model of one module and of a multi-module structure consisting entirely of aluminium (as is explained in 4.1.1) is given in Figure 4.3 (left), without and with gravity. The load on the graph represents the total required load (i.e. the sum of the four horizontal forces). There is a nonlinear increase in this required force for folding when the load-displacement curve of one module is compared with the load-displacement curve of a flat multi-module structure of 9 modules.

There exists an empirical formula, proposed by Gantes (Gantes, 2001), which predicts the results of the analysis in case of a flat structure composed of multiple modules, by using the corresponding results from the deployment analysis of one of the modules, as is explained in appendix D. Nevertheless, the simplifying assumptions (e.g. gravity is not considered) are too restrictive to consider this formula in practical cases.

4.1.1 Gravity

When looking at the load-displacement curves, the important information to consider is the peak load (to achieve the desired flexibility during deployment), the snap-through magnitude (to ensure safety throughout the deployment) and the maximum negative folding force. This negative force should be high enough to prevent the structure from moving back from the folded to the deployed configuration under its own weight. This maximum negative folding force is the 'reserve' that will be useful when gravity is taken into account. When gravity is considered, there should still be a sign reversal in the curve, to prevent the folded structure from unfolding under its own weight.

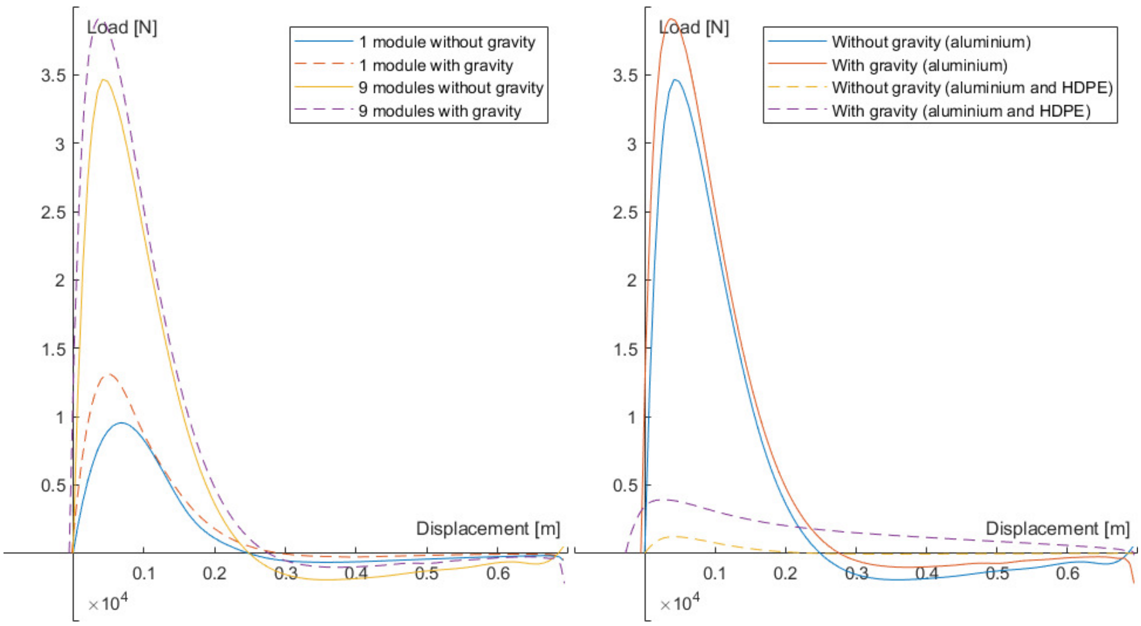

Figure 4.3: Comparison of the total load required for folding of one module and for a multi-module structure consisting of 9 modules made of aluminium (left). Comparison between the deployment behaviour of a multi-unit structure consisting of aluminium and a structure consisting of aluminium and HDPE for the beams that bend during deployment (right).

When taking gravity into account, a higher load is required for folding, because the gravity prevents the structure from folding. For the structure with beams in aluminium and HDPE (Figure 4.3 right), the total weight of the structure is 120 kg. Without gravity, the maximum negative load is -66.7 N. When gravity is applied, the peak load increases with 2.7 kN from 1.206 kN to 3.905 kN. There are no negative required loads any more because the snap-through magnitude and the maximum negative required load are too small for the structure in comparison to its weight. It is a fundamental question of balance and it requires several iterations on the materials and cross-sections of the beams. This balance between gravity and snap-through governs the self-locking of the structure.

To test the above, the deployment behaviour is modelled for a structure which entirely consists of aluminium (Figure 4.3 left). The required load for folding, the snap-through magnitude and the minimum required load are higher for this structure due to the stiffer elements. The total weight of the structure is 182 kg. Without gravity, the maximum negative load is -1.95 kN. When gravity is applied, the peak load increases with 4.46 kN from 34.66 kN to 39.12 kN and the maximum negative load decreases to -1.035 kN. In this case, the snap-through is still present, but the peak force of this structure is 10 times the peak force of the structure consisting of aluminium and HDPE (Figure 4.3 right). This has far-reaching consequences, in the sense that it would be possible to unfold and fold the structure of aluminium and HDPE by hand with around 7 or 8 people, while the deployment of the structure of aluminium is only possible by machine power.

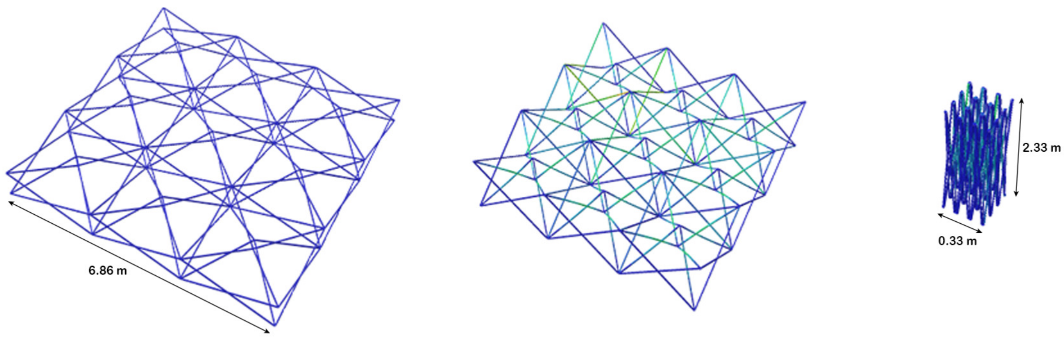

Figure 4.4: Successive folding stages of 3x3 modules.

In this case, the structure completely made of aluminium is chosen for the next simulations, to still have a snap-through effect and negative required loads during folding when gravity is taken into account. When having these negative loads, the folded structure does not go back to the deployed configuration under its own weight.

A design question to explore in the future is how to find the right balance between the stiffness (material and cross-section) of the beams which bend during deployment and the influence of gravity.

4.1.2 Imperfections

To be able to compare the influence of imperfections on a multi-module structure with the influence of imperfections on a single module, a single module with the same dimensions, material characteristics, boundary conditions and applied load is also modelled with random imperfections. The results should not directly be compared to the results in chapter 3, because the deployment behaviour of a bistable scissor structure largely depends on the dimensions, material characteristics and applied loads, as explained in chapter 2.

100 structures are modelled with values for the imperfections chosen according to the imperfections that were acceptable for the single bistable module in chapter 3. Random values for the imperfections on the beam lengths are modelled with a standard deviation of 0.1% of the total beam length. The random values for the position of the pivot point are also defined with a standard deviation of 0.1% of the total beam length and the random values for the misalignment of the hinge axes are defined with a standard deviation of 0.5° misalignment. For each simulation, random values are associated to each member separately, which ensures full randomness. Those 100 simulations do not

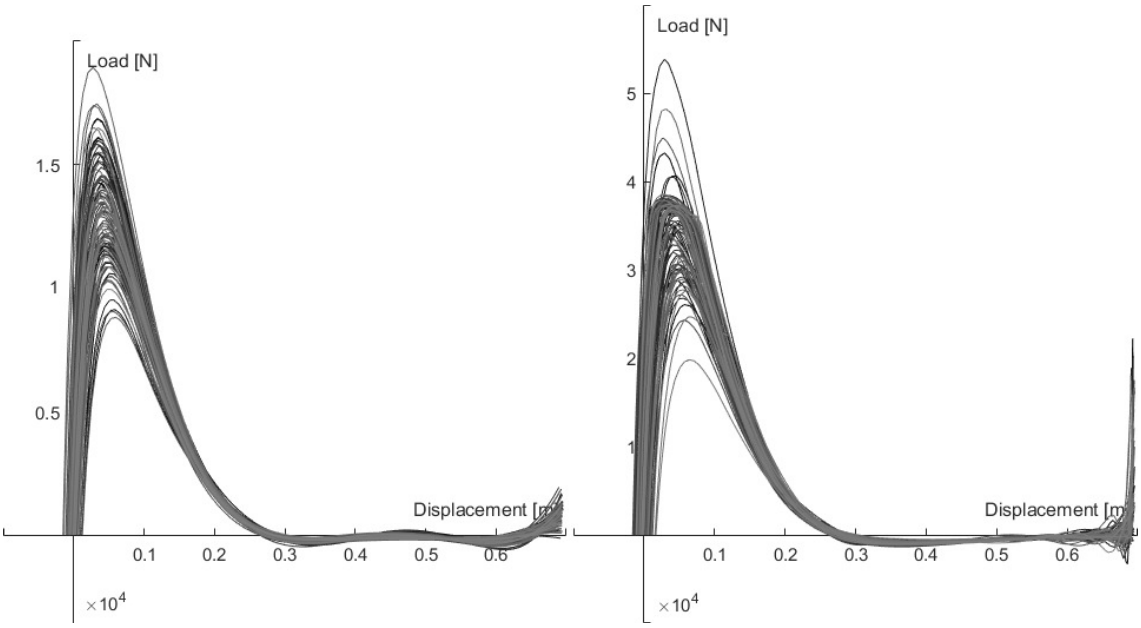

Figure 4.5: Comparison of the load-displacement curves for 100 simulations with random values for the imperfections in 1 module (left) and in 3x3 modules (right).

sample the space, but they are chosen to limit the time to perform the nonlinear analyses, the computational time of one analysis of the structure being 2 to 3 minutes, leading to a total time of around 4 hours for 100 simulations. The results will be a first set of realisations to identify some trends. For quantitative results, much more simulations would be required, which is out of the scope of this dissertation.

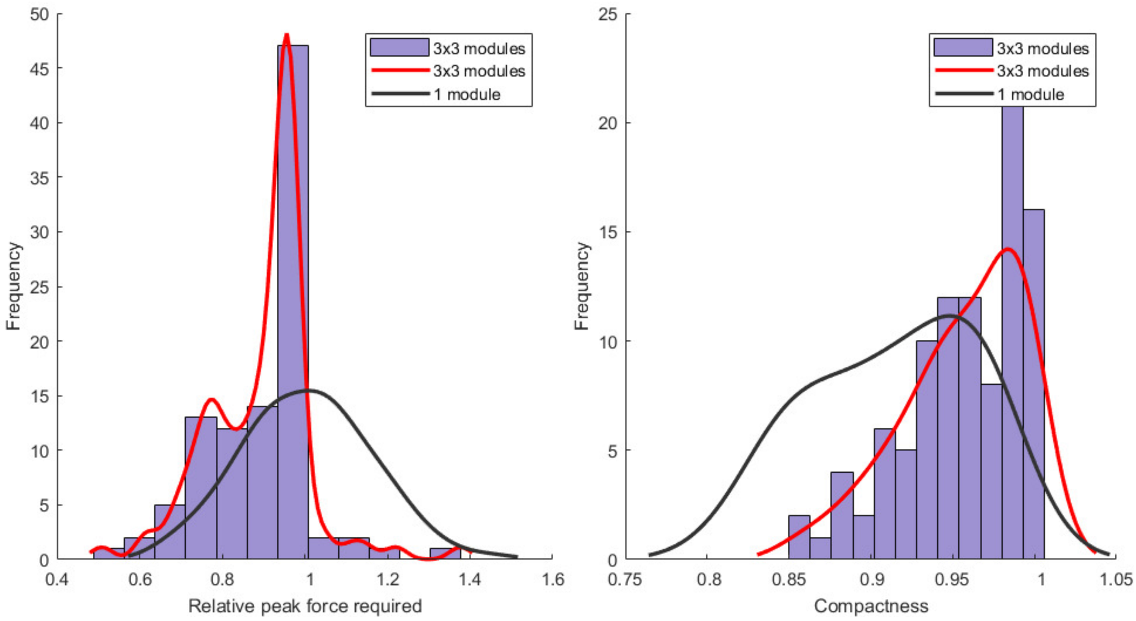

Figure 4.6: Comparison of the probability density functions for the peak load (left) and the compactness (right) for 100 simulations with random values for the imperfections.

The comparison of the load-displacement curves for 100 simulations with random values for all of the imperfections simultaneously in one module and in the structure with 3 by 3 modules, is given in Figure 4.5. Figure 4.6 and 4.7 show the difference between the probability density functions for one module and for a multi-module structure for the peak load, the compactness, the minimum load required for folding and the snap-through magnitude. The peak load, the minimum load and the snap-through magnitude are displayed as relative peak load, minimum load and snap-through magnitude, which is the value of the peak load, minimum load and snap-through magnitude divided by the peak load, minimum load and snap-through magnitude of the structure without imperfections, with gravity taken into account.

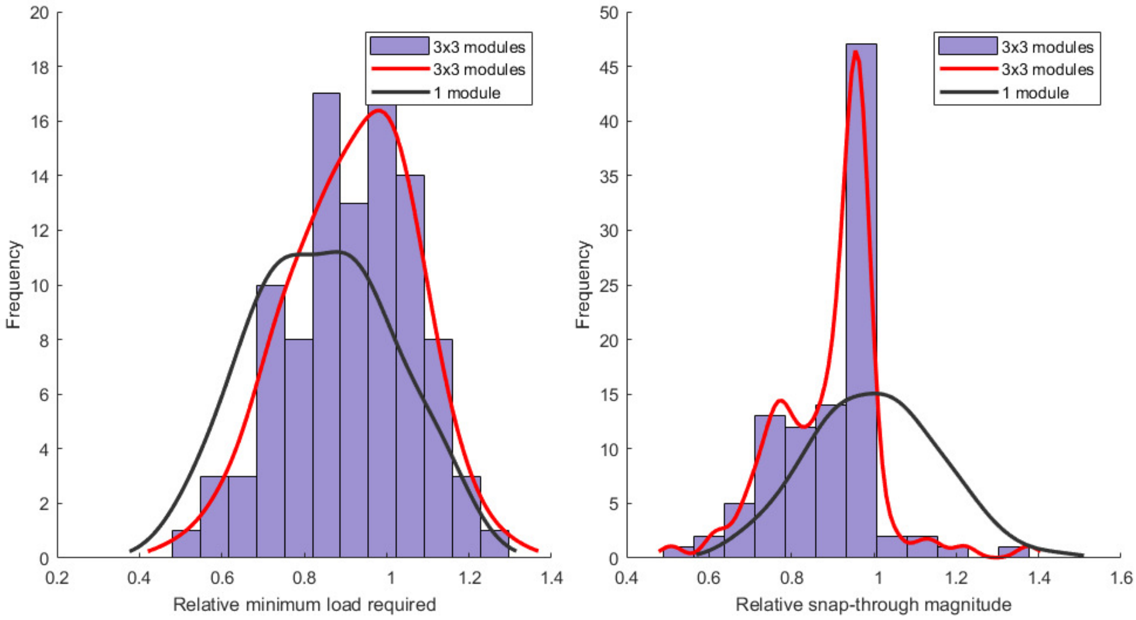

Figure 4.7: Comparison of the probability density functions for the minimum load required (left) and the snap-through magnitude (right) for 100 simulations with random values for the imperfections.

It appears that there is more probability that the peak load and the snap-through magnitude is lower than the peak load and snap-through magnitude for the structure without imperfections, but this can also be due to the low amount of different random realisations. For one module, the results were more symmetric. It appears that the compactness is less influenced by imperfections when several modules are assembled (an average compactness of 0.98 with a minimum of 0.85 instead of an average compactness of 0.95 with a minimum of 0.76). For the minimum load, the results are basically the same as for one module.

To conclude, the minimum and maximum values are in the same magnitude for single and multiple modules. There appears to be a bias to the left for the peak load and the snap-through magnitude, and the compactness is better when multiple modules are assembled. These conclusions have to be checked by more simulations in the future.

4.2 Curved multi-module structures

The difference between curved and flat multi-module structures consists in parallel unit lines during deployment for flat scissor structures, while for curved structures, the unit lines intersect during deployment (see Appendix A). By assembling regular curved modules, a curved structure is created with a constant curvature. Because of this curvature, it is interesting to study curved structures separately. The considered arch can for example be used to construct a cylindrical roof.

To be able to compare the results for the imperfections on the arch with the imperfections on the flat multi-module structure, aluminium is chosen for all the beams of the structure.

4.2.1 Gravity

Without taking into account gravity for curved structures consisting of multiple modules, the same folding mechanism is used as for flat multi-module structures (i.e. four horizontal forces in the corner points), but because the structure is an arch in the deployed configuration, an additional vertical force is needed in the middle of the arch on one of the highest points to pull those points down, to be able to fold the structure (Figure 4.8). Different geometries thus require different loads to transform.

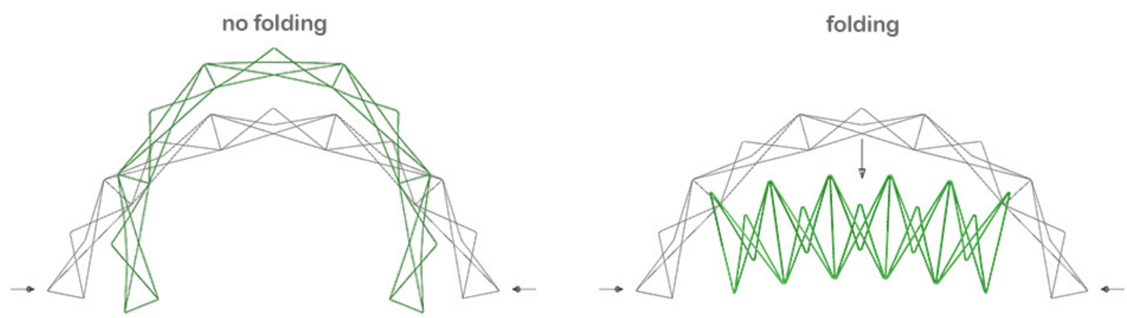

Figure 4.8: Deployed configuration and deformation of the structure after applying four horizontal forces at the corner points (left) and with an additional vertical force in the middle (right).

This additional vertical force becomes more important when the overall shape of the structure is more curved. The higher the part of this vertical force in comparison to the horizontal forces, the lower the total required force will be. For this arch, the vertical load has to be at least 4 times higher than the total horizontal loads, to be able to fold the structure. The amount of force that is required for the folding of a scissor structure depends highly on how the forces are applied. Knowing how to apply the forces is thus a very important parameter in the design and the use of a scissor structure. Applying a non-optimal set of forces can lead to an enormous peak load, to the impossibility to fold the structure or to residual stresses in the folded or unfolded configuration.

Several researchers have proposed solutions for deploying scissor structures. Escrig proposed three different solutions: an electric motor by means of a screw, a hydraulic system and a rope connecting distant joints by means of a tensor engine (Escrig, 1985). Kokawa designed a zigzag-cable system which can be winded up by a winch (Kokawa, 1995, 1996). Small lifting equipment, which would usually be already present for loading and unloading during transport, could be used to lift the structure at a central node (De Temmerman, 2007). In the future, it can be explored which set of forces is optimal.

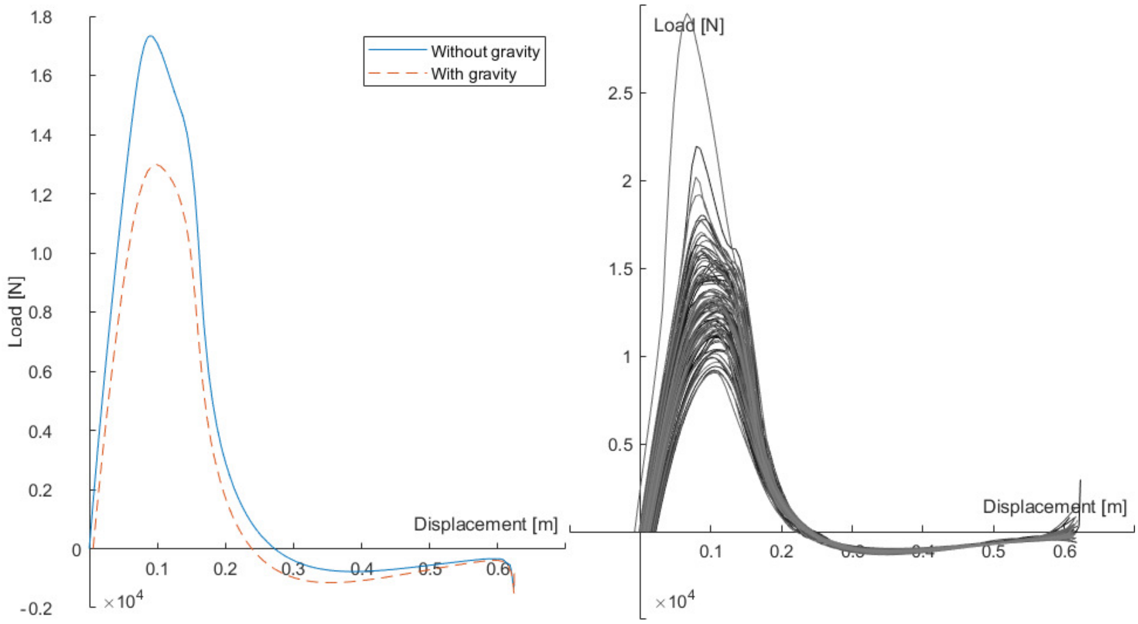

Figure 4.9: Comparison between the folding behaviour with and without gravity (left) and comparison of the load-displacement curves for 100 simulations with random values for the imperfections (right).

In Figure 4.9 (left), the folding behaviour of the arch is given for the idealised model with and without taking gravity into account. The load on the graph represents the total required load (i.e. the sum of the four horizontal forces and the additional vertical force). In the case of curved multi-unit structures, contrary to flat multi-module structures, gravity helps the folding process. The gravity adds an additional set of vertical forces. As mentioned before, the higher this additional vertical force, the lower the total load required to fold the structure. In this case, the total weight of the arch is 106 kg, which is 72 kg less than the flat multi-module structure. When considering gravity, the peak load decreases with 4.35 kN from 17.34 kN to 12.99 kN, while the minimum required load increases from -0.776 kN to -1.151 kN, when the proportion of the vertical load is kept the same in comparison to the horizontal loads.

Because gravity aids the folding process, there is less need for the vertical force in the middle of the structure for folding. However, for the unfolding, this vertical force will be more important to pull the middle of the structure upwards.

4.2.2 Imperfections

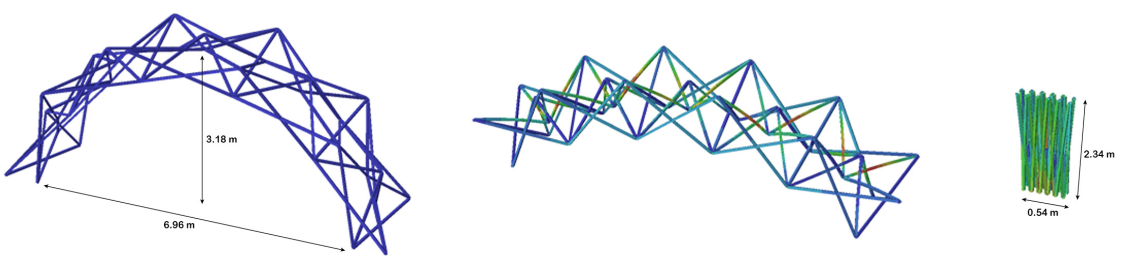

Figure 4.10: Successive folding stages of an arch with 5 modules.

The influence of imperfections is investigated by introducing random imperfections on the beam lengths, the position of the pivot points and the alignments of the hinges simultaneously in the curved structure consisting of 5 modules (Figure 4.10).

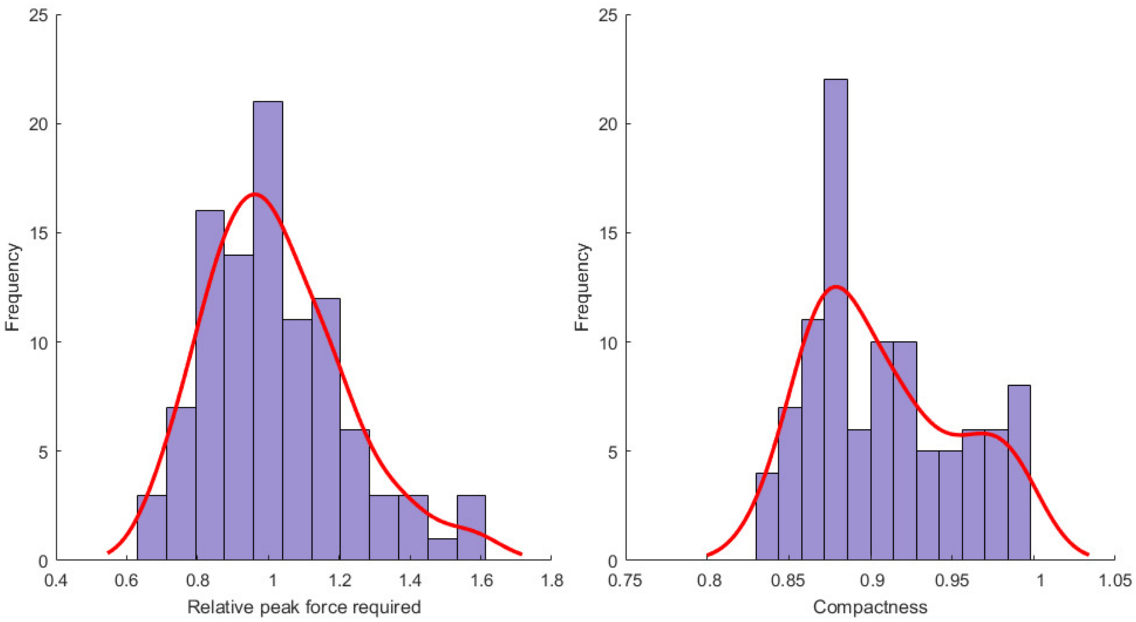

Figure 4.11: Comparison of the probability density functions for the peak load (left) and the compactness (right) for 100 simulations with random values for the imperfections.

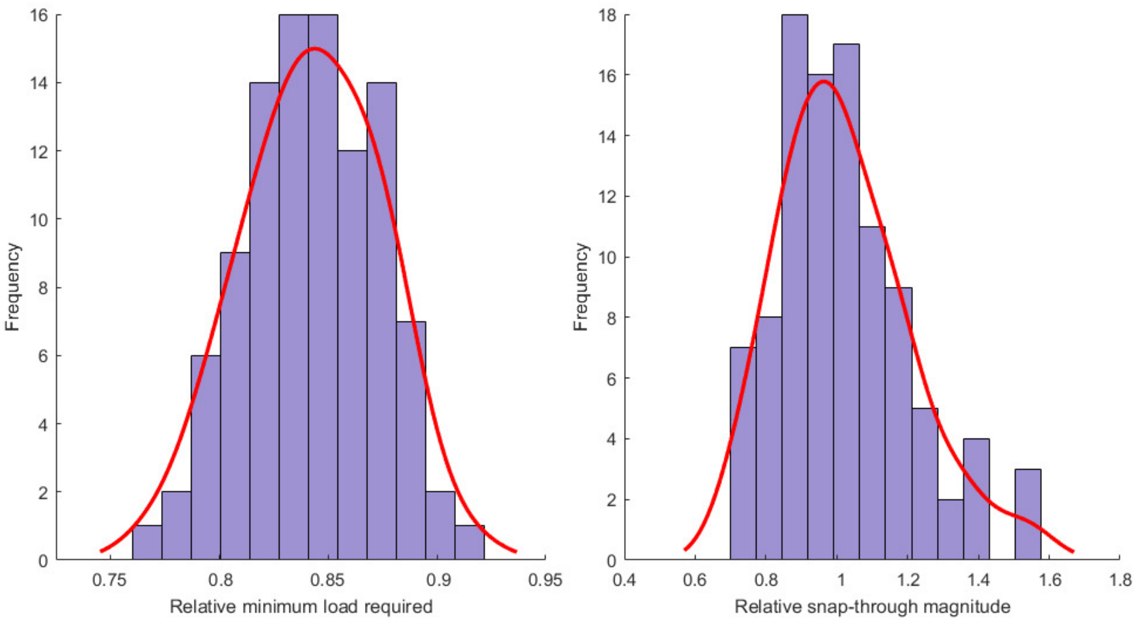

Figure 4.12: Comparison of the probability density functions for the minimum load required (left) and the snap-through magnitude (right) for 100 simulations with random values for the imperfections.

Figure 4.11 and 4.12 show the frequency and probability density functions for the peak load, the compactness, the minimum load and the snap-through magnitude for 100 simulations (deterministic realisations of different sets of random variables).

In general, the probability density functions are less biased distributions than for the flat multi-module structure. The range of the peak load (Figure 4.11 left) is between 0.6 and 1.6 times the peak load of the idealised model. This is a huge variation, which leads to a huge variation for the snap-through magnitude as well (Figure 4.12 right), which is between 0.7 and 1.6 times the snap-through magnitude of the idealised model. The average compactness (Figure 4.11 right) is 0.9 with a minimum of 0.8, which is comparable to the flat structure, and the minimum load (Figure 4.12 left) is between 0.8 and 1.15 times the minimum load of the idealised model, which is less impacted than for the flat structure.

4.3 The Dome

A spherical triangulated double layer grid of basic polar units with concurrent unit lines (see Appendix A) is chosen as last multi-module structure to investigate, because it is composed of several different modules and the surface of the dome is a spherical surface which has a positive double curvature. The grid is a triangulated pattern and the structure is bistable because of angular incompatibilities (see appendix A).

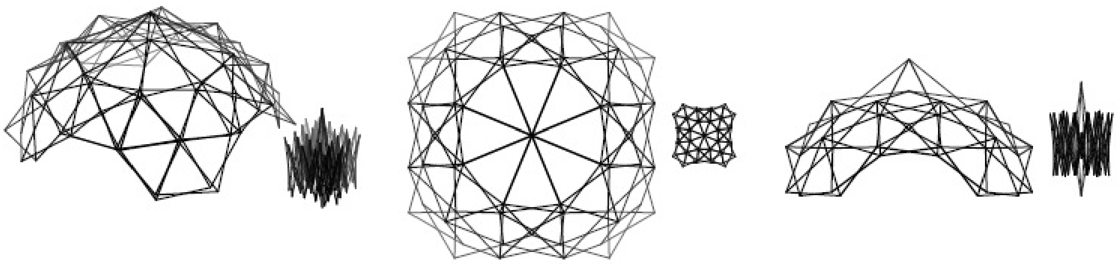

Figure 4.13: Perspective, plan view and side view of a spherical triangulated bistable scissor structure (Roovers, 2017).

The structure of the dome in Figure 4.13, in which the polygonal modules form a part of a truncated cuboctahedron, consists of one octagonal module, four hexagonal modules and four square modules (Gantes, 1996c). The assembly of different polygonal modules makes this structure different from the previously investigated structures. The sides of the polygons have the same length, leading to a structure with seven different beams. The entrance of the structure is 2.2 m high. The whole structure has a diameter of 15.7 m and a height of 6.3 m.

The fins of the joints have to be equal to the amount of beams that are connected in a joint, leading to six different types of joints, one with eight fins, two with six fins, one with five fins, one with four fins and one with three fins. The size of the joint is influenced by the beams it has to connect. The wider the section and the higher the number of beams coming together in one joint, the larger the radius of the joint must be, in order to accommodate all elements without interference during deployment. To accommodate beams with a cross-section of 5 by 5 cm, the radius of the biggest joint has to be 9 cm, while the radius of the other joints is taken equal to 5 cm (Figure 4.14).

The most time-consuming in the modelling of this structure, is to define all the nodes and the hinges. For this structure, 400 hinges had to be defined. Every pivot point in

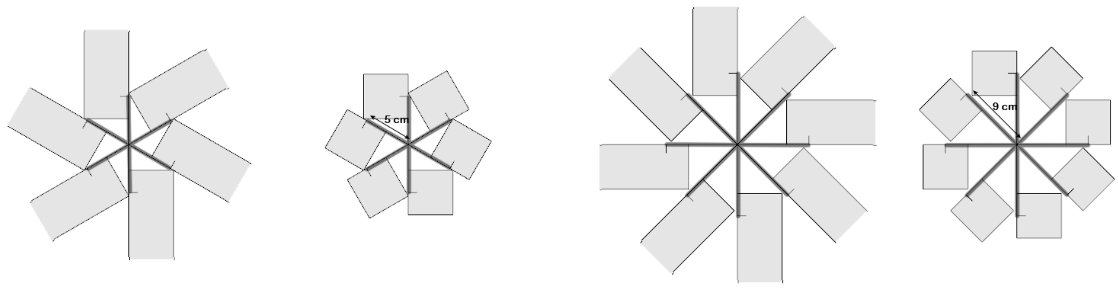

Figure 4.14: Joint with a radius of 5 cm, which connects 6 beams in the unfolded and folded configuration (left) and joint with a radius of 9 cm, which connects 8 beams in the unfolded and folded configuration (right).

each SLE is a hinge, and for the joints, as many hinges have to be defined as there are beams that are connected to the joint. For example, for the largest joint with 8 fins, 8 hinges have to be defined. For each hinge, the hinge orientation has to be defined.

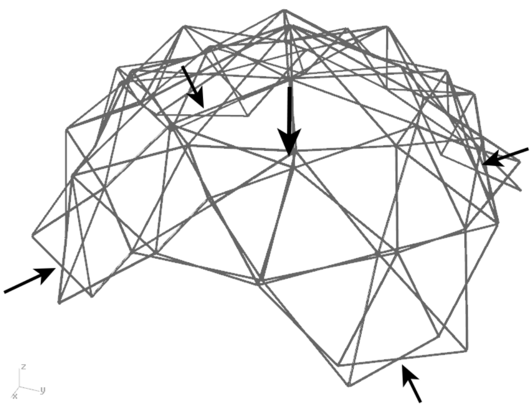

Figure 4.15: Deployment mechanism for a dome.

The used folding mechanism for this dome (Figure 4.15) without gravity is the same folding mechanism as was used for the arch, which means that there are four horizontal forces and one vertical force applied. This additional vertical force in the middle of the structure that was needed to be able to fold the arch, is also needed for the dome. For the dome, this vertical force must be at least 3.5 times the total horizontal forces to be able to fold the structure.

To be able to compare the results for the imperfections on the dome with the imperfections on the arch and the flat multi-module structure, aluminium is chosen for all the beams of the structure.

4.3.1 Gravity

In Figure 4.16 (left), the deployment behaviour of the dome is given for the idealised model with and without taking gravity into account. The load on the graph represents the total required load (i.e. the sum of the four horizontal forces and the vertical force). As was the case for the arch, the gravity helps the folding process, leading to a lower required total load for folding.

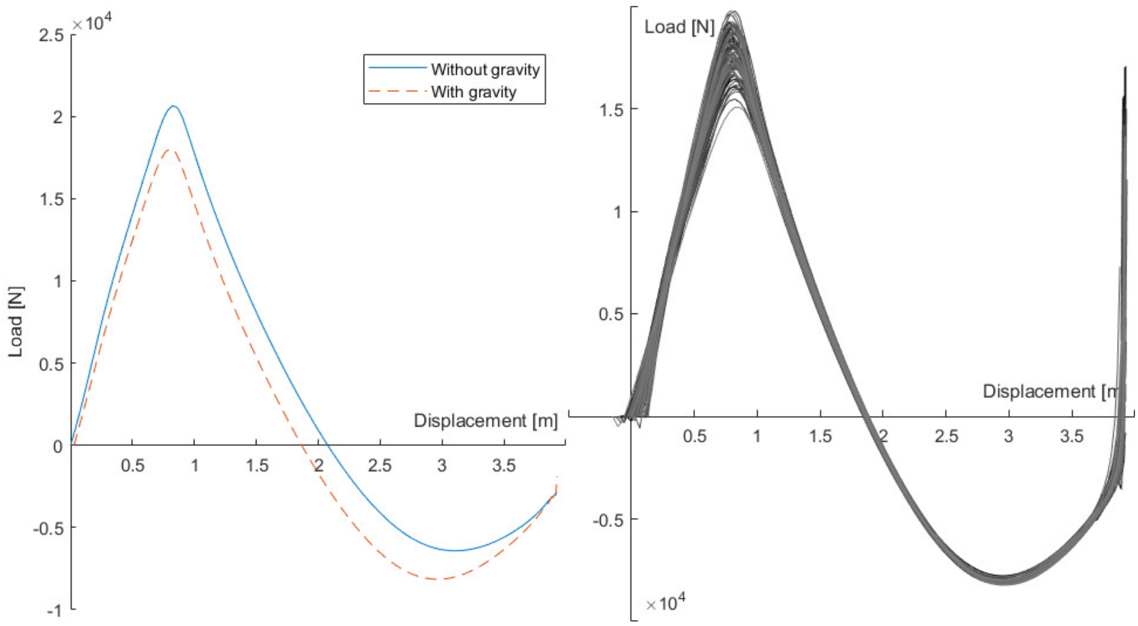

Figure 4.16: Comparison between the folding behaviour with and without gravity (left) and comparison of the load-displacement curves for 100 simulations with random values for the imperfections (right).

The load-displacement curve for this dome has a totally different shape than the previously considered load-displacement curves, in the sense that the negative required loads for folding are more prominent and the negative slope of the graph is less steep. This is due to the fact that the structure is an assembly of octagonal, hexagonal and square modules, which have each a different deployment behaviour, their convoluted effect results in Figure 4.16.

The total weight of the dome is 425 kg, which is 319 kg more than the arch and 243 kg more than the flat multi-module structure. When considering gravity, the peak load decreases with 2.62 kN from 20.65 kN to 18.03 kN, while the minimum required load increases from -6.414 kN to -8.144 kN, when the proportion of the vertical load is kept the same in comparison to the horizontal loads.

4.3.2 Imperfections

The influence of imperfections is investigated by introducing random imperfections on the beam lengths, the position of the pivot points and the alignment of the hinges at the same time in the dome (Figure 4.17).

Figure 4.16 (right) shows the load-displacement curves and Figure 4.18 and 4.19 show the probability density functions for the peak load, the compactness, the minimum load required for folding and the snap-through magnitude for 100 simulations with random values for the imperfections on the beam lengths, the position of the pivot points and the alignment of the hinges at the same time.

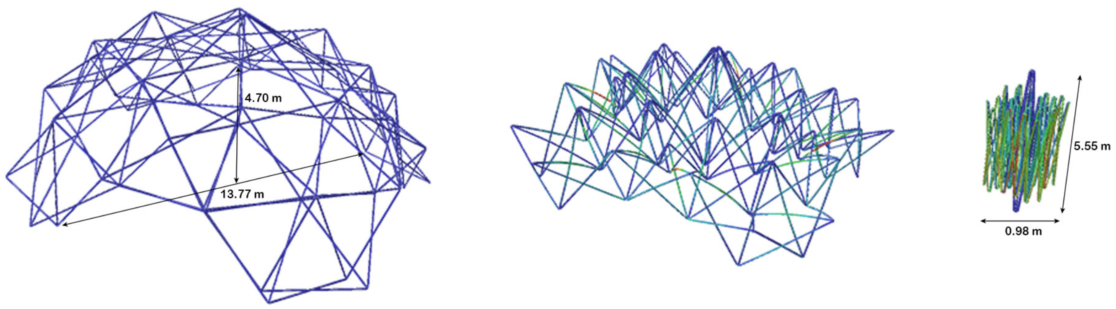

Figure 4.17: Successive folding stages of a dome.

All the probability density functions are globally much narrower for imperfections on the dome than for imperfections on the arch and the flat structure. The range of the peak load (Figure 4.18 left) is between 0.8 and 1.12 times the peak load of the idealised model. The average compactness (Figure 4.18 right) is 0.994 with a minimum of 0.977. The minimum load (Figure 4.19 left) is between 0.95 and 1.015 times the minimum load of the idealised model and the snap-through magnitude (Figure 4.19 right) is between 0.84 and 1.1 times the snap-through magnitude of the idealised model.

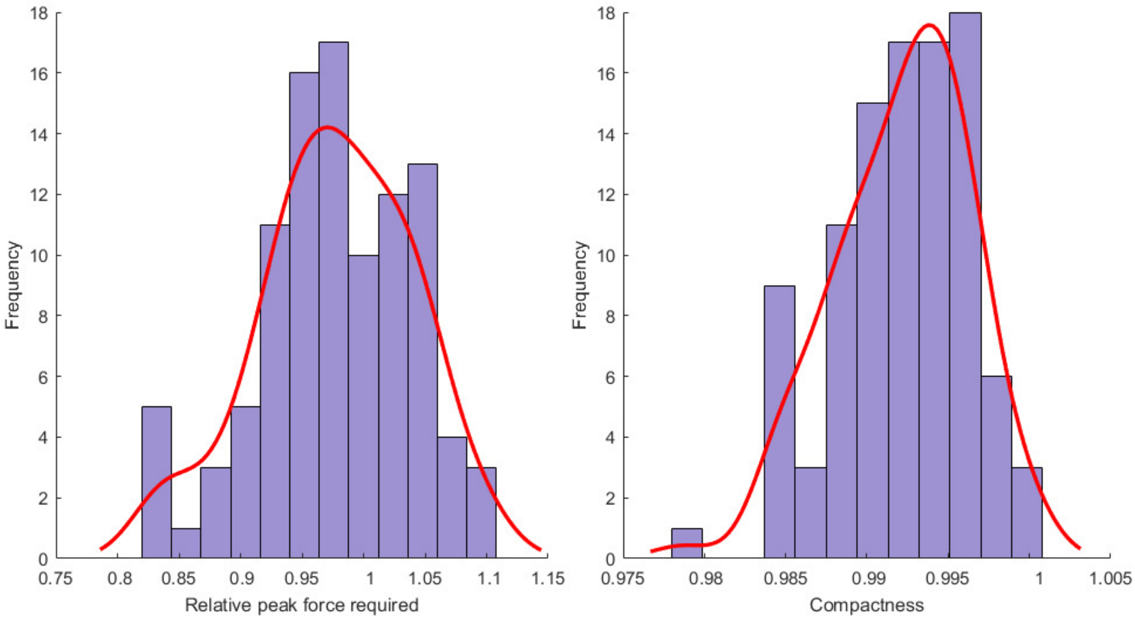

Figure 4.18: Comparison of the probability density functions for the peak load (left) and the compactness (right) for 100 simulations with random values for the imperfections.

The influence of the imperfections is smaller for this dome in comparison to the arch and the flat structure. The influence of imperfections on one module seems to be attenuated by assembling several different modules. It appears that the influence of the imperfections on the flat multi-module structure was the highest, comparable to the influence of imperfections on one module. The influence of the imperfections on the arch was a little bit lower, and the influence of the imperfections on the dome is much lower.

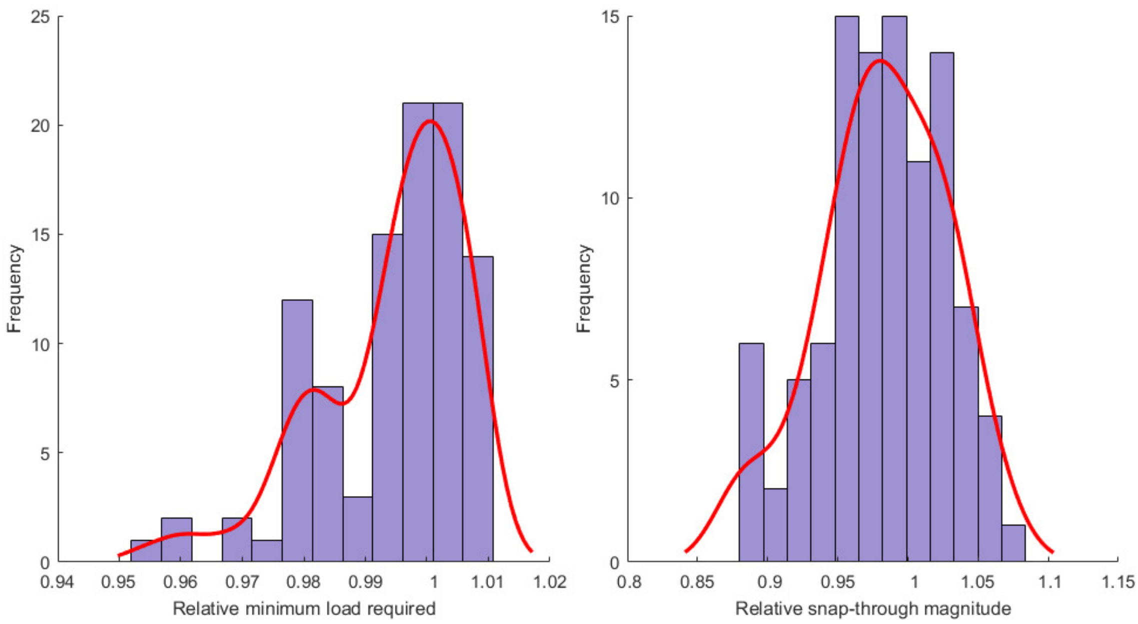

Figure 4.19: Comparison of the probability density functions for the minimum load required (left) and the snap-through magnitude (right) for 100 simulations with random values for the imperfections.

4.4 Discussion

4.4.1 Effect of gravity

Taking gravity into account is important to make the results practically relevant. For flat multi-module structures, a higher load is required for folding when gravity is taken into account, because the gravity prevents the structure from folding. It is important that the snap-through magnitude and the maximum negative required load is high enough to not completely alter the deployment behaviour. It is a question of balance and it requires several iterations to choose the materials and the cross-sections of the beams. Still having negative required loads after applying the gravity is important if some stiffness is desired in both the folded and unfolded configuration.

For curved structures consisting of multiple modules, the same folding mechanism was used with an additional vertical force in the middle of the structure. This vertical force becomes more important when the structure is more curved and decreases the total required load for folding. It has been shown that knowing how to apply the forces is a very important parameter in the design of scissor structures.

For curved multi-module structures (e.g. the arch and the dome), gravity helps the folding process, leading to a lower total required load. Gravity can replace part of the additional vertical force that is needed to fold the structure.

4.4.2 Influence of imperfections

To model multi-module structures, a different folding mechanism in which diagonal horizontal loads were applied at the upper corner nodes was chosen to make the folding more realistic. Random imperfections were introduced in a multi-module structure to know how imperfections are transferred throughout the whole structure.

When implementing imperfections in a flat multi-module structure, the minimum and maximum values are in the same magnitude for single and multiple module. The influence on the compactness seems to be less restrictive as for one module.

In general, for the arch, the influence of the imperfections appears to be smaller than for the flat structure.

The load-displacement curve for the dome has a different shape than the previously considered load-displacement curves, because the dome is an assembly of octogonal, hexagonal and square modules, each with their own deployment behaviour. The influence of imperfections in this dome was very small in comparison to the arch and the flat structure.

Chapter 5

Conclusion and outlook

The aim of the work presented in this dissertation was to develop a 3D nonlinear structural model for the simulation of the transformation of bistable scissor structures. Starting from an initial simplified polygonal module, the computational model was refined in several stages and the influence of the main design parameters and manufacturing imperfections on the transformation response was investigated. The main types of tolerances that were investigated were imperfections on the beam lengths, eccentricity of the pivot points, finite hinge stiffness, hinge misalignment and friction. The computational tool was applied for structures consisting of multiple modules during deployment and the influence of gravity and imperfections was investigated on multi-module structures with the aim of obtaining practically relevant results.

The complexity of the modelling of scissor structures consists in defining each node and each hinge separately. For structures such as the dome investigated in chapter 4, which has 400 hinges, this is time-consuming. The computations themselves are complex as well, because all the analyses are nonlinear. In total the results of around 2000 computations are displayed in this dissertation. Taking into account that the computational time needed for a quarter of a module is only around half a minute and of a whole module around 50 seconds, while this computational time increases to 1.5 minute for the arch, 2 to 3 minutes for the flat multi-module structure and around 4 minutes for the dome, the total computational time of all the simulations is more than 35 hours.

First, a model has been derived that can be used to explore the intensity of the snap-through phenomenon of bistable scissor structures. An initial simplified idealised single square polygonal module was analysed (i.e. corresponding to the design wireframe geometry). The load-displacement curve and the variation of the stress, normal force and bending moment during folding was obtained. The snap-through effect was identified, however ignoring important factors such as joint size and imperfections. The model has been extended to include curved spherical structures as well, for which the type of response was observed to be qualitatively the same.

A parameter study has been carried out to give the designer some general guidelines on how to influence the structural response by changing the main design parameters related to the module geometry and the stiffness of the elements.

Gravity was included in the computational model because it is always present in civil engineering applications. It has been verified that the snap-through response is reversible, in the sense that the load-displacement curves for folding and unfolding are the same, when an idealised structure is modelled and when gravity is taken into account.

A curved pentagonal module was modelled and compared to the results of Gantes (Gantes, 1991). The match was satisfactory, taking into account that not all dimensions and material characteristics were known exactly. A fair agreement was reached to the available experimental data when considering gravity.

Manufacturing defects and imperfect hinge behaviour are naturally present in all engineered structures and were thus investigated in this work. Two types of imperfections were identified, geometrical imperfections (finite hinge size, tolerances on the beam lengths, eccentricity of the pivot points and hinge misalignment) and imperfect hinge behaviour (finite hinge stiffness and friction). Geometrical tolerances were modelled as a fictitious thermal load on the structure so that the resulting stresses are naturally taken into account in the behaviour. To model friction, the Coulomb friction model was used in the hinges (a friction coefficient, a tightening force and the resultant forces from the rotation are taken into account).

To model multi-module structures, a different folding mechanism in which diagonal horizontal loads were applied at the upper corner nodes was chosen to make the folding more realistic. Random imperfections were introduced in multi-module structures to know how imperfections are transferred throughout the whole structure. Gravity was taken into account to make the results practically relevant.

Some important messages resulted from this work and some main contributions are made to the computational investigation of bistable scissor structures:

- When the structure is in a geometrically compatible state, it does not directly mean that it is stress-free or that no external force is required to keep it in this state. This is due to the use of a kinematic design obtained with rigid elements (in which only the geometry is considered without taking statical equilibrium into account) into a structure in which the stiffness and deformability of the beams is properly taken into account. It was shown that compatible configurations can be approached when there is a clever choice of boundary conditions and applied loads.

- Gravity can have a considerable influence on the load-displacement curve, which will depend on the module geometry and the stiffness of the elements and should thus certainly be taken into account during the design phase.

- Including realistic joint dimensions in the numerical model has an overall stiffening effect, which is bigger when the joint dimensions are larger.

- When introducing tolerances on the beam lengths, the peak force changes as well as the minimum force and the snap-through magnitude because the initial configuration changes. A measure for the compactness of the structure was defined, and the higher the imperfection, the lower the compactness of the structure in the folded state. When introducing random imperfections, values for the strain on the beam length with a standard deviation of 0.1% are acceptable (which means that 99.7% of the values are within a range of -0.3% to 0.3% i.e. 3 mm on 1 m span).

- When introducing imperfections on the position of the SLE pivot point, again the initial configuration changes, leading to a change in the peak force, minimum force and the snap-through magnitude and a decrease of the compactness. The compactness decreases comparably for imperfections on the beam length as for a shift of the pivot point.

- For the peak force, the minimum force and the snap-through magnitude, the imperfections on the beam lengths seem to be slightly more important than a shift of the pivot point. As was the case for random imperfections on the beam lengths, values for the strain on the beam length with a standard deviation of 0.1% are acceptable (which means a shift in the pivot point of 1 mm for a beam with a span of 1 m).

- The influence of a misalignment of a hinge in an outer SLE is huge for the peak load, minimum load and snap-through magnitude, but less important for the compactness. A misalignment of a hinge in an inner SLE almost has no influence on the deployment response. When introducing random imperfections, only the results of simulations with a standard deviation of 0.5° are acceptable. The structure is thus most sensitive to the variation of this parameter.

- When using flexible hinges and allowing additional rotations around the other axes, the deployment behaviour of the idealised module is almost not altered, but flexible hinges can counteract the effect of imperfections, for example imperfections on the beam length and more important, it will counteract the influence of hinge misalignment, allowing a higher tolerance for imperfections on the latter.

- For flat multi-module structures, a higher load is required for folding when gravity is taken into account, because the gravity prevents the structure from folding. It is important that the snap-through magnitude and the maximum negative required load is high enough to not completely alter the deployment behaviour. It is a question of balance and it requires several iterations on the materials and the cross-sections of the beams. Still having negative required loads after applying the gravity is important if some stiffness is desired in both the folded and unfolded configuration.

- For curved structures consisting of multiple modules, an additional vertical force in the middle of the structure was required to fold the structure. This vertical force becomes more important when the structure is more curved and decreases the total required load for folding. It has been shown that knowing how to apply the forces is a very important parameter in the design of scissor structures.

- For curved multi-module structures (e.g. the arch and the dome), gravity helps the folding process, leading to a lower total required load. Gravity can replace part of the additional vertical force that is needed to fold the structure.

- When implementing imperfections in a flat multi-module structure, the minimum and maximum values are in the same magnitude for single and multiple module. The influence on the compactness seems to be less restrictive in comparison to one module.

- In general, for the arch, the influence of the imperfections appears to be smaller than for the flat structure.

- The load-displacement curve for the dome has a different shape than the previously considered load-displacement curves, because the dome is an assembly of octogonal, hexagonal and square modules, each with their own deployment behaviour. The influence of imperfections in this dome was very small in comparison to the arch and the flat structure.

5.1 Suggestions for future research

A number of complex questions and challenges have been identified which should be addressed in the design strategy of bistable structures (a non-exhaustive list):

- How to ensure a deployment with realistic deployment force levels, either machine-assisted or human-force driven?

- How to guarantee the safety of the deployment in relation with the snap-through behaviour, which is associated with the magnitude of the deployment force fluctuation?

- How to choose the best snap-through configuration with respect to safety, ease of erection and stiffness in the deployed state? For example, does a square bistable scissor grid or a triangular bistable scissor grid perform better with respect to the ease of erection and the stiffness in the deployed state?

- What are the most critical parameters affecting the safety and deployment force levels? For example, the finite stiffness of the joints is a design parameter and helps accommodating the snap-through, as well as the choice of the material of the elements exhibiting snap-through.

- How does the stage of deployment at which snap-through occurs allow optimizing the stiffness in the deployed state (i.e. if the snap-through occurs close to the deployed configuration, does this 'late'snap-through lead to stiffer structures?)

- How to design the joints, taking into account their stiffness and practical technological solutions?

- What is the influence of imperfections on other polygonal modules?

- What are the quantitative conclusions on imperfections in multi-module structures, when the normal distribution of the random variables is covered better?

- How to find the right balance between the stiffness (material and cross-section) of the beams that bend during deployment and the influence of gravity?

Future research projects can aim at finding answers to these questions using advanced FE simulations.

References

ADINA R&D. (1987). *ADINA-IN: User's Manual*. Massachusetts.

Alegria Mira, L. (2010). *Design and Analysis of a Universal Scissor Component for Mobile Architectural Applications* (Master's thesis, Vrije Universiteit Brussel, Brussels).

Alegria Mira, L. (2014). *Parametric Structural Assessment of Deployable Scissor Systems, Optimising the Universal Scissor Component* (Doctoral dissertation, Vrije Universiteit Brussel, Brussels).

Alegria Mira, L., De Temmerman, N. & Preisinger, C. (2012). Structural optimisation of deployable scissor structures using new computational methods. *WIT Transactions on The Built Environment*, *124*, 469–480.

Crisfield, M. A. (1996a). *Non-linear Finite Element Analysis of Solids and Structures Volume 1: Essentials*. Chichester: John Wiley & Sons.

Crisfield, M. A. (1996b). *Non-linear Finite Element Analysis of Solids and Structures Volume 2: Advanced Topics*. Chichester: John Wiley & Sons.

Dassault Systèmes. (2014). Incremental Control Techniques. Retrieved February 2017, from http://help.solidworks.com/2014/English/SolidWorks/cworks/c_Incremental%20_Control_Techniques.htm

Dassault Systèmes Simulia Corp. (2012b). *Abaqus Scripting User's Manual*.

Dassault Systèmes Simulia Corp. (2012c). *Abaqus/CAE User's Manual*.

De Temmerman, N. (2007). *Design and Analysis of Deployable Bar Structures for Mobile Architectural Applications* (Doctoral dissertation, Vrije Universiteit Brussel, Brussels).

Dupont, A. (2014). *Impact of manufacturing defects on deployable structures* (Master's thesis, Brussels Faculty of Engineering, Brussels).

Escrig, F. (1985). Expandable Space Structures. *Space Structures*, *1*, 79–91.

Escrig, F., Sanchez, J. & Valcarcel, J. P. (1996). Two Way Deployable Spherical Grids. *International Journal of Space Structures*, *11*(1&2), 257–274.

Escrig, F. & Valcarcel, J. P. (1993). Geometry of Expandable Space Structures. *International Journal of Space Structures*, *8*, 71–84.

Euro-bearings Ltd. (2016). Megi bushes. Retrieved April 2017, from https://www.euro-bearings.com/bushes.htm

Eurocode 9. (2007). Design of aluminium structures. European Standards.

Farrugia, P. (2008). *Kinematic Analysis of Foldable Structures* (Doctoral dissertation, University of Surrey, Surrey, UK).

Friedman, N. (2011). *Investigation of Highly Flexible, Deployable Structures: Review, Modeling, Control, Experiments and Applications* (Doctoral dissertation, Ecole Normale Superieure de Cachan, Budapest University of Technology and Economics, Cachan).

Fugier, M. (2013). *Rhinoceros v5.0, Level 1, Training Manual*.

Gantes, C. J. (1991). *A Design Methodology for Deployable Structures* (Doctoral dissertation, Massachusetts Institute of Technology, Massachusetts).

Gantes, C. J. (1993). Geometric constraints in assembling polygonal deployable units to form multi-unit structural systems. *Space Structures*, *4*, 793–803.

Gantes, C. J. (1996a). A Creative Aspect of a Destructive Phenomenon: Using Snap-through Buckling as a Form of Prestressing. In *IASS/IABSE international symposium on conceptual design of structures* (pp. 222–229). Stuttgart.

Gantes, C. J. (1996b). Analytical Predictions of the Snap-through Characteristics of Deployable Structures. In *MARAS '96, 2nd international conference on mobile and rapidly assembled structures* (pp. 83–92). Seville: Computational Mechanics Publications.

Gantes, C. J. (1996c). Deployable Structures for Temporary Sheltering Following Natural Disasters. *Stop Disasters*, *28*, 7–8.

Gantes, C. J. (1997). An Improved Analytical Model for the Prediction of the Nonlinear Behavior of Flat and Curved Deployable Space Frames. *Journal of Constructional Steel Research*, *44*(1-2), 129–158.

Gantes, C. J. (2001). *Deployable Structures - Analysis and Design*. Southampton: WIT Press.

Gantes, C. J., Connor, J. J. & Logcher, R. D. (1990). Finite element analysis of movable deployable roofs and bridges. In *Third biennial symposium on heavy movable structures and movable bridges*. St. Petersburg, Florida.

Gantes, C. J., Connor, J. J. & Logcher, R. D. (1991). Combining Numerical Analysis and Engineering Judgment to Design Deployable Structures. *Computers & Structures*, *40*(2), 431–440.

Gantes, C. J., Connor, J. J. & Logcher, R. D. (1993). Simple Friction Model for Scissor-Type Mobile Structures. *Journal of Engineering Mechanics*, *119*(3), 456–475.

Gantes, C. J., Connor, J. J., Logcher, R. D. & Rosenfeld, Y. (1989). Structural Analysis and Design of Deployable Structures. *Computers & Structures*, *32*, 661–669.

Gantes, C. J. & Konitopoulou, E. (2004). Geometric design of arbitrarily curved bi-stable deployable arches with discrete joint size. *International Journal of Solids and Structures*, *41*, 5517–5540.

Gantes, C. J., Logcher, R. D., Connor, J. J. & Rosenfeld, Y. (1993a). Deployability Conditions for Curved and Flat, Polygonal and Trapezoidal Deployable Structures. *International Journal of Space Structures*, *8*(1&2), 97–106.

Gantes, C. J., Logcher, R. D., Connor, J. J. & Rosenfeld, Y. (1993b). Geometric Design of Deployable Structures with Discrete Joint Size. *International Journal of Space Structures*, *8*(1&2), 107–117.

Gantes, C. J., Tsouknaki, D. N. & Kyritsas, S. C. (1997). Symbolic Manipulation as a Tool for Design of Deployable Domes. *Computers & Structures*, *64*(1-4), 865–878.

Gantes, C. J., Tsouknaki, D. N. & Kyritsas, S. C. (1998). Combining Active and Passive Substructures in Snap-through Type Deployable Structures. In *IUTAM-IASS symposium on deployable structures: theory and applications* (pp. 107–116). Cambridge.

Gaul, L. & Nitsche, R. (2001). The Role of Friction in Mechanical Joints. *Applied Mechanics Reviews*, *54*(2), 93–109.

Grupo Estran. (n.d.). Portfolio digital. Retrieved January 2017, from http://www.grupoestran.com/

Hernandez, C. H. (1996). New ideas on deployable structures. In *Mobile and Rapidly Assembled Structures II* (pp. 64–72). Southampton: Computational Mechanics Publications.

Hoberman, C. (1990). *Reversibly expandable doubly-curved truss structure*. US 4,942,700. United States.

Kaveh, A. & Daravan, A. (1996). Analysis of Pantograph Foldable Structures. *Computers & Structures*, *59*(1), 131–140.

Kawaguchi, K., Inoue, K. & Ogi, Y. (2012). Structural behaviour of a deployable spoke wheel with off-set scissors and radial tension cables for a SSPS system. In *Proceedings of the IASS-APCS 2012 Symposium - From Spatial Structures to Space Structures*. Seoul, Korea.

Kawaguchi, K. & Sato, T. (2015). Development of Deployable Geodesic Full Sphere with Scissors Members. In *Proceedings of the international association for shell and spatial structures (IASS) symposium 2015*. Amsterdam.

Kokawa, T. (1995). A Trial of Expandable Arch. In *Proceedings of IASS*. Milan, Italy.

Kokawa, T. (1996). Scissor arch with zigzag-cable through pulley-joints. In *Proceedings of IASS*. Stuttgart, Germany.

Koumar, A., Tysmans, T., De Temmerman, N., Filomeno Coelho, R. & Alegria Mira, L. (2014). Multi-criteria optimisation of a barrel vault structure for emergency relief. In *Proceedings of the International IASS-SLTE Symposium, Shells, Membranes and Spatial Structures: Footprints*. Brasilia, Brazil.

Krishnapillai, S. & Zalewski, W. P. (1985). *The design of deployable structures*. Department of Architecture, MIT, Cambridge, Massachussets.

Langbecker, T. (1999). Kinematic Analysis of Deployable Scissor Structures. *International Journal of Space Structures*, *14*(1), 1–15.

Langbecker, T. & Albermani, F. (2000). Foldable positive and negative curvature structures: Geometric design and structural response. *Journal of the International Association for Shell and Spatial Structures*, 147–161.

Langbecker, T. & Albermani, F. (2001). Kinematic and non-linear analysis of foldable barrel vaults. *Engineering Structures*, *23*, 158–171.

Latteur, P. (2000). *Optimisation et prédimensionement des arcs et des treillis sur base d'indicateurs morphologiques - Application aux structures soumises en partie ou en totalité au flambement* (Doctoral dissertation, Vrije Universiteit Brussel, Brussels).

Leaveanest Co.Ltd. (2012a). Unfolding a deployable dome. Retrieved January 2017, from https://www.youtube.com/watch?v=VDMarOJQ_E8

Leaveanest Co.Ltd. (2012b). What scissors type structures are. Retrieved January 2017, from https://www.youtube.com/watch?v=3A7BHZKjqlw

Lee, D. S.-H., Larsen, O. P. & Kim, S.-D. (2013). Study of the connection joint for scissor-type deployable structure for the possible application in emergency evacuation shelter. In *Proceedings of the first conference transformables 2013* (pp. 1–5). Spain.

Lee, D. S.-H., Larsen, O. P. & Kim, S.-D. (2014). Design of Deployable Structure for Dome Type Emergency Shelter. In *Proceedings of the IASS-SLTE 2014 symposium 'Shells, Membranes and Spatial Structures: Footprints'* (pp. 1–7). Brazil.

Lee, D. S.-H., Larsen, O. P. & Kim, S.-D. (2016). Computational tools for the design of a deployable dome structure: Beyond their Limits. In *Third International Conference on Structures and Architecture* (pp. 267–274). Portugal.

Massart, T. (2016). CNST-H-418 Nonlinear Modelling. Université Libre de Bruxelles.

Matijevic, I. & Kovacevic, D. (2009). Some disadvantages of standard buckling analysis comparing to incremental geometric nonlinear analysis. *International Journal of Engineering*, *7*(4), 13–16.

Nomadic Display Corp. (n.d.). 10' instand pop up curved backwall. Retrieved November 2016, from http://www.nomadicdisplay.com/displays/

Nunes, E. F. (2016). *Retractable structure for emergency building*. Belo Horizonte: Izabela Hendrix Methodist University Center.

Partyspace BVBA. (n.d.). Partyspace.eu. Retrieved August 2016, from http://www.partyspace.eu/nl

Payne, A. & Issa, R. (2009). *The Grasshopper Primer, Second Edition*.

Pellegrino, S. (2001). *Deployable Structures*. New York: Springer-Verlag Wien GmbH.

Piker, D. (2010). *Kangaroo: Life Physics for Rhino and Grasshopper*.

Piñero, E. P. (1961). A Reticular Movable Theatre. *The Architects' Journal for August*, *30*(134), 299.

Piñero, E. P. (1965). *Three dimensional reticular structure*. US 3,185,164. United States.

Preisinger, C. (2015). *Karamba User Manual for Version 1.1.0*.

Roovers, K. (2017). *Deployable Scissor Grids - Geometry and Kinematics* (Doctoral dissertation, Vrije Universiteit Brussel, Brussels).

Roovers, K. & De Temmerman, N. (2015). Digital design of deployable scissor grids based on circle packing. In *Proceedings of the IASS 2015 symposium 'Future Visions'*. Amsterdam.

Rosenfeld, Y., Ben-Ami, Y. & Logcher, R. D. (1993). A Prototype 'Clicking' Scissor Link Deployable Structure. *Space Structures*, *8*(1-2), 85–95.

Rosenfeld, Y. & Logcher, R. D. (1988). New Concepts for Deployable-Collapsable Structures. *International Journal of Space Structures*, *3*(1), 20–32.

Van Mele, T., De Temmerman, N., De Laet, L. & Mollaert, M. (2010). Scissor-hinged retractable membrane structures. *International Journal of Structural Engineering*, *1*(3/4), 374–396.

Zeigler, T. R. (1976). *Collapsible self-supporting structure*. US 3,968,808. United States.

Zeigler, T. R. (1977). *Collapsible self-supporting structures*. US 4,026,313. United States.

Zeigler, T. R. (1981). *Collapsible self-supporting structures and panels and hub therefor*. US 4,290,244. United States.

Zeigler, T. R. (1984). *Collapsible self-supporting structures*. US 4,437,275. United States.

Zeigler, T. R. (1989). *Hub assembly for collapsible structures*. US 4,838,003. United States.

Zeigler, T. R. (1993). *Polyhedron building system*. US 5,230,196. United States.

Appendix A

Geometry and Kinematics

A.1 Basic concepts

A.1.1 Scissor units

Scissor structures consist of scissor units, also called scissor-like elements (SLE), pantographs or duplets, in which two beams are crosswise interconnected by a revolute joint, referred to as the intermediate hinge point. The distance between the intermediate hinge point and an end point of a scissor unit is called a semi-length. The upper and lower points of a scissor unit are connected by unit lines (Roovers, 2017).

There are three types of scissor units (Figure A.1): the translational unit, the polar unit and the angulated unit. A translational scissor unit is characterized by unit lines that remain parallel during deployment, a polar scissor unit is formed when the unit lines intersect at a variable angle during deployment and an angulated scissor unit consists of a pair of kinked beams and is characterized by unit lines that intersect at an invariant angle (De Temmerman, 2007).

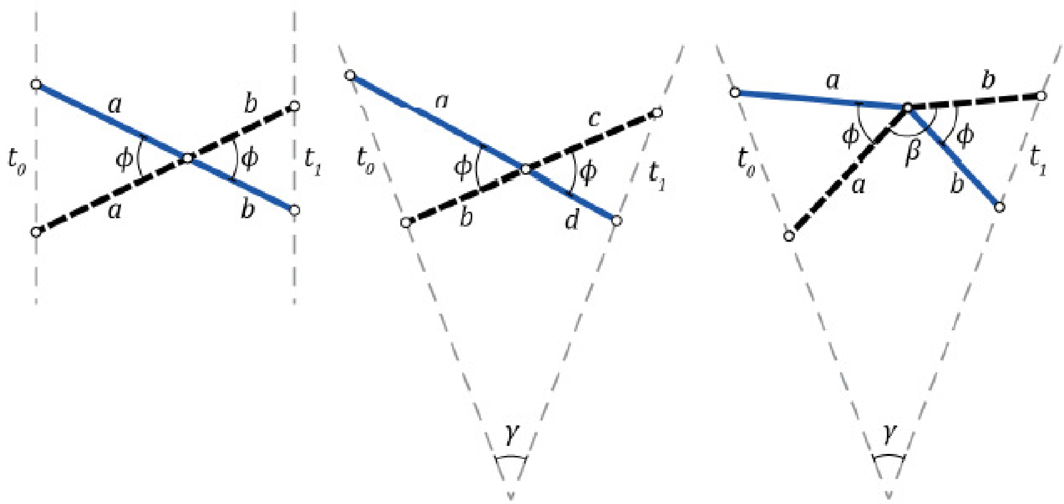

Figure A.1: Translational scissor unit (left), polar scissor unit (middle) and angulated scissor unit (right) (Roovers & De Temmerman, 2015).

A.1.2 Scissor linkages

Scissor linkages are formed by connecting a number of scissor units side by side. The geometric design approach for bistable scissor structures is based on the requirement for geometric compatibility in the deployed as well as in the folded configuration, which means that the beams are located theoretically on one line in the folded configuration. This can be translated into the deployability constraint, a formula derived by Escrig (1985; 1993). As seen in Figure A.2, the deployability constraint is written as:

$$a + b = c + d \tag{A.1}$$

This constraint requires that the sum of the semi-lengths a and b of a scissor unit has to be equal to the sum of the semi-lengths c and d of the adjoining unit. It ensures that all units in the linkage simultaneously reach their most compact state, which is essential to maximize the deployment range of a scissor linkage of translational or polar scissor units.

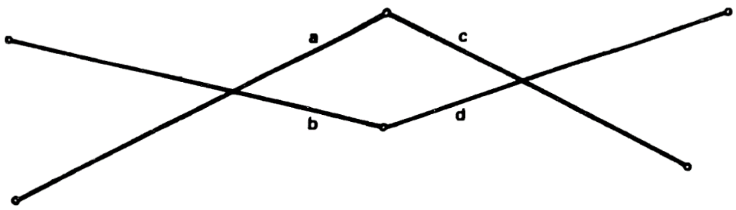

Figure A.2: The deployability constraint (Gantes, 2001).

The most compact state that is reached by angulated units, depends on the kink in the beams, making a general equivalent equation less straightforward to determine (Roovers, 2017). Linkages of angulated units are often dimensioned according to the shape-invariance constraint (Hoberman,(1990)), in which a is equal to c and b is equal to d.

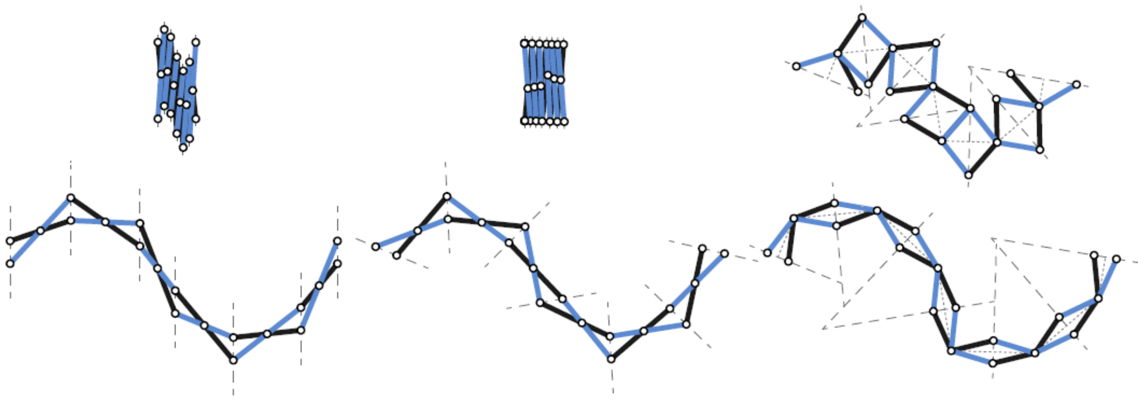

Figure A.3: Curved scissor linkage of translational scissor units (left), polar scissor units (middle) and angulated scissor units (right) in the folded (top) and unfolded (bottom) state (Roovers, 2017).

Basically any not self-intersecting two-dimensional curve (Figure A.3) can be translated into a scissor linkage of any unit type and form (Roovers, 2017).

A.1.3 Scissor modules

When the two ends of a scissor linkage are interconnected to form a closed loop, which requires at least three scissor units, a scissor module is created. In the case of translational and polar units, a scissor module will always describe a spatial prismatic shape. Using angulated units, it becomes possible to form planar closed loops. Attention should be paid to modules which consist of four scissor units or more where the unit lines are either parallel or concurrent throughout deployment (Figure A.4 right). In this specific case, the module obtains additional degrees of freedom (Roovers, 2017).

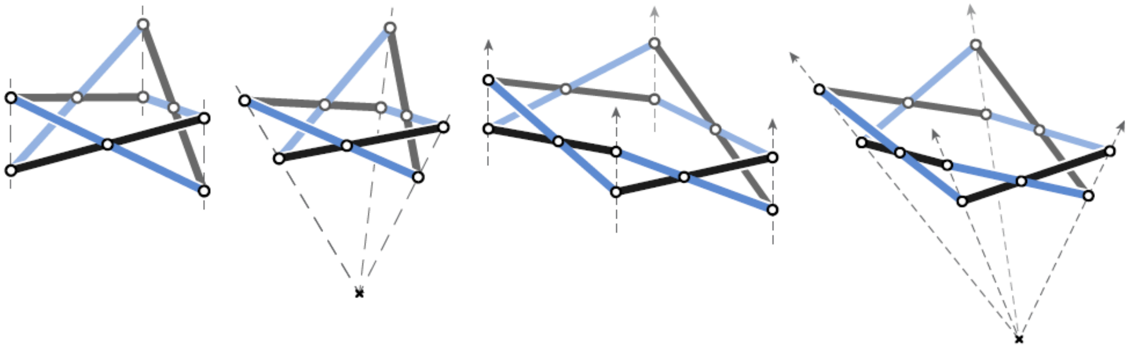

Figure A.4: Two three-unit modules (left) and two four-unit modules, having an additional degree of freedom due to their parallel and concurrent unit lines (right) (Roovers, 2017).

A.1.4 Scissor grids

Scissor grids are formed by combining multiple scissor modules. A single-layer grid (Figure A.5 left) is formed by stacking multiple scissor modules on top of each other, a double-layer grid (Figure A.5 middle) is formed by tessellating scissor modules along a base surface and a multi-layer grid (Figure A.5 right) is formed by stacking multiple double-layer grids. Double-layer grids are mostly used because they allow a broader variety in shapes and patterns and their grids occupy a smaller volume than multi-layer grids. Triangulated patterns are useful for their geometric rigidity, while other patterns offer a greater freedom of shape and tend to produce lighter scissor grids with less complex nodes (Roovers, 2017).

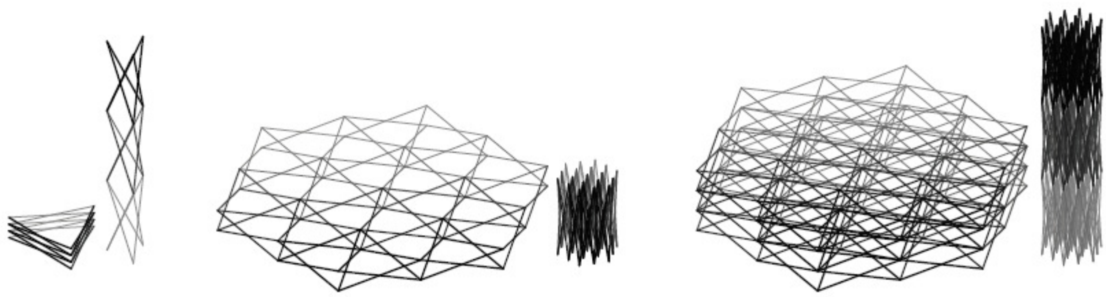

Figure A.5: A single-layer grid (left), a double-layer grid (middle) and a multi-layer grid (right) (Roovers, 2017).

A.2 Deployment behaviour

A.2.1 Geometric incompatibilities

The deployment behaviour of scissor grids is described through its geometric compatibility in the folded and unfolded configuration, as well as during deployment. A scissor grid is geometrically compatible when all the members are straight and without elastic deformation. Scissor grids can be described as 'foldable', 'bistable' or 'incompatible'. Foldable scissor grids are geometrically compatible throughout all stages of deployment and act as pure mechanisms, bistable scissor grids are geometrically compatible in the folded and unfolded stage and incompatible throughout or during a part of the deployment and incompatible scissor grids are geometrically compatible during maximum one deployment stage, and incompatible during all others. Foldable scissor grids can easily be converted into bistable grids and bistable grids into incompatible grids by adding some elements that introduce incompatibilities. The opposite is generally not possible (Roovers, 2017).

If a scissor grid is incompatible during only a part of the deployment, it depends on the moment when the incompatibility occurs whether the structure is self-locking or not and thus whether it is interesting to design or not. Incompatible scissor structures, which are not often designed because of the undesired residual stresses inside the elements which reduce the structural performance (Gantes, Tsouknaki & Kyritsas, 1997), can also show a snap-through effect by having larger incompatibilities during deployment than in the folded or unfolded configuration (Roovers, 2017). Although often undesired, these residual stresses inside the elements might prove helpful when folding of unfolding the structure. Nevertheless they are out of the scope of this thesis.

There are two types of geometric incompatibilities, observed by Roovers (Roovers, 2017), which he presented as angular and peripheral incompatibilities. Angular incompatibilities occur during deployment because the interior angles no longer add up to 2π because of the varying angles between the unit lines. The incompatibilities can be overcome by bending in the members. Peripheral incompatibilities on the other hand occur when the length of the beams at the perimeter is insufficient to encircle the grid that lies within. The beams at the perimeter are too short to close the modules during deployment in a compatible manner because they are deformed to the extent that two of the scissor units become aligned. The scissor grid cannot deform further without removing these beams, increasing their length or allowing bending in the members inside the grid. Peripheral incompatibilities tend to create a larger snap-through effect, because the deformations that are required are much larger and concentrated at the perimeter.

A.2.2 Bistable scissor grids

Two-dimensional scissor linkages which comply with the deployability constraint are always geometrically compatible during deployment, since the bistable deployment is caused by geometric incompatibilities associated with a three-dimensional configuration. Whether or not a certain configuration leads to a snap-through effect, depends on the specific combination of the grid type, unit type and curvature.

Designing single curvature structures with translational and/or polar units in a two- or three-way grid with a constant unit thickness leads to structures behaving like a mechanism. The same applies to doubly curved deployable grids with translational units (Figure A.6 left). It is possible to make flat structures bistable by integrating curved linkages on the diagonals of the grid to create a snap-through effect.

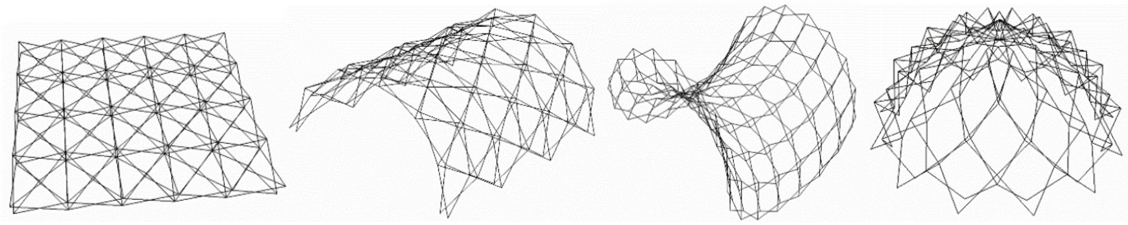

Figure A.6: Mechanisms: from left to right: plane translational units on a four-way grid, polar units on a three-way grid, translational units on a two-way grid and polar units on a lamella grid (De Temmerman, 2007).

On the contrary, doubly curved structures with polar units almost always exhibit a snap-through effect because of angular deformations (Figure A.6 right) (De Temmerman, 2007). An exception is the lamella grid (Figure A.6 right). Three-dimensional structures with angulated units are out of the scope of this thesis. Although they can be bistable, the simplicity and compactness in the folded state of translational and polar units is preferable.

A.3 Geometric modelling

In theory, the folded state of a scissor structure can be a one-dimensional configuration corresponding to the most compact form. An approach that is used to achieve this requirement is to use the deployability constraint (equation A.1). A number of equations can be used to represent the foldability conditions, sometimes in conjunction with other geometric constraints, to obtain the configuration of scissor structures that are at least geometrically compatible in the folded and unfolded state. The constraint equations are very often particular to the structure being considered and the geometric approach is therefore problem specific (Farrugia, 2008).

Another method which can be used to design scissor structures is the geometric construction method, which is more intuitive. It consists in drawing the geometry of the scissor structure while using the graphic representation of the deployability constraint (i.e. ellipses). Digital parametric design tools present a powerful means to handle the high degree of complexity in an interactive and efficient manner (Roovers & De Temmerman, 2015).

A.3.1 Review of geometric design approaches

Escrig explored different configuration assemblies of SLE's to obtain various forms (Escrig, 1985; Escrig & Valcarcel, 1993). He proposed a set of constraints using the deployability constraint in an attempt to generalise the design of scissor structures. He pointed out that snap-through deployable structures are obtained by mapping SLE's on geodesic and three-way spherical grids. Escrig, Sanchez and Valcarcel presented different methods of tessellating a spherical surface into a rhombic grid of which the lines are then replaced by SLE's (Figure A.7). The results show that there are geometric incompatibilities during deployment in the structure (Escrig, Sanchez & Valcarcel, 1996).

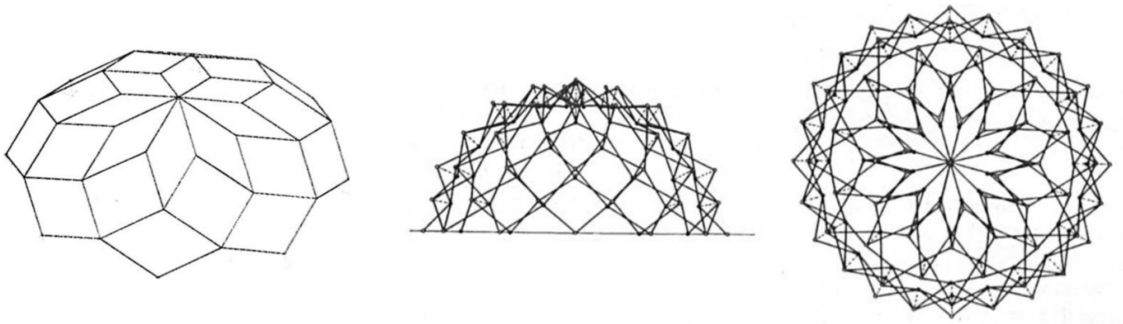

Figure A.7: Tessellated spherical surface of which the lines are replaced by SLEs (Escrig et al., 1996).

Clarke used projective geometry to determine the geometric constraints that can be used to design scissor structures composed of three-unit modules (Figure A.8) in accordance to Zeigler's deployable domes (Zeigler, 1976). These structures also have geometric incompatibilities during deployment (Farrugia, 2008).

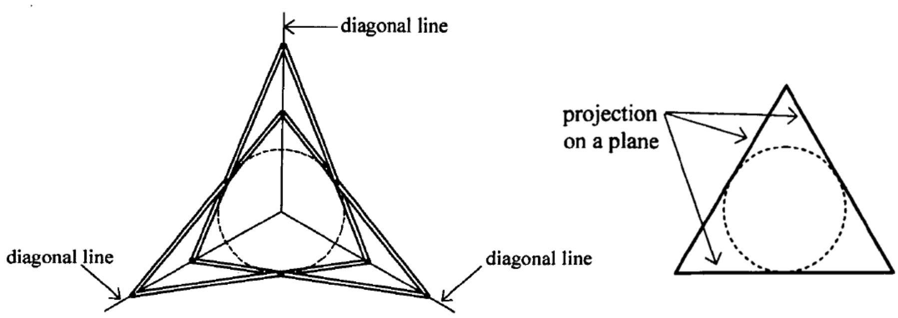

Figure A.8: A perspective view of a three-unit module, used in Zeigler's deployable domes (Farrugia, 2008).

Rosenfeld and Logcher, who focused on the structures invented by Krishnapillai (Krishnapillai & Zalewski, 1985), extended and applied the foldability conditions proposed by Escrig to obtain geometric constraint equations for bistable scissor structures (Rosenfeld & Logcher, 1988).

Gantes used a similar approach to determine the geometry of bistable scissor structures which are composed of polygonal modules by solving simultaneously equations that are obtained explicitly for each type of module (Gantes, Logcher, Connor & Rosenfeld, 1993a). The geometric constraint equations are derived by applying equation A.1 for all scissor-like elements of a module, taking also symmetry and other special conditions into account. The design procedure must be preceded by the choice of design parameters, which are often some external dimensions which are imposed by architectural requirements. The other quantities that define the geometry are the unknown variables.

Following this approach, a system of simultaneous nonlinear equations will have to be solved (Gantes, 1991). The approach is not intended as a general method for obtaining the geometry of all bistable scissor structures, because the set of simultaneous equations has to be found and assembled for each particular module.

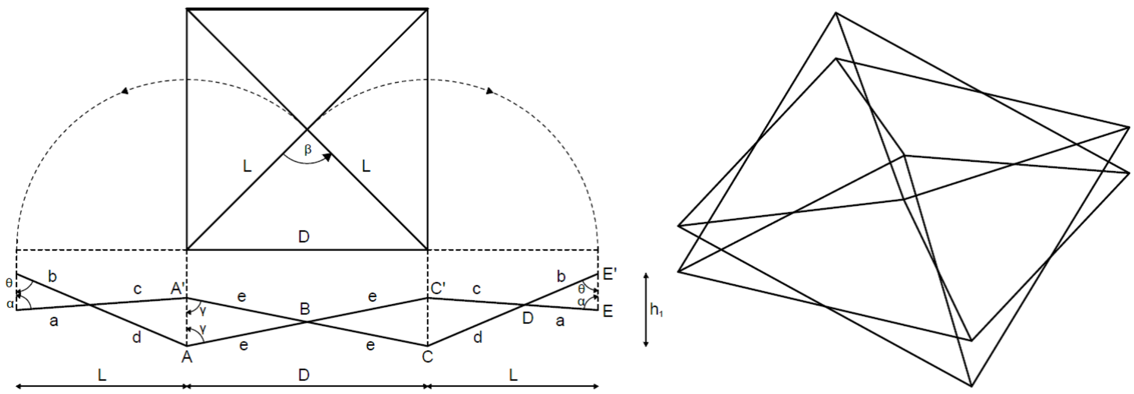

Figure A.9: Geometric characteristics of a flat square module.

Gantes has extended his approach to include the discrete size of the joints, because otherwise there are residual stresses inside the elements during each stage of deployment because of the difficulty in building physical models with infinitesimal joints (Gantes, Logcher, Connor & Rosenfeld, 1993b). Gantes defined geometric constraints for flat polygonal (Figure A.9) and trapezoidal modules, as well as for curved polygonal modules with constant curvature and arbitrary curvature. Additional constraints have been imposed by Gantes on the geometric configuration to obtain the desired overall shape (Gantes, 2001):

- Each module has to satisfy the constraint equations.
- For flat structures, the polygonal plan views must fill the plane, which can only be the case for equilateral triangles, squares and hexagons.
- For curved structures, the polygonal plan views must form part of a convex polyhedron that is inscribed in a sphere and all external nodes have to lie on a part of this sphere.
- Adjacent modules must share the same nodes across their interfaces.
- For semi-regular polyhedra, some additional constraints have to be enforced, for example all modules must have the same curvature and the lines connecting corresponding upper and lower nodes must be concurrent.

Previous approaches had the disadvantage of being design specific, requiring new derivations for each combination of modules. Proposals for a more systematic kinematic analysis of scissor linkages include the foldability vectors presented by Langbecker. He defined a series of foldability equations using geometry and trigonometry, by means of foldability vectors which represent the direction of motion of a duplet (Langbecker, 1999; Langbecker & Albermani, 2000, 2001).

At last, a lot of effort has been done by De Temmerman and Roovers to unravel the general principles that govern the motion and shape of scissor grids, revealing various new and interesting design possibilities (Roovers, 2017).

A.3.2 Geometric construction

Mathematics form a good tool to prove that a given assembly is compatible. It is however impractical and cumbersome as a tool to search for new design possibilities or to study a variety of shapes, due to the amount of parameters and equations that arise using irregular or generalised units or when creating larger assemblies. A more efficient and intuitive design approach can be provided by integrating graphical design methods in digital design environments in the form of parametric models (Roovers, 2017).

A.3.2.1 Flat structures

The locus of all valid intermediate hinges that comply with the deployability constraint (equation A.1) is an ellipse, with the common end nodes of both units as its foci (De Temmerman, 2007). This graphic representation of the deployability constraint makes it possible to draw the geometry of scissor structures.

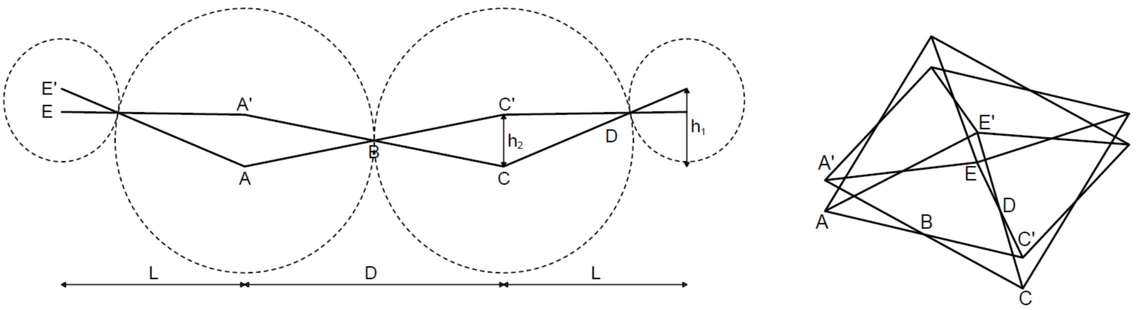

Figure A.10: Ellipses as the graphic representation of the deployability constraint for flat polygonal modules.

Polygonal modules with translational linkages (Figure A.10) can be designed by geometric construction, in accordance to Gantes' design approach (Gantes, 1991), if L, h_1 and h_2 are known. By drawing an ellipse with A and A' as its foci while B is a point on the ellipse, the intermediate hinge between $E'A$ and EA' can be determined. The same applies to the intermediate hinge between $E'C$ and EC'.

A.3.2.2 Curved structures

Polygonal modules for curved structures with constant curvature (Figure A.11) can be similarly designed by geometric construction if L, h_1, h_2 and ϕ are known. The only difference is that the unit lines intersect at a predetermined angle instead of being parallel.

Polygonal modules for arbitrarily curved structures (Figure A.12) can be constructed by following Gantes' approach (Gantes & Konitopoulou, 2004).

An easier way of designing curved scissor structures is to design a doubly curved grid of two-dimensional polar linkages. These structures almost always exhibit a snap-through

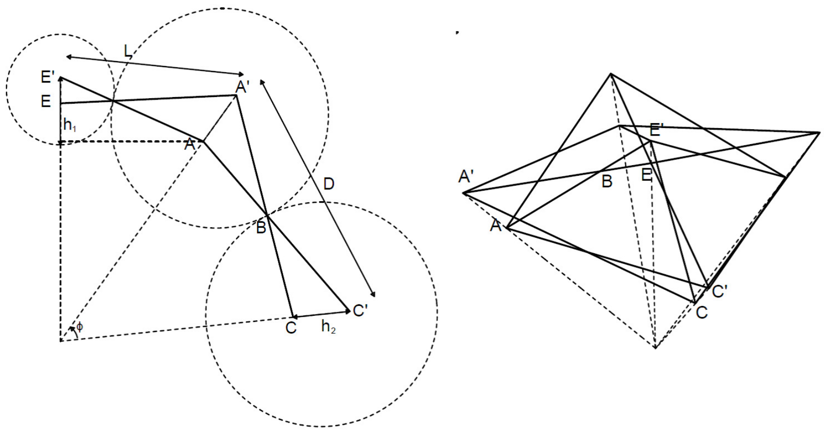

Figure A.11: Ellipses as the graphic representation of the deployability constraint for curved polygonal modules.

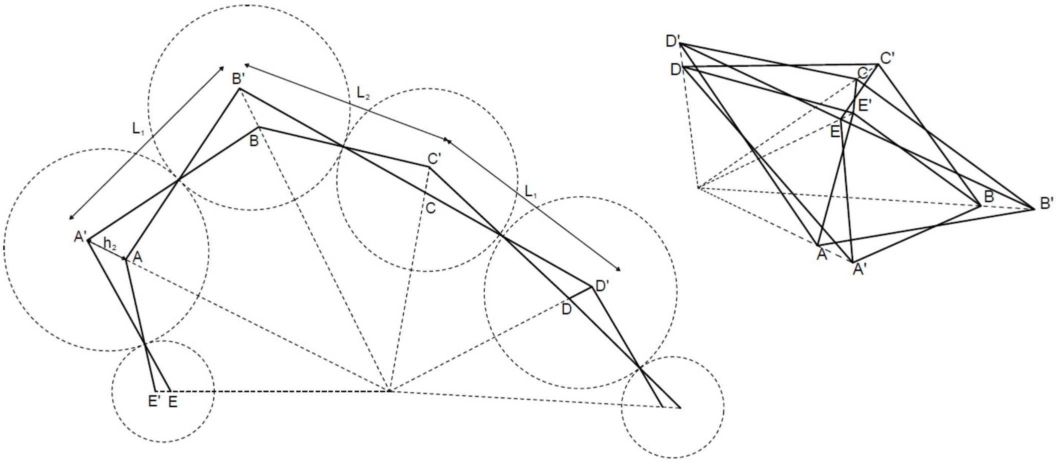

Figure A.12: Ellipses as the graphic representation of the deployability constraint for arbitrarily curved polygonal modules.

effect because of angular deformations. The disadvantage of this type of structures is the absence of clear polygonal modules and the lack of knowledge about which elements will bend in the deployment procedure, which makes the snap-through effect harder to control.

A.3.2.3 Digital modelling

Digital parametric design environments present a powerful means to handle the high degree of complexity of the design process of scissor structures in an interactive and efficient manner. General design methods to generate certain types of scissor units can be translated into algorithms, which ask the user for a number of input parameters and output the geometry of the desired structure (Figure A.13). These tools were created using the 3D modelling software Rhinoceros® (Fugier, 2013) and its generic design plug-in Grasshopper® (Payne & Issa, 2009).

These tools can further be extended by using for example the interactive live physics plug-in Kangaroo (Piker, 2010) to simulate the deployment (Figure A.14), or by using the tool Karamba (Preisinger, 2015) to structurally analyse the grid (Alegria Mira, 2014;

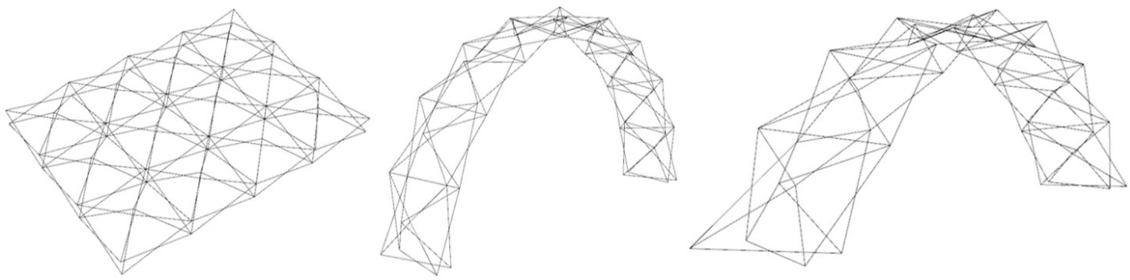

Figure A.13: A tool to create flat (left), constantly curved (middle) and arbitrarily curved (right) square bistable polygonal modules, with as input parameters a curve, the amount of modules, the height of the first module and the height of the middle point of each module.

Alegria Mira, De Temmerman & Preisinger, 2012). A method that is also found to be useful in the design of scissor grids is based on circle packing (Figure A.15), which allows exploring a wide variety of deployable scissor grids (Roovers & De Temmerman, 2015).

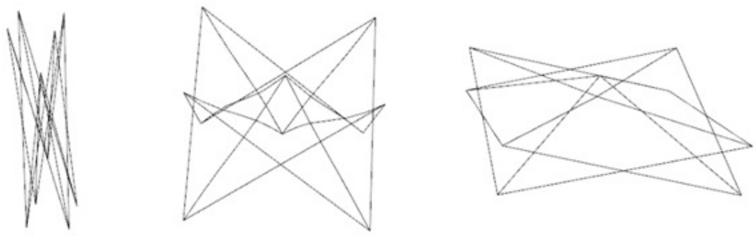

Figure A.14: Subsequent stages in the deployment of a flat square bistable module.

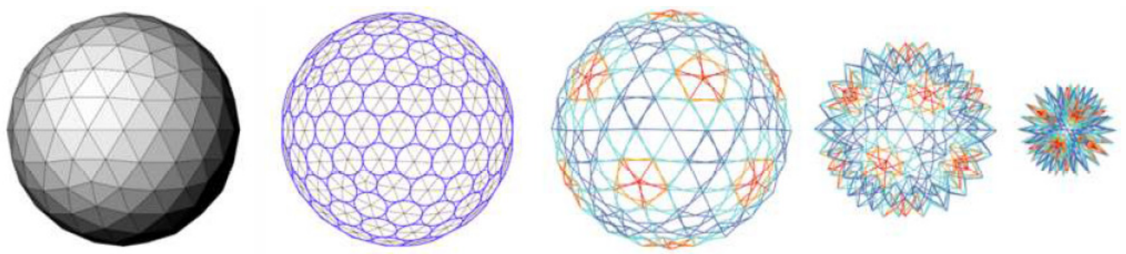

Figure A.15: A grid that has been optimised to hold a circle packing to form the basis of a scissor structure. The resulting scissor grid consists of four different elements (different colours) and is shown in three deployment stages (Roovers & De Temmerman, 2015).

Appendix B

Non-linear finite element analysis

Since scissor structures are subjected to large displacements, a nonlinear finite element analysis is necessary to be able to determine their behaviour.

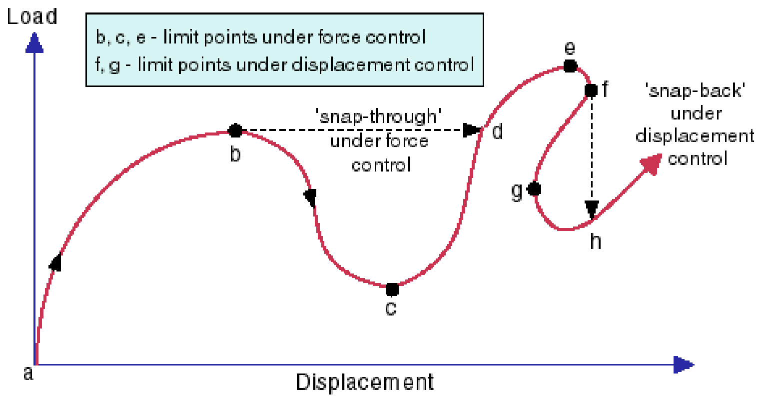

Figure B.1: Snap-through and snap-back behaviour (Dassault Systèmes, 2014).

A complex response is displayed in Figure B.1. Two effects are shown that can occur during a geometrically nonlinear analysis. The classical method of controlling the load case by a force or by a displacement might introduce errors if respectively the force or the displacement decreases during the analysis (Dupont, 2014). Both force control and displacement control will breakdown in the neighbourhood of local maxima (known as snap-through for force control and snap-back for displacement control). Arc-length control will successfully overcome these difficulties (Dassault Systèmes, 2014). Since bistable structures exhibit a snap-through effect, an arc-length method is required for the present work.

The principle is to resolve equilibrium expressed as:

$$^{t+\Delta t}f_{int} = {}^{t+\Delta t}f_{ext} \tag{B.1}$$

with t a parameter which defines the sequence of the different mechanical events (i.e. a fictitious 'time' parameter). An increment is defined as the set of operations needed to go from one state t to the next $t + \Delta t$. This relationship leads to the following equation by developing it to the first order at time t:

$$(\frac{\partial f_{int}}{\partial q})\Delta q \simeq {}^{t+\Delta t}f_{ext} - {}^{t}f_{int} \tag{B.2}$$

with $(\frac{\partial f_{int}}{\partial q})$ called K_t or tangent stiffness. Since the convergence of such calculations is local at each step, an incremental iterative process has to be applied in order to determine the final response (Dupont, 2014). In incremental procedures, the load is applied with discrete, successive steps and the structural response is evaluated at discrete points. In order to deal with the snap-through behaviour of bistable scissor structures, the Riks continuation method is used.

B.1 Riks method

The essence of the Riks method is that the solution is viewed as the discovery of a single equilibrium path in a space defined by the nodal variables and the loading parameter (Figure B.2).

Because the modified Riks method solves simultaneously for loads and displacements, another quantity must be used to measure the progress of the solution. Abaqus uses the 'arc length' Δl along the equilibrium path in the load-displacement space. This approach provides solutions regardless of whether the response is stable or unstable (Dassault Systèmes Simulia Corp., 2012c).

While using arc-length control, the current load magnitude, which is controlled by a varying scalar quantity ω (load proportionality factor) and a unit force system f_{ext}, is not constant during the iterations of a given loading step:

$$^{t+\Delta t}f_{int}{}^{(i)} = {}^{t+\Delta t}\omega^{(i)} f_{ext} \tag{B.3}$$

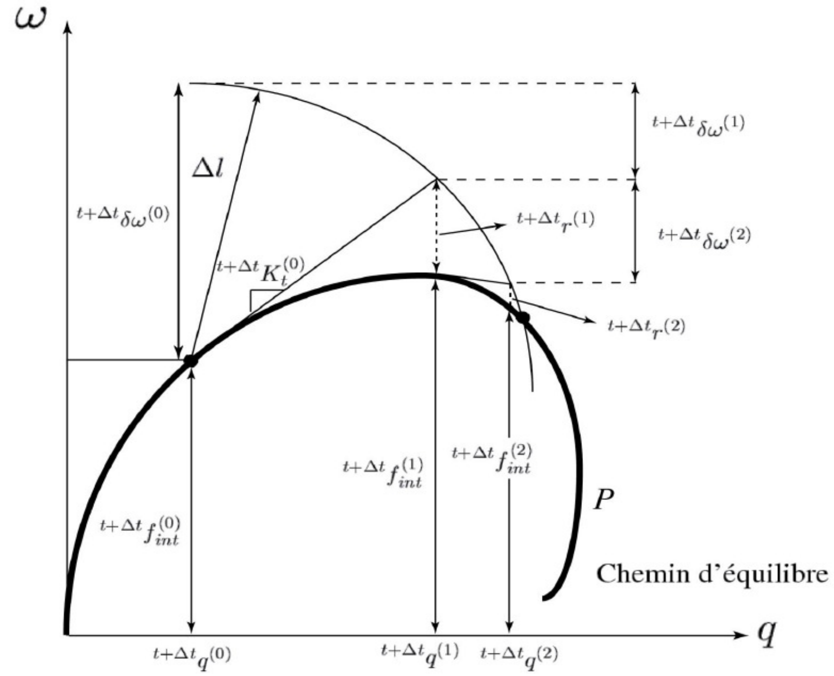

Figure B.2: The modified Riks method or arc-length method (Massart, 2016).

Abaqus uses Newton's method to solve the nonlinear equilibrium equations. Because ω evolves over the successive iterations, a new equation is introduced in order to determine the value of ω:

$$ {}^{t+\Delta t}\Delta q^{(i),T\,t+\Delta t}\Delta q^{(i)} + ({}^{t+\Delta t}\Delta\omega^{(i)})^2\Psi^2 {f_{ext}^{(u)}}^T f_{ext}^{(u)} = \Delta l^2 \tag{B.4} $$

with Ψ a parameter of dimensional consistency which is equal to 1 if a spherical arc length is used (Massart, 2016). The graphical method for one step is described in Figure B.2. For subsequent iterations and increments the value of ω is computed automatically. A maximum value of the load proportionality factor or of the displacement can be specified to end the analysis.

Appendix C

Friction model proposed by Gantes

The main idea behind the friction model proposed by Gantes is that the two beams of a scissor-like element lie theoretically in a plane. In reality, the beams have a certain width while their end nodes are forced to lie in a common plane. This causes deformation of the beams (Figure C.1 top). Because of this deformation, transverse forces between the beams are generated. These forces add up to a total frictional moment that resists rotation. The macroscopic effect of friction, which has a huge influence on the results, can be taken into account by using appropriate nonlinear rotational springs at all pivotal connections (Gantes, Connor & Logcher, 1993).

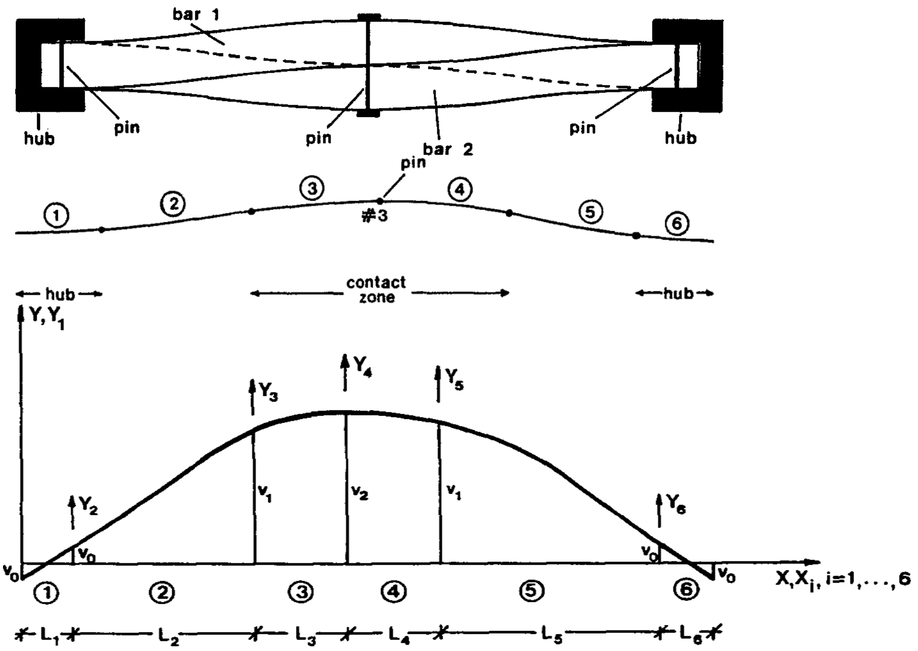

Figure C.1: Top view of a scissor-like element with discrete member width (top), assumed deformation of beams (middle) and details of deformation of beams (bottom) (Gantes, Connor & Logcher, 1993).

This approximate friction model has been thought up by Gantes to overcome the high computational cost and convergence difficulties that are associated with available numerical algorithms for contact problems with friction. The disadvantage of such an approach is that it cannot capture local effects (Gantes, 2001). With the software that is available today, the high computational cost and convergence difficulties are somewhat reduced.

Nevertheless, Gantes'approach can still be used for SLE's in which the beams lie in one plane.

The frictional moments that resist rotation have to be derived as functions of the constant geometry, material characteristics and the varying angle ϕ between the two beams of a scissor-like element during deployment. The Coulomb theory is used for the sake of simplicity. In order to calculate the transverse forces between the two beams (Figure C.1 bottom), some assumptions have to be made. Considering the slot of the joint is a little larger having a width of b_h, while the width of the beam is b, some rotation of the beam takes place until its sides are in contact with the joint. Further, at the pivotal connection there is no contact between the beams caused by a tiny margin in the length of the pin. Following these assumptions, the beam can be thought of as consisting of six segments (Figure C.1 middle). The first and sixth are in the slots of the end joints and the pin separates segments three and four (Gantes, 2001).

Three sources of friction could be identified: friction between the bars and between the beams and the joints in the form of line forces at the contact lines, and friction between the beams and the pins. The friction between the beams and the pins was neglected because it can be easily minimized through lubrication. The friction between the beams and the joints can also be neglected, because it gives a moment that is smaller than 5% compared to the moment at the pivot (Gantes, 1991).

v_0, v_1 and v_2 are known:

$$v_0 = \frac{b_h - b}{2} \tag{C.1}$$

$$v_1 = \frac{b}{2} \tag{C.2}$$

$$v_2 = kb \tag{C.3}$$

where k is factor slightly larger than 0.5 which depends on the extensibility of the pin at the pivotal connection. It is assumed that the two bars are of approximately the same length and the same stiffness.

It can be assumed that the segments have cubic shapes. Their shape, slope and bending moment are given by:

$$v(X_i) = a_i X_i^3 + b_i X_i^2 + c_i X_i + d_i \tag{C.4}$$

$$v'(X_i) = 3a_i X_i^2 + 2b_i X_i + c_i \tag{C.5}$$

$$M(X_i) = EI(6a_i X_i + 2b_i) \tag{C.6}$$

with (X_i, Y_i), $i = 1, ..., 6$ the local coordinate systems for each segment. The 24 unknown coefficients a_i, b_i, c_i, d_i, $i = 1, ..., 6$ can be calculated from the known end displacements at each segment, the moment and slope continuity at the interfaces between the segments and the zero moments at the two ends. These boundary conditions result in a system of 24 linear equations for the 24 unknowns. The concentrated transverse forces F_i, $i = 1, ..., 7$ are given by:

$$F_i = 6(a_i - a_{i-1})EI \tag{C.7}$$

with $a_0 = a_7 = 0$.

The lengths L_i are not constant along the height h of the beam. Gantes proposed two approaches. Either the exact values of L_i should be calculated referring to a specific longitudinal fibre of the beam, leading to an 'exact' model, or some average values could be used, leading to an 'approximate' model (Gantes, 1991). Gantes found a reasonably good agreement between these two approaches. Hence, the 'approximate' model will be used in future analyses.

With B and C the lengths between the three pivots of the beam, A the distance between the pivots at the hinges and the ends of the beam and D the distance between the pivots at the hinges and the edges of the joint, the lengths L_i can be calculated as follows:

$$L_1 = A + D \tag{C.8}$$

$$L_2 = B - D - \frac{h}{2\sin\phi} \tag{C.9}$$

$$L_3 = \frac{h}{2\sin\phi} \tag{C.10}$$

$$L_4 = \frac{h}{2\sin\phi} \tag{C.11}$$

$$L_5 = C - D - \frac{h}{2\sin\phi} \tag{C.12}$$

$$L_6 = A + D \tag{C.13}$$

The friction forces are obtained by multiplying the concentrated transverse forces by the friction coefficient μ. The approximate expression for the total resisting moment due to friction at the pivot is:

$$M_3 = 2\mu F_3 \frac{h}{2\sin\phi} = \frac{1}{2}\mu h^2 b^3 E \frac{a_3 - a_2}{\sin\phi} \tag{C.14}$$

The moment increases rapidly near the folded configuration (Figure C.2 left), when the discrete width of the beams prevents them from folding completely. The nonlinear torsional springs are incorporated in the model using spring-like elastic connector behaviour. The required input format for the nonlinear elastic behaviour is through a sequence of moments with their corresponding rotation.

The load-displacement curve resulting from this friction model is given in Figure C.2 (right). Friction between the members is a concern during the deployment of a bistable scissor structure since an additional force is necessary to overcome friction (Gantes, 2001). In this case, a friction coefficient of 0.36 was used, which was found experimentally by Gantes to be the friction coefficient between two beams in HDPE.

In Gantes's model, the end nodes of the beams of a scissor-like element are forced to be in a common plane, which causes deformation of the beams. Because of this deformation, forces between the beams are generated which add up to a frictional moment that resists rotation. Better solutions exist in which the beams do not lie in one plane and in practice, friction is often designed to be reduced. Dupont found that the influence of friction is small in comparison to other imperfections such as tolerances on the beam lengths (Dupont, 2014).

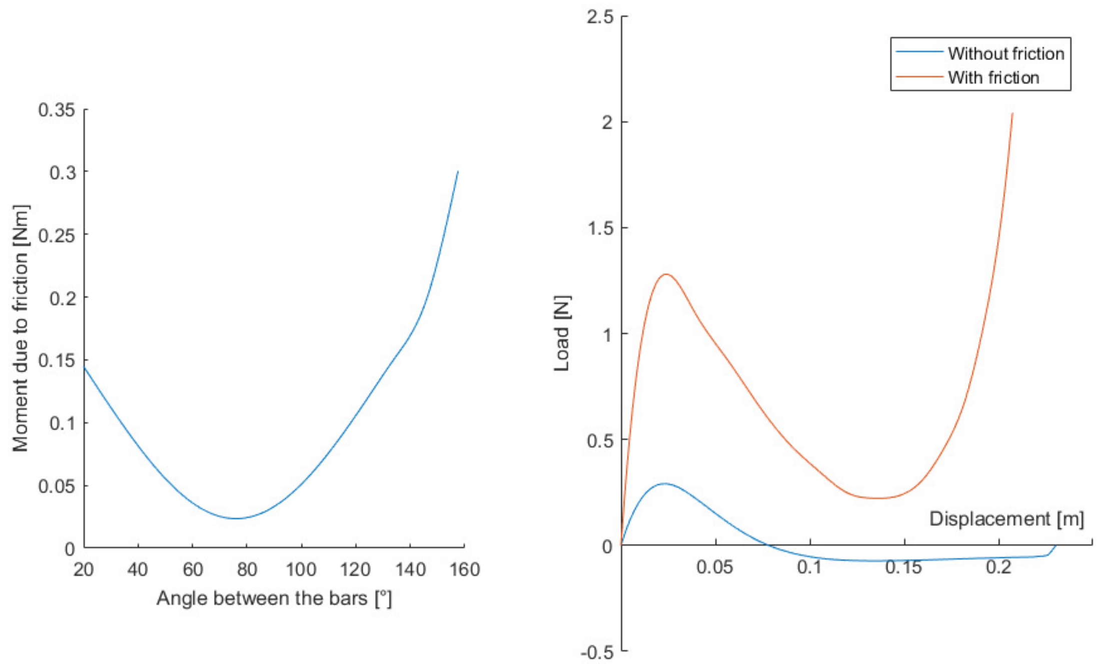

Figure C.2: Variation of the friction moment during folding (left) and influence of friction when using the friction model of Gantes (right).

Appendix D

Approximate model for flat multi-module structures

It has been shown by Gantes that the results of the analysis can be predicted quite well in case of a flat structure composed of multiple modules, both for the stress inside the members as for the required load, by using the corresponding results from the deployment analysis of one of the modules (Gantes, Connor & Logcher, 1991). The results of the load comparison can be generalized to predict the deployment load of a structure consisting of m by n modules. The following empirical formula is proposed by Gantes for the prediction of the deployment load:

$$P_{mn}^{pred} = P_{11}\sqrt[3]{\frac{2}{\frac{1}{m^3}+\frac{1}{n^3}}} \tag{D.1}$$

where P_{11} is the deployment load of a single module. This approximate model can save time when the cost of a nonlinear analysis for the structure is high. Gantes also derived approximate analytical models that can be used to predict the intensity of the snap-through phenomenon for both flat and curved modules (Gantes, 2001). The final analytical expressions are relatively simple and estimate the change of the required load during deployment, but the derivation of the model is rather cumbersome, it does not evaluate the value of the required loads and it can only be used for structures made of identical polygonal modules. Today's computational tools allow for more complexity in the analyses.

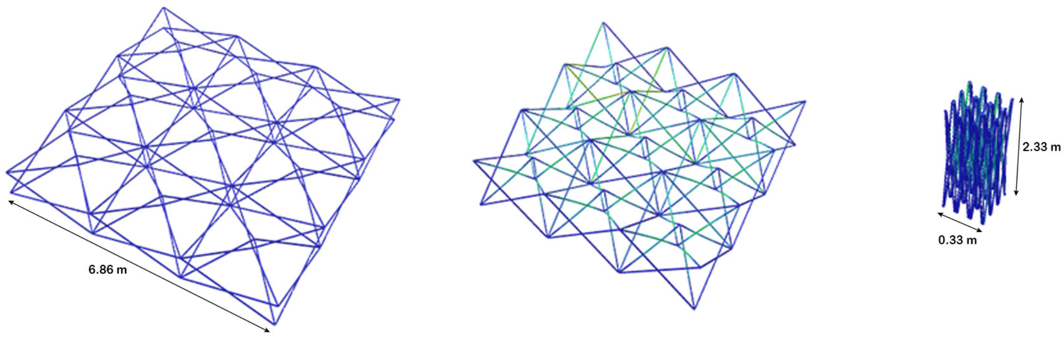

Figure D.1: Successive deployment stages of 3x3 modules.

To verify equation D.1, multi-module structures of 1x2, 1x3, 2x2, 2x3 and 3x3 modules

(Figure D.1) were modelled to compare the maximum deployment load with the expectations. The results are given in table D.1. The accuracy of Gantes' equation is good, not only for the maximum deployment load, but also for the load-displacement curves (Figure D.2). The results of the deployment analysis of single modules can definitely be used for the prediction of corresponding quantities for multi-module structures during preliminary design (Gantes, 1991). To have more accurate results, or to model curved or more complex scissor structures, modelling the whole structure is recommended.

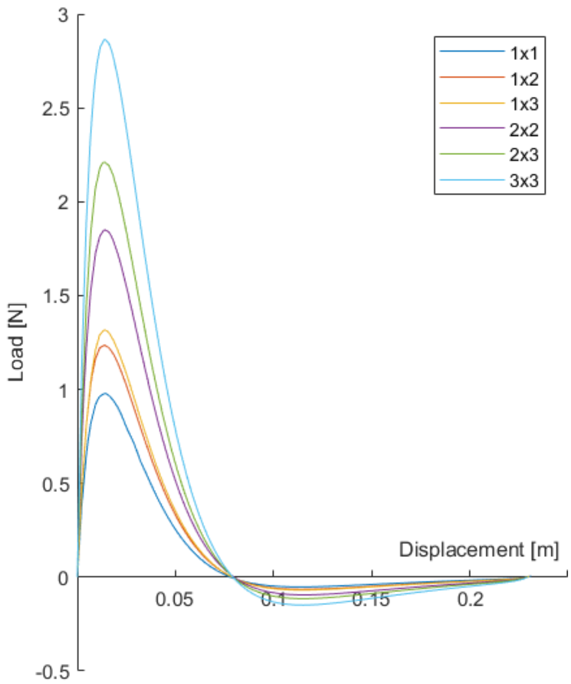

Figure D.2: Load-displacement curves for 1x1, 1x2, 1x3, 2x2, 2x3 and 3x3 modules.

Table D.1: Accuracy of predicted maximum deployment loads according to formula D.1

$\mathbf{m}$	$\mathbf{n}$	$\mathbf{P_{mn}}$ (N)	$\mathbf{P_{mn}^{pred}}$ (N)
1	1	0.9783	0.9783
1	2	1.236	1.185
1	3	1.319	1.218
2	2	1.850	1.957
2	3	2.211	2.261
3	3	2.865	2.935